Winter 3-16-2015

Facile Methods for the Analysis of Lysophosphatidic Acids in Human Plasma

Jialu Wang
Portland State University

Facile Methods for the Analysis of Lysophosphatidic Acids in Human Plasma

by

Jialu Wang

A dissertation submitted in partial fulfillment of the
requirements for the degree of

Doctor of Philosophy
in
Chemistry

Dissertation Committee:
Robert M. Strongin, Chair
Reuben H. Simoyi
David Stuart
Jonathan Abramson

Portland State University
2015

Abstract

Lysophosphatidic acid (LPA) influences many physiological processes, such as brain and vascular development. It is associated with several diseases including ovarian cancer, breast cancer, prostate cancer, colorectal cancer, hepatocellular carcinoma, multiple myeloma atherosclerotic diseases, cardiovascular diseases, pulmonary inflammatory diseases and renal diseases. LPA plasma and serum levels have been reported to be important values in diagnosing ovarian cancer and other diseases. However, the extraction and quantification of LPA in plasma are very challenging because of the low physiological concentration and similar structures of LPA to other phospholipids. Many previous studies have not described the separation of LPA from other phospholipids, which may make analyses more challenging than necessary.

We developed an SPE extraction method for plasma LPA that can extract LPA at high purity. We also developed an HPLC post-column fluorescence detection method that allows the efficient quantification of LPA. These methods were used in a clinical study for ovarian cancer diagnosis to help validate LPA as a biomarker of ovarian cancer. Moreover, molecular imprinted polymers (MIPs) were designed and synthesized as material for the improved extraction of LPA. Compared to the commercially available materials, the MIP developed shows enhanced selectivity for LPA. The extraction was overall relatively more efficient and less labor-intensive.

Acknowledgements

This dissertation could not have been accomplished without the help and support from many generous people. I am sincerely grateful to all of them.

First, I would like to express my thanks and great appreciation to my advisor Professor Robert M. Strongin for his guidance and encouragement. He taught me how to be a researcher with his intelligence and enthusiasm about science. He taught me how to face challenges, solve problems and be an independent thinker with his patience and optimism. I have learned much more than chemistry from him and he is going to be a continuous inspiration for me.

I would like to thank my committee members Professor Jonathan Abramson, Professor Reuben H. Simoyi and Professor David Stuart for their valuable suggestions and feedbacks on my research work. Thanks for their support and advices the whole time. I would also like to thank Dr. Martha Sibrian-Vazquez, Dr. Jorge O. Escobedo and Dr. Mark Lowry for sharing their experiences, ideas and techniques with me. They spent lots of time and effort in helping me with this research. Thanks also go to my colleagues, Shelly Chu, Lei Wang, Aabha Barve and Lovemore Hakuna for their generous help and support. They are not only good colleagues in the lab, but also wonderful friends in life.

Finally, I would like to acknowledge my family for supporting and encouraging me all the time. A special acknowledgement goes to my boyfriend Zhenkun Yang for being understanding and caring. He is always cheering me up and helping me through those disappointing times. I could not finish my Ph.D study without his support and encouragement.

Table of Contents

Abstract ..... **i**

Acknowledgements ..... **ii**

List of Tables ..... **vi**

List of Figures ..... **viii**

List of Schemes ..... **xi**

List of Abbreviations ..... **xii**

Chapter 1 Introduction **1**

1.1 Structure and formation of LPA 1

1.2 LPA as a biomarker of ovarian cancer 2

1.3 LPA and other diseases 5

1.4 Challenge of LPA analysis in human plasma 5

Chapter 2 Extraction and HPLC post-column quantification of LPA in plasma **8**

2.1 Introduction 8

2.2 Experimental 10

2.2.1 Materials 10

2.2.2 Instrumentation 11

2.2.3 Extraction and LPA enrichment procedure for plasma samples 12

2.2.4 Fluorescence determination of linearity and dynamic range for DiA: LPA 18:0 model system 12

2.2.5 HPLC post-column procedure for plasma analysis 13

2.2.6 LC-ESI/MS/MS validation procedure for plasma analysis 13

2.3 Results and discussion 13

2.3.1 Selection of the post-column reagent 13

2.3.2 Probe concentration and flow rate 17

2.3.3 Mobile phase composition, pH and effects of other additives 17

2.3.4 Separation conditions 20

2.3.5 Detection parameters 20

2.3.6 Linearity and dynamic range 22

2.3.7 Quantification of LPAs in human plasma 25
2.3.8 Method validation via LC-ESI/MS/MS 31
2.4 Conclusion 39

Chapter 3 Clinical study of LPA levels in ovarian cancer patients 41

3.1 Introduction 41
3.2 Experimental 42
3.3 Results and discussion 42

Chapter 4 Molecular imprinted polymer synthesis and evaluation 50

4.1 Introduction 50
4.2 Experimental 53
4.2.1 Instruments and materials 53
4.2.2 Synthesis of monomer **1**. 54
4.2.3 Synthesis of monomer **2** 59
4.2.4 Synthesis of monomer **3** and **4**. 59
4.2.5 Preparation of imprinted polymer and non-imprinted polymer 66
4.2.6 ^{1}H NMR titrations 66
4.2.7 Job plots for monomers with template 67
4.2.8 LPA enrichment procedure with MIP 67
4.2.9 LC-ESI/MS procedure for plasma analysis 67
4.2.10 Swelling of polymers 68
4.3 Results and discussion 68
4.3.1 Monomer selection and synthesis 68
4.3.2 Characterization of monomer binding properties 70
4.3.3 Infrared spectroscopy of MIP 77
4.3.4 SEM microphotographs of polymers 78
4.3.5 Swelling of polymers 80
4.3.6 Formulation optimization of MIP 80
4.3.7 SPE protocol optimization 85
4.3.8 LPA extraction and quantification in plasma 86
4.4 Conclusion 90

Chapter 5 Future Work **91**

5.1 Optimization of current formulations of MIP 91

5.2 MIP with other functional monomers 91

5.3 MIP for specific LPA subspecies 91

5.4 Molecularly imprinted membrane (MIM) for LPA analysis 92

5.5 MIPs with fluorescent probes 92

References **93**

List of Tables

Table 2.1 Effect of column length on the resolution (R_s) and theoretical plates (N) for the separation of LPAs.[a] 18

Table 2.2 Effect of pH on the resolution (R_s) and theoretical plates (N) for the separation of LPAs.[a] 19

Table 2.3 Resolution (R_s) and theoretical plates (N) for the final optimal conditions. The column size is 50×2.0 mm.[a] 19

Table 2.4 Data obtained from calibration curves for LPA species via the HPLC post-column method. 24

Table 2.5 Recoveries of individual LPA species after SPE enrichment. 27

Table 2.6 Statistical values obtained for the individual LPA species in the LC-ESI/MS/MS method (n = 3). 32

Table 2.7 Results for LPA analysis in human plasma (donor A) using the HPLC post-column fluorescence and LC-ESI/MS/MS methods. 33

Table 2.8 Results for LPA analysis in human plasma (donor B) using the HPLC post-column fluorescence and LC-ESI/MS/MS methods. 34

Table 2.9 Results for LPA analysis in human plasma (donor C) using the HPLC post-column fluorescence and LC-ESI/MS/MS methods. 35

Table 2.10 Results for LPA analysis in human plasma (donor D) using the HPLC post-column fluorescence and LC-ESI/MS/MS methods. 36

Table 2.11 Results for LPA analysis in human plasma (donor E) using the HPLC post-column fluorescence and LC-ESI/MS/MS methods. 37

Table 4.1 Data for the Job plot performed by ^{1}H NMR titration in $CDCl_3$. 72

Table 4.2 Data of ^{1}H NMR titration of monomer **1** and template in $CDCl_3$. 75

Table 4.3 Swelling factor and density of Non-imprinted and imprinted polymers .. 80

Table 4.4 Formulations of MIP and NIP. 83

Table 4.5 Statistical values from calibration curves for LPA species with LC/MS as the quantification method. 86

Table 4.6 Recoveries of individual LPA species after SPE. (n = 3) 87

Table 4.7 Results for LPA analysis in human plasma using LC-ESI/MS. 88

List of Figures

Figure 1.1 Structures of lysophosphatidic acids (LPAs)..... 1

Figure 1.2 Two distinct enzymatic mechanisms of LPA generation..... 2

Figure 1.3 Ovarian cancer five-year relative survival rates..... 3

Figure 1.4 Comparison of LPA and CA125 as biomarkers for ovarian cancer at different stages..... 4

Figure 1.5 Structure comparison of PA and LPA..... 6

Figure 1.6 Structures of representative lysophospholipids..... 7

Figure 2.1 Structures of probe candidates including DiA, DPH, DSHP, NAO and BBOT. 15

Figure 2.2 Absorption spectra (top) and fluorescence spectra (bottom) of 3 μM aqueous solutions of DiA alone (dashed lines) and in the presence of 10 μM LPA 18:0 (solid lines). Excitation/emisson wavelengths: 470/590 nm. 16

Figure 2.3 HPLC trace of a LPA mixture (10 μM LPA 14:0, 16:0, 18:0, 18:1, 20:4 and 20 μM LPA 17:0). Chromatographic conditions: column: Luna™ C8, 3 μm, 50 × 2.0 mm; mobile phase: MeOH: phosphate buffer (50 mM, pH 2.5) 16:5; flow rate: 0.32 mL/min; injection volume: 20 μL; sample concentration: 10 μM in MeOH: H_2O 9:1; post-column reagent: 10 μM DiA in H_2O; reagent flow rate: 0.62 mL/min; excitation/emission wavelengths: 450/570 nm..... 21

Figure 2.4 Emission spectra and calibration curve (inset) of 2.67 μM DiA upon titration with LPA (18:0)..... 22

Figure 2.5 Calibration curves of specific LPA subspecies obtained by HPLC-post column fluorescence detection. The area ratio is the peak area of individual LPAs divided by the peak area of the internal standard (LPA 17:0). Data points represent the average of 4 runs..... 23

Figure 2.6 Mass spectra of phospholipids mixture in negative mode..... 29

Figure 2.7 Mass spectra of phospholipids mixture in positive mode..... 29

Figure 2.8 Mass spectra of plasma extract in negative mode..... 30

Figure 2.9 Mass spectra of plasma extract in positive mode..... 30

Figure 2.10 Calibration curves of LPAs using the LC-ESI/MS/MS method. The area ratio is the peak area of individual LPAs divided by the peak area of the internal standard (LPA 17:0). 31

Figure 2.11 Chromatograms of a mixture containing 10 μM of each LPA species and LPAs isolated from human plasma (donor A) using the post-column detection method. 38

Figure 2.12 LC-ESI/MS/MS traces of a 10 μM standard mixture of LPAs. Column: Luna™ C8 (50 × 2 mm, 3 μm) at 40 ºC. Injection volume: 10 μL. Mobile phase: 9:1 MeOH:aqueous HCOOH (pH 2.5) at a flow rate of 0.4 mL/min. Parent and daughter ions were detected in the negative ion mode, sprayer voltage; 3.0 kV, capillary temperature at 300 ºC. 39

Figure 3.1 LPA 14:0 concentrations in plasma and serum samples of 183 patients.44

Figure 3.2 LPA 20:4 concentrations in plasma and serum samples of 183 patients.45

Figure 3.3 LPA 16:0 concentrations in plasma and serum samples of 183 patients.46

Figure 3.4 LPA 18:1 concentrations in plasma and serum samples of 183 patients.47

Figure 3.5 LPA 18:0 concentrations in plasma and serum samples of 183 patients.48

Figure 3.6 Total LPA concentrations in plasma and serum samples of 183 patients. 49

Figure 4.1 Energy-minimized model of the complex of a tris-urea scaffold and LPA 18:1. 52

Figure 4.2 ^{1}H-NMR spectrum of monomer **1**. 55

Figure 4.3 ^{13}C-NMR spectrum of monomer **1**. 56

Figure 4.4 ^{1}H-NMR spectrum of monomer **2**. 57

Figure 4.5 ^{13}C-NMR spectrum of monomer 58

Figure 4.6 ^{1}H-NMR spectrum of monomer **3**. 62

Figure 4.7 ^{13}C-NMR spectrum of monomer **3**. 63

Figure 4.8 ^{1}H-NMR spectrum of monomer **4**. 64

Figure 4.9 ^{13}C-NMR spectrum of monomer **4**. 65

Figure 4.10 Chemical structures of selected functional monomers. 69

Figure 4.11 ^{1}H NMR spectra of Job plot data for trisurea and octadecylphosphonic acid. Each spectrum is labeled with the mixture numbers in Table 3.1. 73

Figure 4.12 Job plot of monomer 1 with octadecylphosphonic acid in CDCl3 showing a maximum at 0.5 mole fraction of trisurea..... 74

Figure 4.13 ^{1}H NMR titration spectra of trisurea and octadecylphosphonic acid. Each spectrum is labeled with the mixture number in Table 3.2..... 76

Figure 4.14 ^{1}H NMR titration of monomer **1** using octadecylphosphonic acid as the guest. 77

Figure 4.15 IR spectra of (a) non-imprinted polymer and (b) imprinted polymer after template removal..... 78

Figure 4.16 SEM microphotographs of non-imprinted (a) and imprinted (b) polymers. 79

Figure 4.17 Structures of OPA, MAA, 4-vinylpyridine, EGDMA and AIBN. 82

Figure 4.18 Percent recoveries of LPA and possible interferences in preliminary screening experiments of three formulations of MIP..... 84

Figure 4.19 Calibration curves of LPA subspecies with LC/MS as the quantification method. The area ratio is the peak area of individual LPA divided by the peak area of the internal standard (LPA 17:0). Data points represent the average of 3 runs. 87

Figure 4.20 LC-ESI/MS traces. (a) A 10 uM standard mixtures of LPAs. (b) Plasma sample. Column: Luna ™ C-8 (50 × 2 mm, 3 µm) at 40 ºC. Injection volume: 10 µL. Mobile phase: 9:1 MeOH–HCOOH (pH 2.5). Flow rate: 0.6 mL/min. Ions were detected in negative ion mode. Sprayer voltage: 3.0 kV and Capillary temperature at 300 ºC..... 89

List of Schemes

Scheme 4.1 Synthesis of monomer **1**. 69

Scheme 4.2 Synthesis of monomer **2**. 70

Scheme 4.3 Synthesis of monomer **3** and **4**. 70

List of Abbreviations

LPA	lysophosphatidic acid
MIP	molecularly imprinted polymers
LPC	lysophosphatidylcholine
ATX	autotaxin
PLA1	phospholipase A1
PLA2	phospholipase A2
CA125	cancer antigen 125
MMP-9	matrix metallopeptidase 9
LPE	lysophosphatidylethanolamine
LPS	lysophosphatidylserine
PA	phosphatidic acids
LPI	lysophosphatidylinositol
LPG	lysophosphatidylglycerol
LC-MS	liquid chromatography–mass spectrometry
DiA	4-(4-(dihexadecylamino)styryl)-N-methylpyridinium iodide
GC	gas chromatography
CE	capillary electrophoresis
TLC	thin layer chromatography
HPLC	high performance liquid chromatography
ELSD	evaporative light-scattering detection
LC-MS/MS	liquid chromatography-tandem mass spectrometry
LC-ESI/MS/MS	liquid chromatography-electrospray ionization-tandem mass spectrometry

SPE	solid phase extraction
BBOT	2,5-bis-2-(5-*tert*-butyl)benzoxazolylthiophene
DPH	1,6-diphenyl-1,3,5-hexatriene
DSHP	4-(4-dimethylaminostyryl)-1-hexadecylpyridinium
NAO	10-N-Nonyl acridine orange
CL	cardiolipin
S/N	signal-to-noise
LOD	limit of detection
PC	phosphatidylcholine
LMSD	LIPID MAPS Structure Database
LLE	liquid-liquid extraction
MAA	methacrylic acid
EGDMA	ethylene glycol dimethacrylate
AIBN	2,2'-azobisisobutyronitrile
NIP	non-imprinted polymer
FTIR	fourier transform infrared spectroscopy
SEM	scanning electron microscope

Chapter 1 Introduction

1.1 Structure and formation of LPA

Lysophosphatidic acid (LPA) is a phospholipid that consists of a phosphate head group, a glycerol backbone and an alkyl chain structure. LPA has many subspecies based on differing length and saturation of the alkyl chain. The structures of five major LPA species are shown in Figure 1.1.

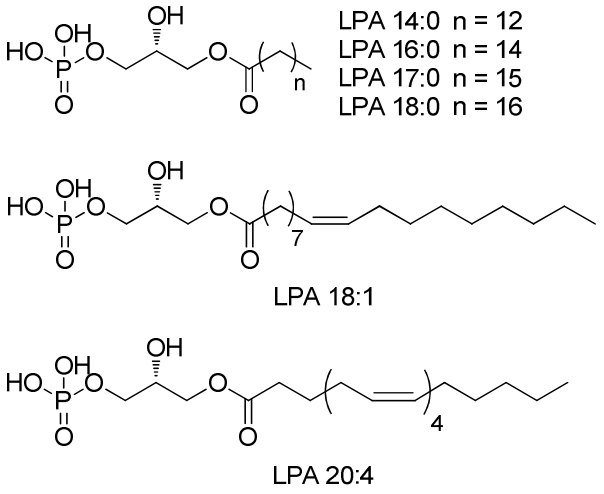

Figure 1.1 Structures of lysophosphatidic acids (LPAs).

LPA can be produced by at least two distinct enzymatic mechanisms. The main source is the hydrolysis of lysophosphatidylcholine (LPC) by lysophospholipase D (lyso-PLD), such as autotaxin (ATX). It can also be generated from the hydrolysis of PA via phospholipase A_1 (PLA_1) or phospholipase A_2 (PLA_2). [1] Figure 1.2 shows the two mechanisms using LPA 18:1 as an example.

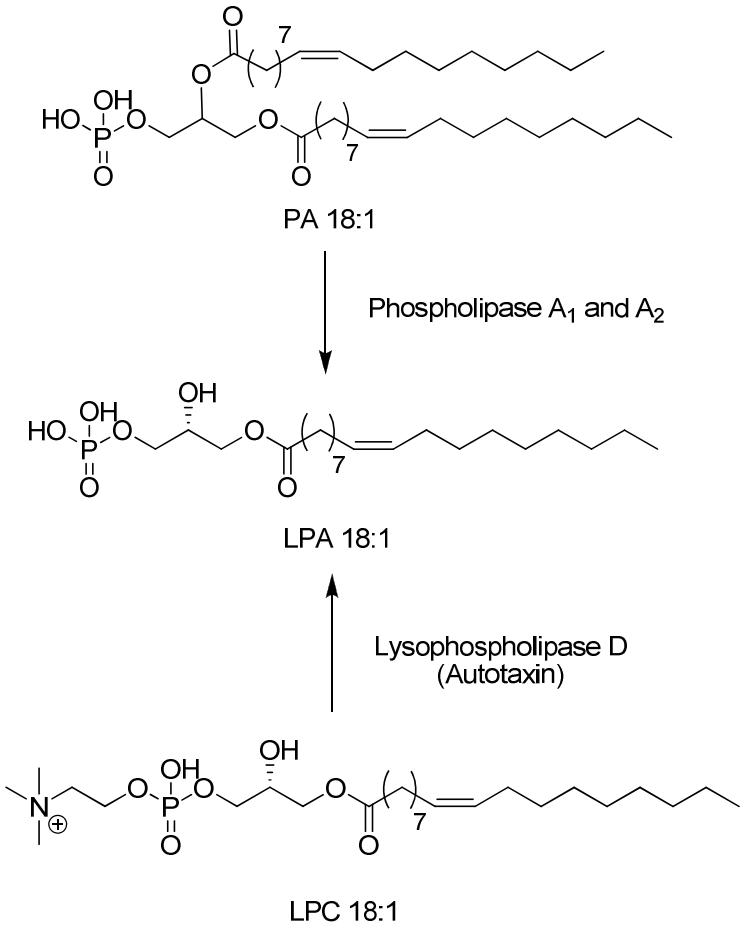

Figure 1.2 Two distinct enzymatic mechanisms of LPA generation.

As a bioactive phospholipid, LPA can activate specific cell-surface G protein-coupled receptors that initiate many cellular processes, such as cell proliferation [2] [3], migration [4] and platelet aggregation [5,6]. LPA also influences many physiological processes such as brain development [7], vascular development [8], wound healing and pathological conditions, including autoimmune disorders and tumor metastasis. [9] [10] [11]

1.2 LPA as a biomarker of ovarian cancer

There are more than 20,000 new cases of ovarian cancer in the US every year. More than 60 % of all patients die from this disease. [12] The early stages of the disease are

difficult to diagnose because of a lack of specific symptoms. The majority of patients are diagnosed with stage III or IV disease, while *ca*. 30% of are diagnosed at stage I or II. An important determinant of ovarian cancer survival is the stage of the disease at diagnosis. [13] The five-year survival relative survival rates are more than 90% for stage I, while only less than 10% for stage IV. (Figure 1.3)

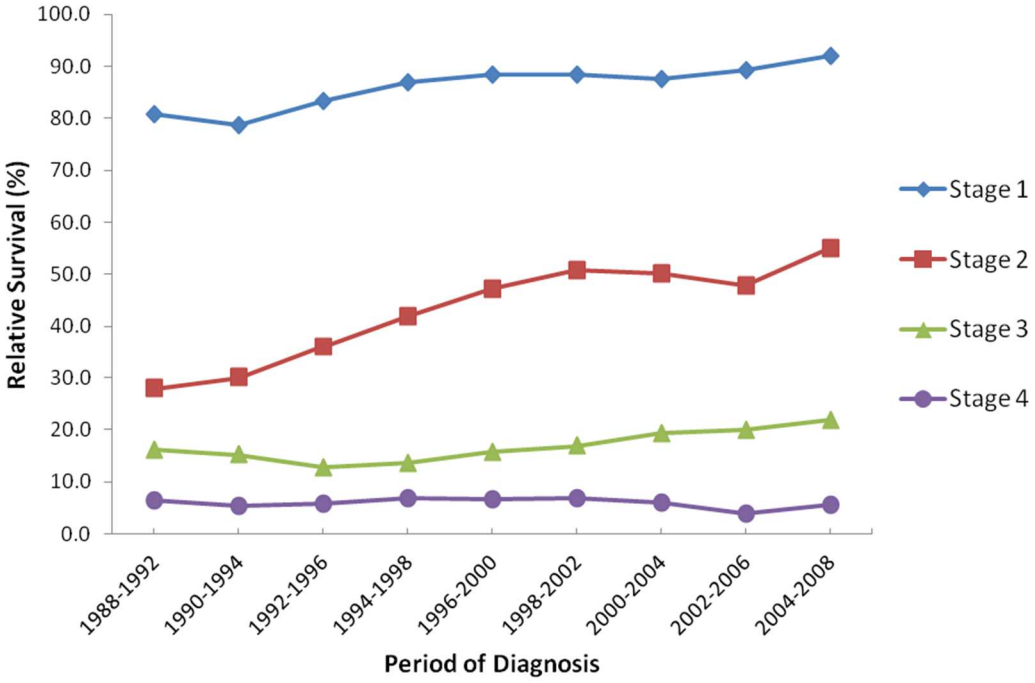

Figure 1.3 Ovarian cancer five-year relative survival rates.

Currently, there is no accurate and effective screening test for the early detection of ovarian cancer. Pelvic exam is a common way to diagnose ovarian cancer. However, it only detects the disease occasionally and usually when the disease is advanced. The combination of a thorough pelvic exam, an ultrasound and a blood test for the biomarker CA125 are suggested, but are not proven completely effective yet.

In 1998, Xu et al. found that increased LPA levels in human plasma were related to ovarian cancer. LPA as a biomarker showed advantages in early stage detection compared to CA125, which was used as the conventional biomarker control for ovarian cancer diagnosis. According to their results, 90% of the stage I patients have an elevated level of LPA while only 20% have an elevated level of CA125. [14] Figure 1.4 shows the percentage of patients that have elevated levels of LPA and CA125 in different stages.

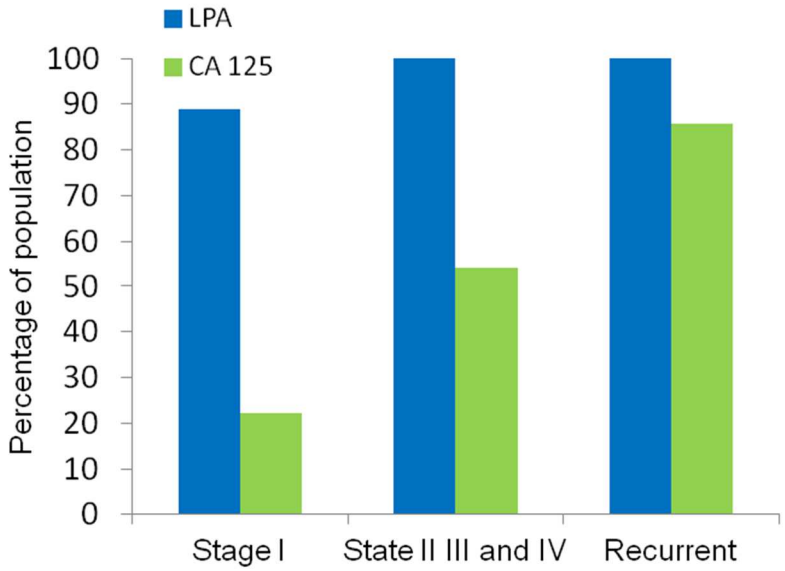

Figure 1.4 Comparison of LPA and CA125 as biomarkers for ovarian cancer at different stages.

After this result was published, many other groups studied the correlation of LPA and ovarian cancer and reported LPA as a perspective marker [15] [16, 17] [18, 19] although some groups had different opinions [20]. Liu et al. [21] reported that LPA promoted ovarian cancer progression by inducing MMP-9 expression and MMP-9-catalyzed E-cadherin ectodomain shedding.

1.3 LPA and other diseases

LPA influences many physiological processes, such as brain[7] and vascular development [8] and is involved in many diseases apart from ovarian cancer [14], such as breast cancer [22], prostate cancer [23], colorectal cancer [24], hepatocellular carcinoma [25], multiple myeloma [26] atherosclerotic diseases [27] [28], cardiovascular diseases [29], pulmonary inflammatory diseases [30], renal diseases [31, 32].

1.4 Challenge of LPA analysis in human plasma

Quantification of LPA in plasma is very challenging because of its low physiological concentration. The concentration of phospholipids in human plasma is > 2000 μM [33]. Among the several classes of phospholipids that are present in human plasma, LPA represents a relatively very small fraction, and reported concentrations of total LPA vary. A generally reported range is 1-5 μM [34]. This makes it very challenging for the selective isolation and enrichment of these analytes. Moreover, some studies showed that not total LPA, but certain subspecies of LPA are the biomarkers of ovarian cancer. [17] Thus, it is necessary to separate and quantify each individual LPA species.

Additionally, other phospholipids could interfere both the extraction and detection because of their similar structures to LPA. For example, the lysophospholipids such as lysophosphatidylethanolamine (LPE), lysophosphatidylcholine (LPC) and lysophosphatidylserine (LPS) have similar structures to LPA, with only different head groups. Phosphatidic acids (PA) have the same head group as LPA, but have an extra alkyl chain than LPA. Structures of representative lysophospholipids are shown in Figures 1.5 and 1.6. Moreover, the concentrations of some of these phospholipids are

much higher than LPA in human plasma. For example, the concentration of LPC is around 300 μM.[35] It is not only difficult to quantify LPA in the presence of LPC, but it is also challenging to separate them because of the similar properties.

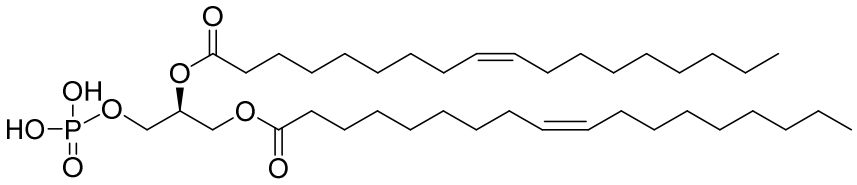

Phosphatidic acid (PA) 18:1

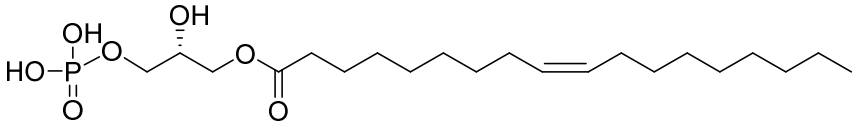

Lysophosphatidic acid (LPA) 18:1

Figure 1.5 Structure comparison of PA and LPA.

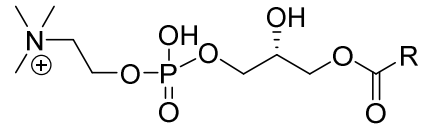

Lyso-phosphatidylcholine (LPC) 18:1

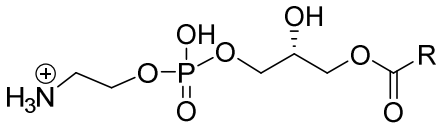

Lyso-Phosphatidylethanolamine (LPE) 18:1

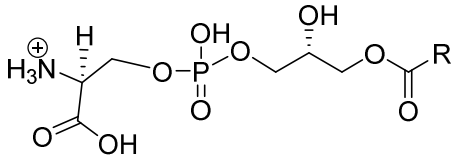

Lyso-Phosphatidylserine (LPS) 18:1

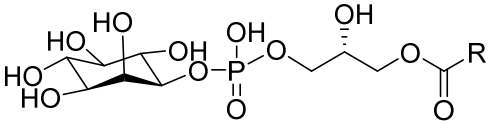

Lyso-Phosphatidylinositol (LPI) 18:1

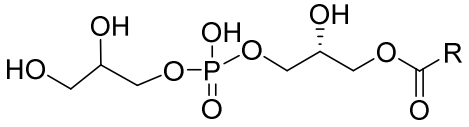

Lyso-Phosphatidylglycerol (LPG) 18:1

Figure 1.6 Structures of representative lysophospholipids.

Chapter 2 Extraction and HPLC post-column quantification of LPA in plasma

2.1 Introduction

HPLC post-column fluorescence probe-assisted methods have been reported for phospholipids previously [36-38]. However, they had not found utility in LPA analyses. A commercially available fluorescent probe 4-(4-(dihexadecylamino) styryl)-N-methylpyridinium iodide (DiA) is used in this study as a post-column reagent for the detection and quantification of LPA. Structure of DiA is shown in Figure 2.1 One may separate and quantify six individual LPA subspecies at physiological levels in plasma with a C-8 column in 15 minutes. In contrast to the currently used liquid chromatography–mass spectrometry (LC-MS) methods, LPA levels obtained by optical method are not susceptible to ionization-related issues.

To date, a number of separation and detection methods to determine LPA levels have been developed. In 1998, Xu et al. [14] used a gas chromatography (GC) method to quantify total levels of LPA in plasma. Chen et al.[39] used capillary electrophoresis (CE) to quantify individual LPAs with an indirect ultraviolet (UV) detection method. However, to separate LPA from other lipids before detection, many of these early studies employed two-dimensional thin layer chromatography (TLC). [14, 15, 39, 40] High performance liquid chromatography (HPLC) has been used to separate LPA. Solid supports have included

---

normal phase (used in hydrophilic interaction chromatography), reversed phase (C8, C18) and diol-bonded phases.

For example, Holland et al.[41] used a diol-bonded phase to separate LPA from other phospholipid classes with evaporative light-scattering detection (ELSD). This avoids the 2-D TLC step; however, LPA recovery is 53.4% and there is no effort to separate LPA subspecies. LC-MS has also been used to quantify LPAs. [3] More recently liquid chromatography-tandem mass spectrometry (LC-MS/MS) has become the method of choice.[15, 42, 43] However, there are reports that LC-MS/MS methods currently have some drawbacks. First, not all endogenous matrix components are efficiently separated from the target analytes. This leads to matrix effects that hamper the efficiency and reproducibility of the ionization process.[44-47] Phospholipids, especially glycerophosphocholines and lysophosphatidylcholines, are cited as the major causes of matrix effects due to their highly ionic character. This affects the electrospray MS source by either suppressing or enhancing ionization. This cannot be compensated for by adding internal standards, including isotopically labelled phospholipids. Wang et al.[45] demonstrated that slight differences in retention times between the analyte and the isotopically-labelled internal standard cause differences in ion suppression between the two. In their study, the results vary up to 52% in peak areas from one plasma sample to another because of matrix effects resulting in up to 18.9 % of variation in concentration. Matrix effects may also result in retention time shifts, elevated baselines and divergent calibration curves. Second, conversion of lysophosphatidylcholine (LPC) and lysophosphatidylserine (LPS) to LPA occurs at the ion source of electrospray ionization tandem mass spectrometry. Shan et al.[48] found that unidentified compounds in plasma

produce the same parent-to-daughter ion transition as LPA in a direct flow injection liquid chromatography-electrospray ionization-tandem mass spectrometry (LC-ESI/MS/MS) method and could reduce the accuracy of the analysis of LPA. Zhao et al.[49] later reported that LPC and LPS lose their respective choline or serine moieties at ion source to generate LPA-like signals.

In order to overcome the limitations described above, we propose a straightforward method combining a modified Bligh and Dyer [50] procedure with a solid phase extraction (SPE) protocol. This isolates plasma LPA effectively enough to permit the rapid detection of each of the subspecies via a standard HPLC fluorescence detector.

HPLC post-column fluorescence probe-assisted methods have been reported for phospholipids previously; [36-38] however, they had not found utility in LPA analyses. A commercially available fluorescent probe 4-(4-(dihexadecylamino) styryl)-N-methylpyridinium iodide (DiA) is used in this study as a post-column reagent for the detection and quantification of LPA. One may separate and quantify six individual LPA subspecies at physiological levels in plasma with a C8 column in 15 minutes. In contrast to the currently used LC-MS methods, LPA levels obtained by optical method are not susceptible to ionization-related issues.

2.2 Experimental

2.2.1 Materials

All lysophosphatidic acids including 1-myristoyl-2-hydroxy-sn-glycero-3-phosphate (LPA 14:0), 1-palmitoyl-2-hydroxy-sn-glycero-3-phosphate (LPA 16:0), 1-

heptadecanoyl-2-hydroxy-sn-glycero-3-phosphate (LPA 17:0), 1-stearoyl-2-hydroxy-sn-glycero-3-phosphate (LPA 18:0), 1-oleoyl-2-hydroxy-sn-glycero-3-phosphate (LPA 18:1) and 1-arachidonoyl-2-hydroxy-sn-glycero-3-phosphate (LPA 20:4) were purchased from Avanti Polar Lipids (Alabaster, AL, USA). 4-(4-(Dihexadecylamino) styryl)-N-methylpyridinium iodide (DiA) was purchased from AnaSpec (Fremont, CA, USA). HPLC grade MeOH was purchased from Fisher Scientific. Ultra pure water was obtained from a Milli-Q™ system. Phosphoric acid and monosodium phosphate were purchased from Sigma-Aldrich (St. Louis, MO, USA). Waters OASIS™ HLB (3 cc, 60 mg, 30 μm) SPE cartridges were purchased from Waters Corporation (Milford, MA, USA). Lyophilized Human Plasma was purchased from Sigma-Aldrich. Human plasma was collected by Lampire Biological Laboratories Inc., from female donors, processed to obtain platelet-free plasma, and frozen at -80 ºC.

2.2.2 Instrumentation

Fluorescence measurements were performed on a Cary Eclipse™ fluorescence spectrophotometer, and absorption spectra performed on a Cary 50™ UV-Vis spectrophotometer (Agilent Technologies). The HPLC system consists of a 1525 binary HPLC delivery system, a 2475 multi lambda fluorescence detector (Waters). A Luna™ C8 (50 × 2 mm, 3 μm) column connected to a guard cartridge with 2.0 to 3.0 mm internal diameters (Phenomenex) was used for all the separations. The reagent is pumped by a reagent manager (Waters). The DiA solution and the liquid eluting from the column are merged through a metal mixing tee and delivered to the detector. The data is collected and processed with the Empower™ software suite (Waters). In the LC-ESI/MS/MS

control method, LPAs were separated in an Accela UPLC system (Thermo Fisher, San Jose, CA) and detected *via* an LTQ-Orbitrap XL Discovery instrument (San Jose, CA, USA), equipped with an ESI ion max source.

2.2.3 Extraction and LPA enrichment procedure for plasma samples

Human plasma (0.8 mL) is mixed with 4 mL MeOH: $CHCl_3$ 2:1, and vortexed at 2000 rpm for 30 s. The mixture is incubated at 4 ºC for 20 min, warmed to rt and centrifuged at 2000 rpm for 10 min. The supernatant is decanted from the precipitated proteins and extracted with 2 mL phosphate buffer saline (10 mM, pH 7.4) and vortexed at 2000 rpm for 30 s. The aqueous phase containing the LPAs is washed two times with 1.33 mL $CHCl_3$ to remove the remaining neutral lipids. The aqueous layer is acidified to pH 2.0 with concentrated H_3PO_4 to protonate the LPAs to convert them to their neutral form.[51] An SPE cartridge is preconditioned with 6 mL MeOH, followed by 3 mL H_2O. The acidified LPAs solution is loaded onto the cartridge and rinsed with 3 mL H_2O followed by 1 mL $CHCl_3$. The SPE cartridge is dried by applying an N_2 stream, and LPAs are eluted with 4 mL of MeOH. The solvent is evaporated and the residue is reconstituted in 0.16 mL MeOH: H_2O 9:1.

2.2.4 Fluorescence determination of linearity and dynamic range for DiA: LPA 18:0 model system

Stock solutions of varying concentrations (0–150 μM) of LPA (18:0) were prepared in a mixture of MeOH–$CHCl_3$ 1:1. To avoid aggregation of the lipids, films of each sample were prepared by evaporation under an Ar stream, and the films

reconstituted in MeOH. Choline chloride (final concentration 6.4 mM) [52] was added before mixing with DiA (final concentration 2.67 μM) aqueous solution.

2.2.5 HPLC post-column procedure for plasma analysis

Samples (20 μL) are injected and eluted with a 16:5 mixture of MeOH-phosphate buffer (50 mM, pH 2.5) through a Luna C-8 (50 × 2 mm, 3 μm) column equipped with a guard column. The end of the column is connected to a mixing tee allowing contact with the post-column reagent solution (DiA, 10 μM). The flow rate of the mobile phase is set to 0.32 mL min^{-1} and 0.62 mL min^{-1} for the post-column reagent. The entire procedure is performed at room temperature.

2.2.6 LC-ESI/MS/MS validation procedure for plasma analysis

Chromatography was performed on a Luna C-8 (50 × 2 mm, 3 μm) column at 40 ºC with an injection volume of 10 μL. The mobile phase MeOH–HCOOH (10 mM, pH 2.5) 9:1 was delivered at a flow rate of 0.4 mL min^{-1}. Ions were created in negative ion mode by setting the sprayer voltage at 3.0 kV and the capillary temperature at 300 ºC.

2.3 Results and discussion

2.3.1 Selection of the post-column reagent

Typically, fluorescent probes used for the post-column detection of phospholipids rely on the formation of aggregated non-fluorescent π-stacked assemblies. These assemblies are disrupted, upon interaction with phospholipids, thereby restoring probe fluorescence. Examples of phosphoplipid-interacting probes include 2,5-bis-2-(5-*tert*-

butyl)benzoxazolylthiophene (BBOT), 1,6-diphenyl-1,3,5-hexatriene (DPH) and 4-(4-dimethylaminostyryl)-1-hexadecylpyridinium (DSHP). [37] [53-55] [56] Structures of BBOT, DPH and DSHP are shown in Figure They are mainly used for the detection and quantification of triglycerides, ceramides, glycosphingolipids and phosphatidylcholines. In our hands, we found that both BBOT and DPH did not produce usable fluorescence emission enhancement in the presence of lysophosphatidic acids. Other fluorescent probes with amphiphilic properties were evaluated. 10-N-Nonyl acridine orange (NAO) has been used in the analysis of certain phospholipids such as cardiolipin (CL); [36] [57, 58] however, it did not produce a useful spectral response in LPA-containing solutions. The amphiphilic cyanine-type probe 4-(4-(dihexadecylamino)styryl)- N-methylpyridinium iodide (DiA) afforded the most promising results for LPA detection. These results can be explained considering the structural characteristics of BBOT and DPH, which are essentially non-polar probes, while LPA (and PA) are amphiphilic charged molecules. Better binding is expected to occur with DiA through electrostatic interactions between the quaternary ammonium moiety and the phosphate group of LPA. Probe structures including DiA, DSHP, BBOT, DPH and NAO are shown in Figure 2.1.

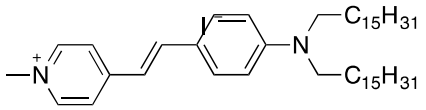

4-(4-(dihexadecylamino)styryl)-N-methylpyridinium iodide (DiA)

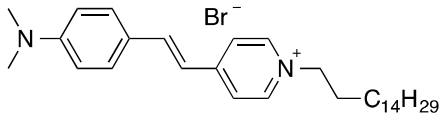

4-(4-dimethylaminostyryl)-1-hexadecylpyridinium (DSHP)

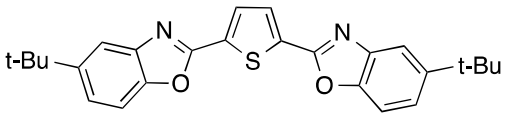

2,5-Bis(5-tert-butyl-benzoxazol-2-yl)thiophene (BBOT)

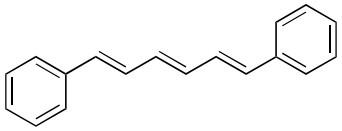

1,6-Diphenyl-1,3,5-hexatriene (DPH)

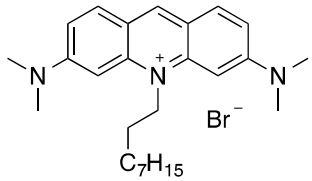

Acridine Orange 10-nonyl bromide (NAO)

Figure 2.1 Structures of probe candidates including DiA, DPH, DSHP, NAO and BBOT.

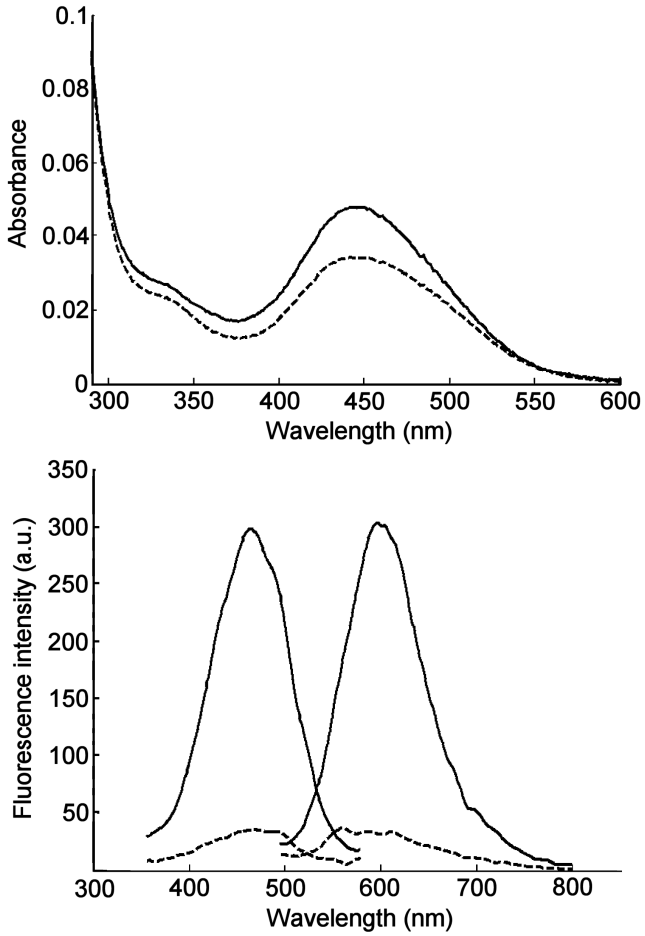

Figure 2.2 Absorption spectra (top) and fluorescence spectra (bottom) of 3 μM aqueous solutions of DiA alone (dashed lines) and in the presence of 10 μM LPA 18:0 (solid lines). Excitation/emisson wavelengths: 470/590 nm.

An aqueous probe solution (3 μM) responds to the addition of 10 μM LPA 18:0 with a 40% increase at 445 nm in absorption. Importantly, the probe exhibits weak fluorescence in the absence of LPA and a 700% increase in fluorescence emission upon addition of 10 μM LPA. (Figure 2.2) It is notable that a relatively small increase in the extinction coefficient of DiA upon addition of LPA produced a dramatic increase in the

fluorescence response. It is known that DiA exhibits minimal fluorescence in aqueous solution, yet the fluorescence emission has been found to increase greatly when bound to membrane environments. [59] It follows that LPA bound DiA would exhibit similar increases in fluorescence.

2.3.2 Probe concentration and flow rate

Solutions of DiA with concentrations ranging from 3 to 20 μM were evaluated for LPA screening. The 10 μM DiA solution exhibited the best signal-to-noise (S/N) ratio, with a relatively low fluorescence background. The optimal reagent flow rate for post-column detection was found to be 0.62 mL min^{-1}. Higher flow rates resulted in relatively better signal to noise ratios, however, a trade-off was dilution of the sample. To best prepare a DiA solution in H_2O, we found that DiA should be pre-dissolved in a small amount of acetone (1% of H_2O volume).

2.3.3 Mobile phase composition, pH and effects of other additives

Common solvent mixtures (MeOH–H_2O, MeCN–H_2O) used for reversed-phase chromatography did not enable resolution of the targeted individual LPA subspecies. Subspecies separation was dependent on buffer pH and concentration. Of the buffer systems evaluated, phosphate afforded optimal separation and peak shapes. Optimal resolution was achieved using MeOH–50 mM phosphate buffer, pH 2.5 in a ratio 16/5. The parameters characterizing the chromatographic system for optimal separation of LPAs are reported in Table 2.1-2.3.

Table 2.1 Effect of column length on the resolution (R_s) and theoretical plates (N) for the separation of LPAs.[a]

	LPA 14:0		LPA 20:4		LPA 16:0		LPA 18:1		LPA 17:0		LPA 18:0
column length (mm)	N (RT, min)	R_s	N (RT, min)	R_s	N (RT, min)	R_s	N (RT, min)	R_s	N (RT, min)	R_s	N (RT, min)
100[b]	312 (4.44)	2.31	192 (5.56)	1.35	1715 (6.53)	NA	NA (7.89)	NA	2712 (8.71)	7.74	3001 (11.87)
50[c]	1280 (3.83)	4.40	1486 (4.72)	3.52	1917 (5.44)	4.30	1748 (6.61)	2.57	3416 (7.32)	10.04	4361 (10.50)

[a]LPA concentration: 80 μM; mobile phase: 4/1 MeOH/50 mM pH 3.0 phosphate buffer; injection volume: 5 μL.

[b]Discovery Bio wide pore (Supelco), C-8, 3 μm, 2.1 mm diameter. Flow rate: 0.20 mL/min.

[c]Luna (Phenomenex), C-8, 3 μm, 2.0 mm diameter. Flow rate: 0.27 mL/min.

Table 2.2 Effect of pH on the resolution (R_s) and theoretical plates (N) for the separation of LPAs.[a]

	LPA 14:0		LPA 20:4		LPA 16:0		LPA 18:1		LPA 17:0		LPA 18:0
pH	N (RT, min)	R_s	N (RT, min)	R_s	N (RT, min)	R_s	N (RT, min)	R_s	N (RT, min)	R_s	N (RT, min)
3.0	996 (3.01)	7.93	1302 (4.69)	3.14	1040 (5.59)	4.22	1860 (6.92)	1.65	397 (7.78)	5.66	2176 (11.12)
2.5	1331 (3.16)	9.71	2000 (4.85)	3.41	1862 (5.61)	4.82	1625 (6.99)	2.56	1630 (7.88)	7.57	1828 (11.21)

[a]LPA concentration is 5 μM; column: Luna C-8 50 × 2.0 mm; mobile phase: 7/2 MeOH/50 mM phosphate buffer; flowrate: 0.27 mL/min. Injection volume: 20 μL.

Table 2.3 Resolution (R_s) and theoretical plates (N) for the final optimal conditions. The column size is 50×2.0 mm.[a]

LPA 14:0		LPA 20:4		LPA 16:0		LPA 18:1		LPA 17:0		LPA 18:0
N (RT, min)	R_s	N (RT, min)	R_s	N (RT, min)	R_s	N (RT, min)	R_s	N (RT, min)	R_s	N (RT, min)
848 (3.96)	6.25	1149 (5.76)	3.75	2531 (6.84)	5.71	2105 (8.58)	2.65	1278 (9.72)	8.28	2635 (13.96)

[a]LPA concentration is 10 μM; mobile phase: 16/5 MeOH/50 mM phosphate buffer; flowrate: 0.32 mL/min. Injection volume: 20 μL.

2.3.4 Separation conditions

Of the reversed phase columns evaluated, the best results were obtained with a C-8 column with a particle size of 3 μm. A 100 × 2.1 mm column enabled separation of all LPAs but caused excessive back-pressure, and limited optimization of the composition/flow rate of mobile phase. A shorter 50 × 2 mm column enabled increased flow rate affording sharper peaks and significantly reduced analysis time (~ 15 min). The parameters characterizing the chromatographic system for optimal separation of LPAs are reported in Table 2.1–2.3. Minimizing the length of the tubing between the HPLC column and post-column mixing tee is also critical for maximizing peak-to-peak resolution and limits of detection.

2.3.5 Detection parameters

Determination of the optimum excitation and emission wavelengths for the HPLC fluorescence detection system were performed as follows. The 3-D scanning mode in a Waters 2475 fluorescence detector allowed us to establish the optimal excitation and emission wavelengths that resulted in the highest signals and best peak shapes based on the wavelength dependence of the excitation source and PMT detector employed by the Waters 2475 fluorescence detection system. The largest LPA induced fluorescence emission enhancement was observed to be near 570 nm when run in emission scanning mode with excitation at 470 nm chosen based upon the excitation spectra in Figure 2.2. The detector gain was set to 100. Subsequently, the acquisition was set to excitation scanning mode (330–530 nm) keeping the emission wavelength constant (570 nm)

allowing collection of an excitation spectrum. The peak excitation wavelength resulting in the greatest fluorescence enhancement was determined to be 450 nm. Consistent with Figure 2.2, the post-column fluorescence response to LPA was much greater than absorption. Fixed excitation and emission wavelengths of 450 and 570 nm, respectively were used in all analyses and presented in all subsequent chromatograms. Figure 2.3 shows a representative HPLC trace using the optimized conditions for the separation of LPA 14:0, 16:0, 17:0, 18:0, 18:1 and 20:4.

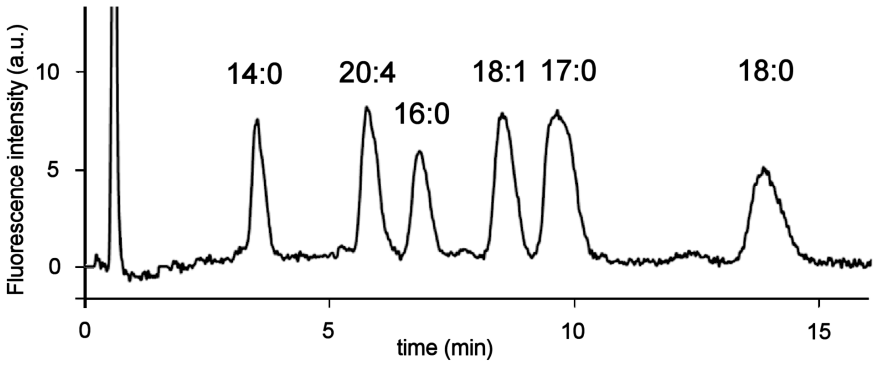

Figure 2.3 HPLC trace of a LPA mixture (10 μM LPA 14:0, 16:0, 18:0, 18:1, 20:4 and 20 μM LPA 17:0). Chromatographic conditions: column: Luna™ C8, 3 μm, 50 × 2.0 mm; mobile phase: MeOH: phosphate buffer (50 mM, pH 2.5) 16:5; flow rate: 0.32 mL/min; injection volume: 20 μL; sample concentration: 10 μM in MeOH: H_2O 9:1; post-column reagent: 10 μM DiA in H_2O; reagent flow rate: 0.62 mL/min; excitation/emission wavelengths: 450/570 nm.

2.3.6 Linearity and dynamic range

In order to determine the linear response of DiA to the presence of LPA, an initial evaluation using LPA (18:0) as a model compound was carried out using direct fluorescence spectrophotometry. Emission spectra were collected upon excitation at 470 nm. As shown in Figure 2.4, the plot of maximum fluorescence emission vs. concentration confirms a good linear relationship (R^2 = 0.994) between the fluorescence intensity and LPA (18:0) concentrations ranging from 1 to 16 μM.

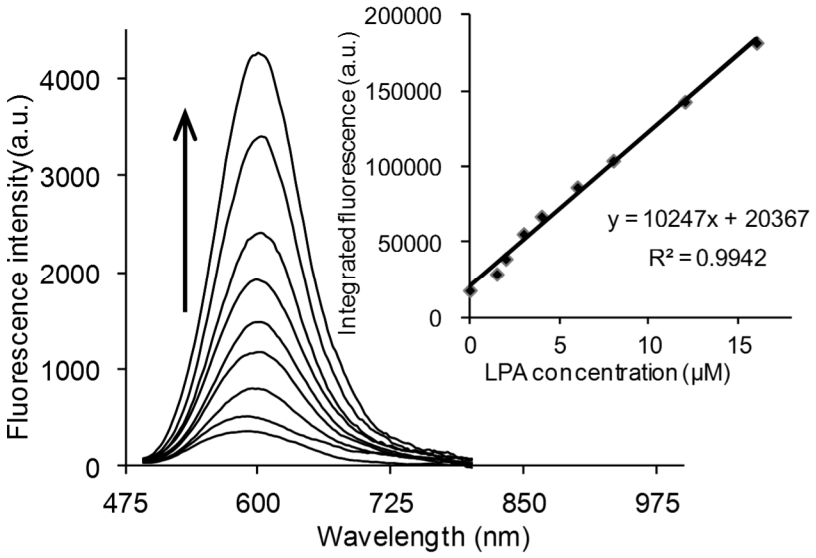

Figure 2.4 Emission spectra and calibration curve (inset) of 2.67 μM DiA upon titration with LPA (18:0).

Based on the above results, we anticipated that a similar linear response would be obtained for the individual LPAs after reversed phase HPLC separation. After

optimization of separation and detection conditions as described above, mixtures of LPAs with concentrations ranging from 0.5 – 40 μM were evaluated.

All LPAs showed a linear response in the 0.5 – 25 μM concentration range, although LPA 14:0, LPA 18:0 and LPA 18:1 exhibit linearity up to 40 μM. LPA (17:0), a non-natural LPA, was added to these mixtures as an internal standard for further quantification. Figure 2.5 shows calibration curves for the individual LPA species evaluated in this study. Acceptable correlation factors (R^2) were obtained for all LPA subspecies. The limit of detection (LOD) for each was determined as the amount of analyte that corresponds to three times the signal of the background noise. Data from calibration curves are shown in Table 2.4.

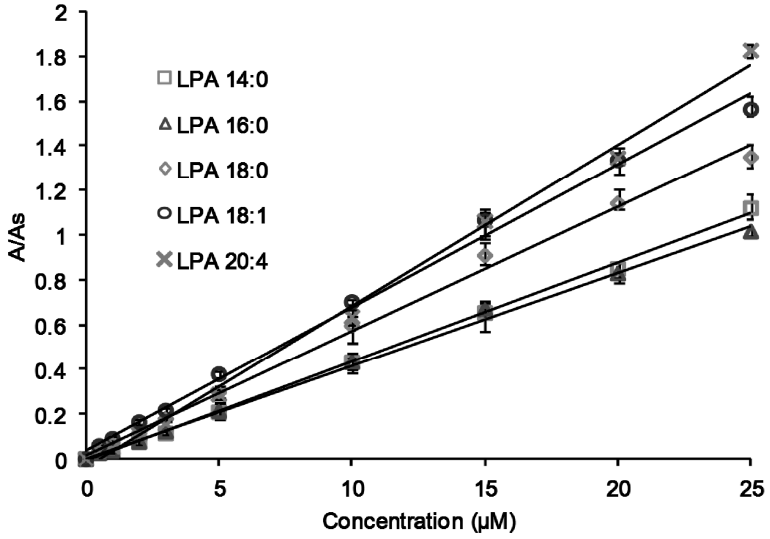

Figure 2.5 Calibration curves of specific LPA subspecies obtained by HPLC-post column fluorescence detection. The area ratio is the peak area of individual LPAs divided by the peak area of the internal standard (LPA 17:0). Data points represent the average of 4 runs.

Table 2.4 Data obtained from calibration curves for LPA species via the HPLC post-column method.

LPA species	Retention time (min)	Linear range (μM)	R^2	LOD (μM)
14:0	3.50	0-40	0.9962	0.147
20:4	5.56	0-25	0.9962	0.161
16:0	6.64	0-25	0.9963	0.173
18:1	8.35	0-40	0.9949	0.074
18:0	13.75	0-40	0.9943	0.272

2.3.7 Quantification of LPAs in human plasma

Biological concentrations of phospholipids in human plasma are higher than 3 mM. [33] Among the several classes of phospholipids that are present in human plasma, LPAs represent a relatively very small fraction, and reported concentrations of total LPA vary. A generally reported range is 1-5 μM.[34] This imposes a challenge for the selective isolation/enrichment of these analytes. Solid phase extraction (SPE) is a common method for the removal of potential interferences from biological samples and has been used for the isolation and enrichment of the different classes of phospholipids.[60-62] Typical SPE materials include normal phase (e.g. silica), reversed phase (C4, C8 or C18), ionic exchange and hybrid solid supports. The SPE enrichment procedure developed herein specifically for LPAs increases their concentration 5-fold. Several solid supports were initially evaluated in control mixtures containing LPA 14:0, 16:0, 17:0, 18:0, 18:1 and 20:4. Three different commercial reversed phase C8 SPE cartridges, including Waters (Sep-pak™ Plus C-8, 200 mg, 37-55 μm), Supelco (Discovery™ DSC-8, 3 mL, 500 mg, 50 μm) and Waters (OASIS™ HLB 3 mL, 60 mg, 30 μm) were evaluated. The OASIS™ HLB proved optimal in terms of LPA recoveries (93-103%). As part of the method development, a liquid-liquid extraction prior to the SPE procedure was used to aid in removing relatively abundant and potentially interfering phospholipids. Typical procedures for lysophospholipids reported in the literature involve acidification of plasma prior to a liquid-liquid extraction.[15, 63] In our hands, this procedure gave very low LPA recoveries. We determined that pH control was critical to achieve the selective removal of interferences. At physiological pH, LPAs are negatively charged.[51] Thus, performing the liquid-liquid extraction at pH 7.4 removes neutral phospholipids (e.g. LPC, LPS, etc.).

The best recoveries were obtained when samples were loaded onto the SPE cartridge at pH 2.0. Selective elution of LPAs from the SPE cartridges was achieved using MeOH. This removes relatively hydrophobic species (e.g. phosphatidic acids). Table 2.5 shows the recoveries obtained for LPA control samples. In general, the recoveries are in the 74-94% range. In addition, we evaluated the effect of other phospholipids that have been identified to be present in human plasma and can result in potential false positives for LPAs. It is known that phospholipids are prone to either chemical or enzymatic hydrolysis. Phosphatidic acids (PAs) can be hydrolyzed enzymatically during sample storage, producing the corresponding LPAs, resulting in false positive LPA readings. Due to the acidic conditions in which the LPA solid phase extraction is carried out, we performed control experiments to investigate PA hydrolysis consisting in submitting PA standards to the whole extraction procedure. The resulting chromatograms did not show any signal within 1 hour, hence, none of PA 14:0, 16:0, 18:0 or 18:1 are hydrolyzed under the conditions used for the SPE-based LPA enrichment reported herein. Phosphatidylcholines (PCs) represent the major components of biological membranes and are also prone to hydrolysis producing the corresponding LPCs or PAs. Evaluation of the hydrolysis of PC in the same fashion as with PA resulted in the absence of any hydrolysis product confirming that PC or its hydrolysis products do not interfere in our sample protocol.

Table 2.5 Recoveries of individual LPA species after SPE enrichment.

LPA species	Measured by HPLC- post column (n = 3)		Measured by LC- ESI/MS/MS (n =3)	
	Recovery (%)	σ (%)	Recovery (%)	σ (%)
14:0	93.5	4.8	93.7	2.9
20:4	73.8	4.3	76.6	1.2
16:0	94.2	5.4	95.7	4.6
18:1	76.9	4.9	77.6	1.7
17:0	85.1	3.8	85.0	4.6
18:0	76.9	4.4	73.1	2.4

An LC/MS full scan in both negative and positive modes was also used to determine the presence of non-LPA phospholipids in plasma to confirm the effectiveness of the new sample preparation extraction steps. A control mixture of 22 phospholipids was initially tested, and all lipids were detectable in negative and/or positive mode. Mass spectra are shown in Figure 2.6-2.9. A plasma extract was tested using the same method. Results were compared to the LIPID MAPS Structure Database (LMSD).[64] No potentially interfering lipids found in the database were detected in negative mode. Limited amounts of LPC 16:0 were detected in positive mode. To further determine the extent of the interference from LPC, an LC-ESI/MS/MS method was used to detect LPC subspecies. The concentration was estimated to be 0.06, 0.01 and 0.05 μM for LPC 16:0, LPC 18:0 and LPC 18:1 respectively. These concentrations represent less than 0.1 % of the total LPCs in human plasma,[35, 65] thus LPC interference is not significant in our method.

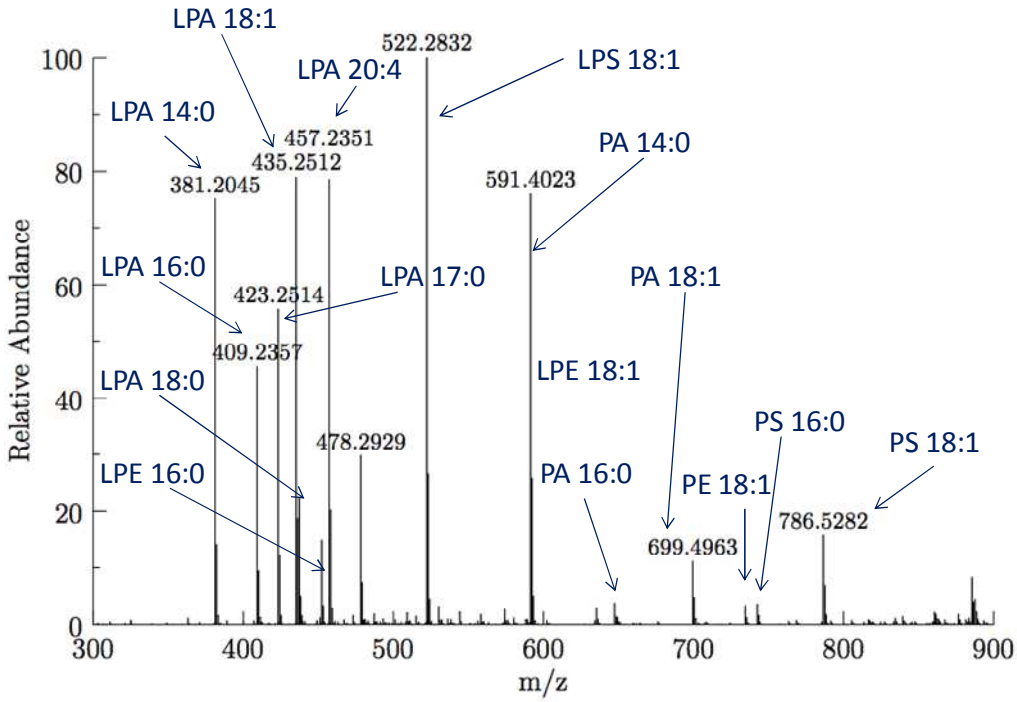

Figure 2.6 Mass spectra of phospholipids mixture in negative mode

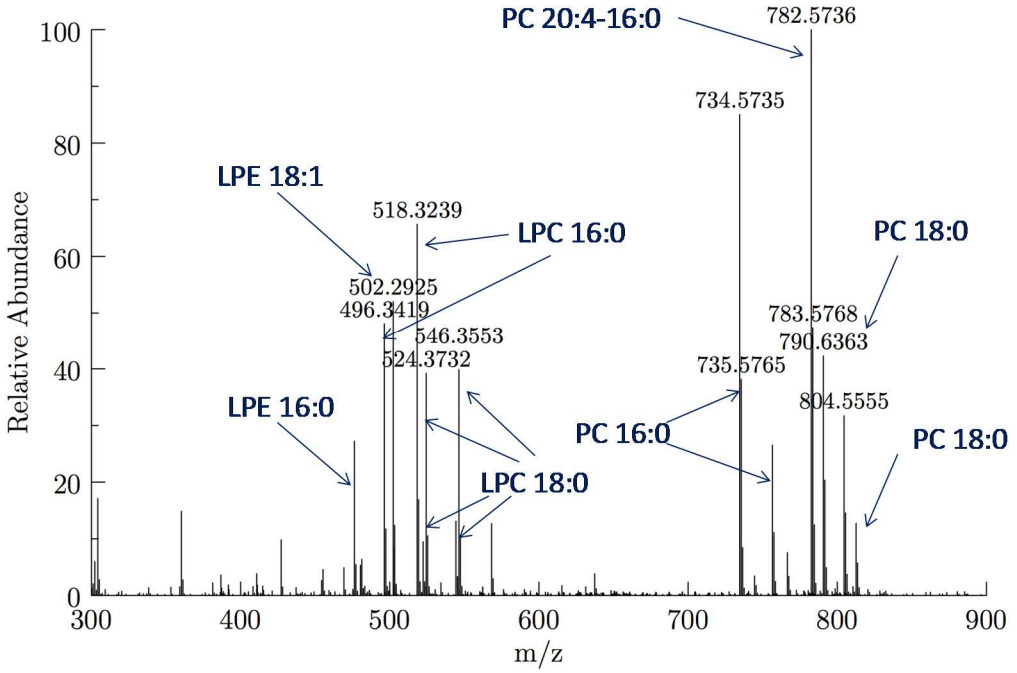

Figure 2.7 Mass spectra of phospholipids mixture in positive mode

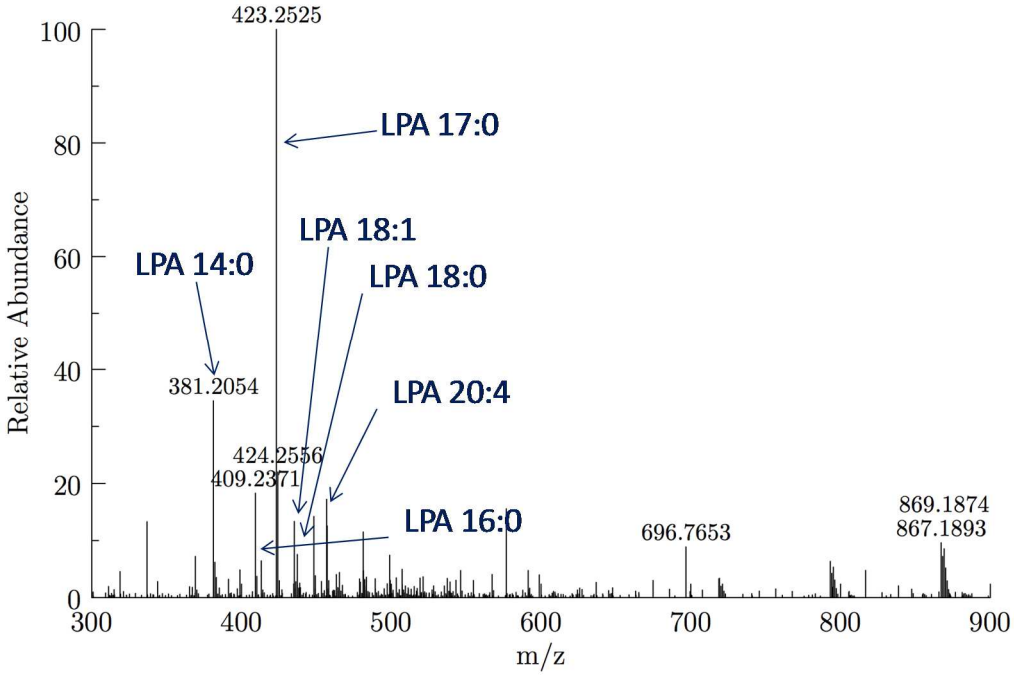

Figure 2.8 Mass spectra of plasma extract in negative mode

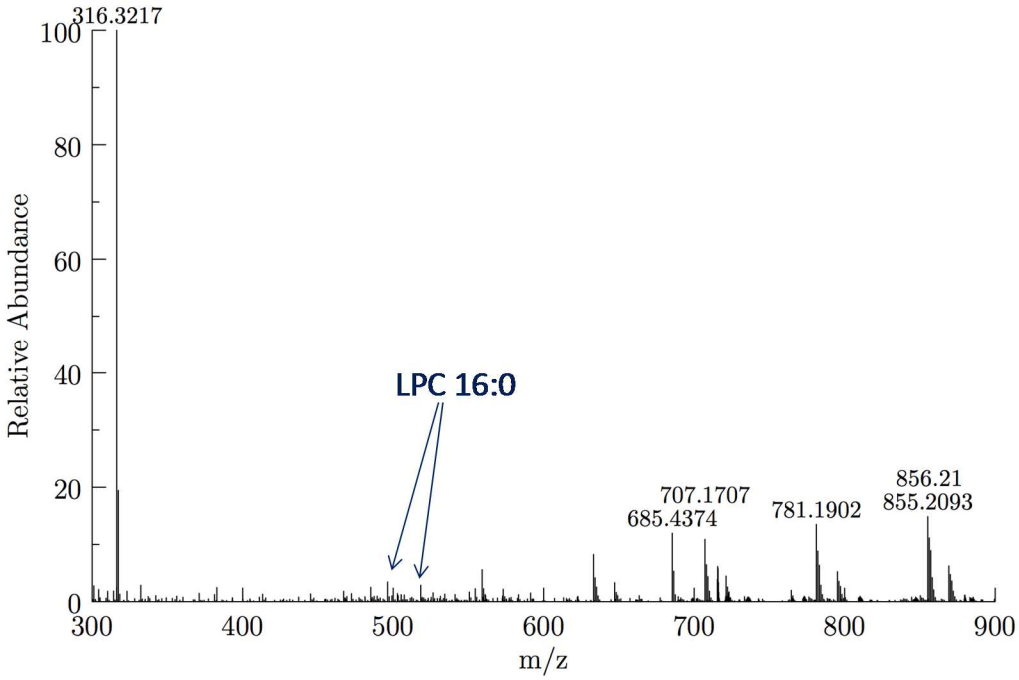

Figure 2.9 Mass spectra of plasma extract in positive mode

2.3.8 Method validation via LC-ESI/MS/MS

Mixtures of LPAs with concentrations ranging from 0.5 – 40 μM were evaluated using the LC-ESI/MS/MS method. We found a linear response for all the LPAs throughout this range. To compare to the new HPLC post-column method, we selected a working concentration range of 0.5 – 25 μM. LPA (17:0) was also used as an internal standard. Figure 2.10 shows calibration curves for the individual LPA species evaluated with the LC-ESI/MS/MS method. Acceptable correlation factors (R^2) were obtained for all the LPAs (Table 2.5). The limit of detection (LOD) for each LPA species was determined as the amount of analyte that corresponds to three times the signal of the background noise.

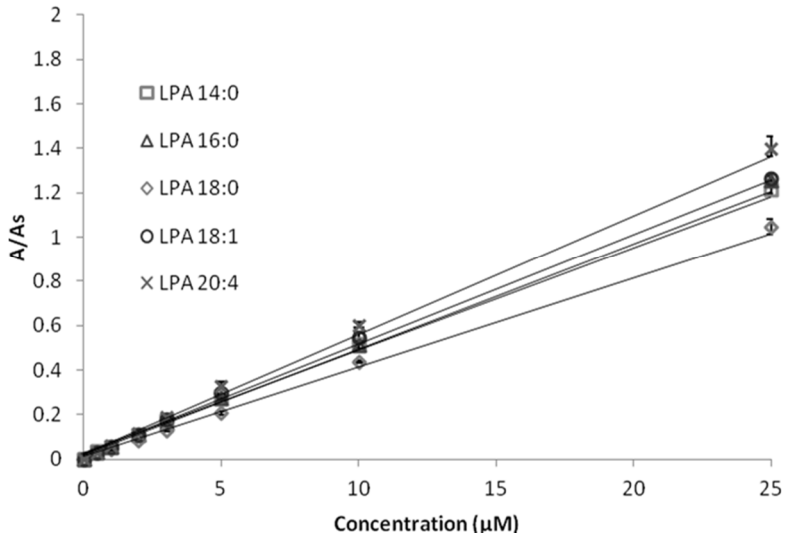

Figure 2.10 Calibration curves of LPAs using the LC-ESI/MS/MS method. The area ratio is the peak area of individual LPAs divided by the peak area of the internal standard (LPA 17:0).

Table 2.6 Statistical values obtained for the individual LPA species in the LC-ESI/MS/MS method (n = 3).

LPA species	Retention time (min)	Linear range (μM)	R^2	LOD (μM)
14:0	6.30	0-40	0.9991	0.0067
20:4	7.55	0-40	0.9990	0.0099
16:0	8.29	0-40	0.9998	0.0123
18:1	9.10	0-40	0.9993	0.0066
18:0	11.22	0-40	0.9991	0.0156

Native LPA concentrations were determined in blind human plasma samples from five different donors using both the MS and the optical methods. In addition, to further evaluate other potential matrix interferences, these plasma samples were also spiked with 0.5 μM of each LPA species. Data from the samples collected from all five donors is presented in Table 2.7-2.11. In each experiment, 800 μL of human plasma was used. All samples were prepared and analyzed in triplicate. Result shows that LPAs concentrations determined by the LC-ESI/MS/MS and HPLC optical post-column techniques are in close agreement. Experimental recoveries were mostly higher in the HPLC-post column method. Representative HPLC traces are shown in Figure 2.11 and Figure 2.12.

Table 2.7 Results for LPA analysis in human plasma (donor A) using the HPLC post-column fluorescence and LC-ESI/MS/MS methods.

	non-spiked (μM) average, σ		spiked with 0.5 μM LPA (μM) average, σ		Recovery (%)	
	HPLC post-column	LC-ESI/MS/MS	HPLC post-column	LC-ESI/MS/MS	HPLC post-column	LC-ESI/MS/MS
LPA 14:0	0.90 (0.01)	0.92 (0.01)	1.31 (0.09)	1.33 (0.05)	82	82
LPA 20:4	0.63 (0.02)	0.64 (0.03)	1.09 (0.05)	1.06 (0.03)	94	84
LPA 16:0	0.76 (0.03)	0.74 (0.01)	1.19 (0.09)	1.19 (0.01)	86	90
LPA 18:1	0.68 (0.01)	0.65 (0.02)	1.18 (0.01)	1.10 (0.03)	98	90
LPA 18:0	0.56 (0.02)	0.60 (0.01)	1.06 (0.03)	1.05 (0.01)	100	88
Total LPA	3.5 3(0.03)	3.56 (0.02)	5.83 (0.22)	5.73 (0.11)	92	87

Table 2.8 Results for LPA analysis in human plasma (donor B) using the HPLC post-column fluorescence and LC-ESI/MS/MS methods.

	non-spiked (μM) average, σ		spiked with 0.5 μM LPA (μM) average, σ		Recovery (%)	
	HPLC post-column	LC-ESI/MS/MS	HPLC post-column	LC-ESI/MS/MS	HPLC post-column	LC-ESI/MS/MS
LPA 14:0	0.97(0.03)	1.03(0.01)	1.43(0.04)	1.45(0.03)	94	82
LPA 20:4	0.98(0.01)	0.94(0.01)	1.41(0.02)	1.43(0.01)	86	100
LPA 16:0	0.96(0.02)	1.04(0.02)	1.45(0.03)	1.60(0.03)	98	112
LPA 18:1	1.05(0.00)	1.03(0.02)	1.47(0.02)	1.55(0.02)	84	102
LPA 18:0	0.99(0.01)	0.93(0.01)	1.56(0.04)	1.47(0.01)	114	110
Total LPA	4.96(0.04)	4.97(0.04)	7.33(0.01)	7.50(0.08)	95	101

Table 2.9 Results for LPA analysis in human plasma (donor C) using the HPLC post-column fluorescence and LC-ESI/MS/MS methods.

	non-spiked (μM) average, σ		spiked with 0.5 μM LPA (μM) average, σ		Recovery (%)	
	HPLC post-column	LC-ESI/MS/MS	HPLC post-column	LC-ESI/MS/MS	HPLC post-column	LC-ESI/MS/MS
LPA 14:0	0.76(0.01)	0.68(0.02)	1.25(0.02)	1.21(0.04)	98	106
LPA 20:4	0.21(0.02)	0.27(0.02)	0.64(0.01)	0.67(0.05)	84	80
LPA 16:0	0.55(0.01)	0.42(0.04)	1.05(0.05)	0.97(0.04)	100	112
LPA 18:1	0.37(0.01)	0.32(0.01)	0.96(0.05)	0.79(0.06)	120	96
LPA 18:0	0.29(0.03)	0.23(0.01)	0.79(0.01)	0.79(0.02)	102	112
Total LPA	2.18(0.02)	1.91(0.09)	4.69(0.08)	4.44(0.12)	100	101

Table 2.10 Results for LPA analysis in human plasma (donor D) using the HPLC post-column fluorescence and LC-ESI/MS/MS methods.

	non-spiked (μM) average, σ		spiked with 0.5 μM LPA (μM) average, σ		Recovery (%)	
	HPLC post-column	LC-ESI/MS/MS	HPLC post-column	LC-ESI/MS/MS	HPLC post-column	LC-ESI/MS/MS
LPA 14:0	0.24(0.00)	0.23(0.01)	0.65(0.02)	0.68(0.02)	82	92
LPA 20:4	0.26(0.01)	0.28(0.01)	0.67(0.01)	0.65(0.04)	82	74
LPA 16:0	0.45(0.03)	0.43(0.01)	0.88(0.02)	0.83(0.04)	88	80
LPA 18:1	0.30(0.02)	0.38(0.01)	0.87(0.02)	0.85(0.03)	114	94
LPA 18:0	0.33(0.02)	0.31(0.00)	0.85(0.02)	0.82(0.01)	104	102
Total LPA	1.57(0.03)	1.63(0.03)	3.91(0.03)	3.83(0.12)	94	88

Table 2.11 Results for LPA analysis in human plasma (donor E) using the HPLC post-column fluorescence and LC-ESI/MS/MS methods.

	non-spiked (μM) average, σ		spiked with 0.5 μM LPA (μM) average, σ		Recovery (%)	
	HPLC post-column	LC-ESI/MS/MS	HPLC post-column	LC-ESI/MS/MS	HPLC post-column	LC-ESI/MS/MS
LPA 14:0	0.17(0.00)	0.18(0.01)	0.61(0.02)	0.60(0.00)	86	84
LPA 20:4	0.20(0.02)	0.23(0.01)	0.75(0.01)	0.77(0.01)	110	110
LPA 16:0	0.29(0.00)	0.28(0.02)	0.71(0.00)	0.76(0.01)	84	96
LPA 18:1	0.53(0.01)	0.47(0.02)	0.97(0.02)	1.03(0.00)	90	112
LPA 18:0	0.33(0.00)	0.30(0.01)	0.84(0.01)	0.89(0.00)	102	118
Total LPA	1.52(0.02)	1.45(0.05)	3.88(0.04)	4.06(0.01)	94	104

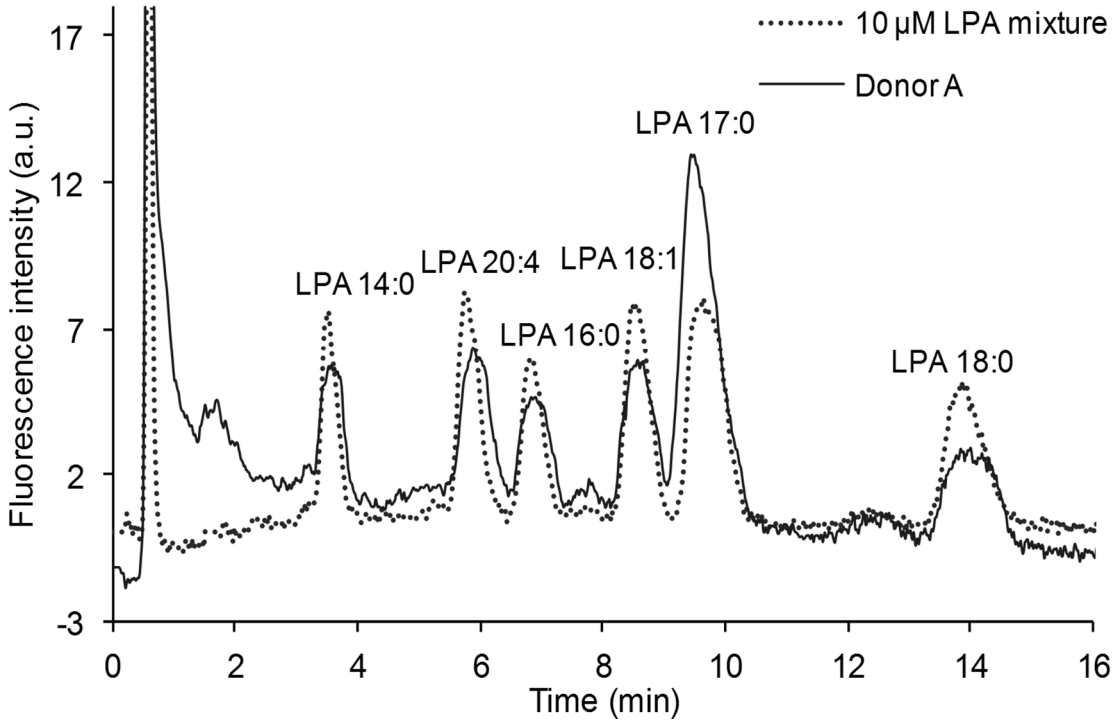

Figure 2.11 Chromatograms of a mixture containing 10 µM of each LPA species and LPAs isolated from human plasma (donor A) using the post-column detection method.

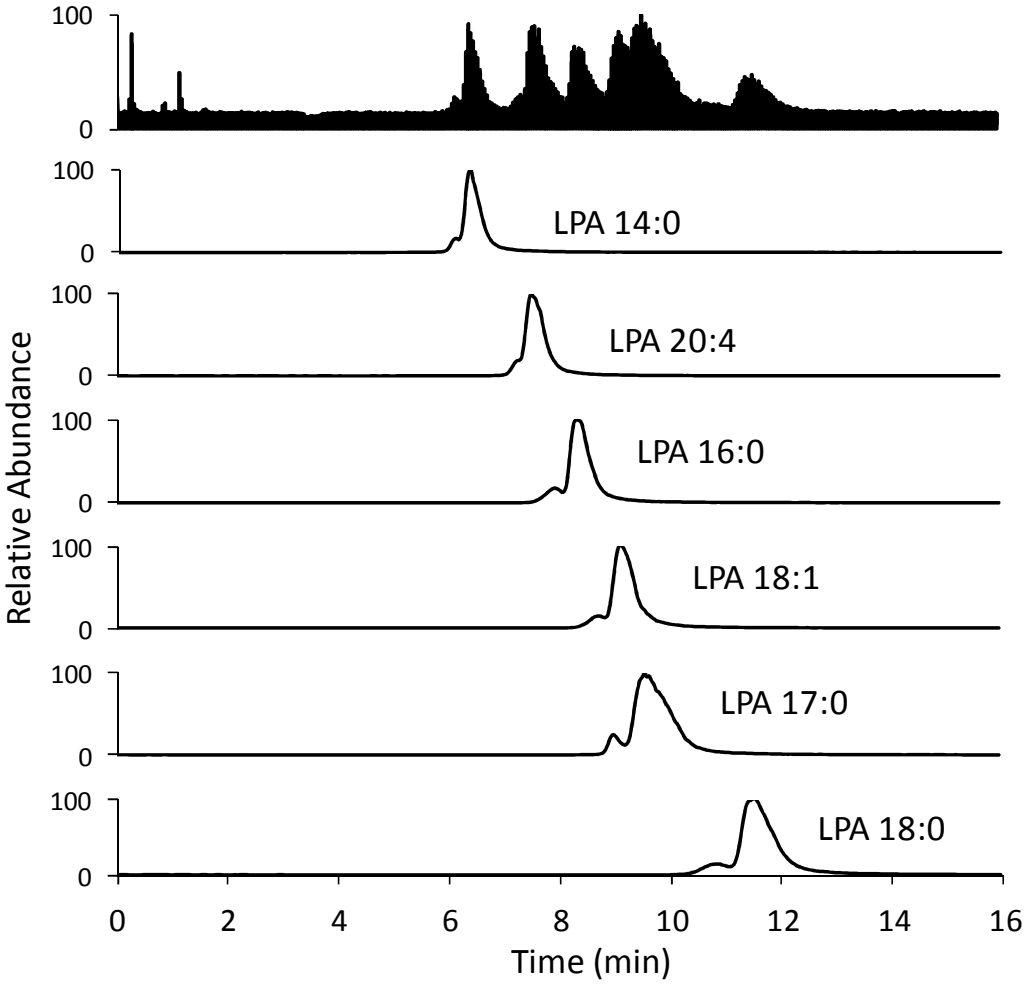

Figure 2.12 LC-ESI/MS/MS traces of a 10 μM standard mixture of LPAs. Column: Luna™ C8 (50 × 2 mm, 3 μm) at 40 ºC. Injection volume: 10 μL. Mobile phase: 9:1 MeOH:aqueous HCOOH (pH 2.5) at a flow rate of 0.4 mL/min. Parent and daughter ions were detected in the negative ion mode, sprayer voltage; 3.0 kV, capillary temperature at 300 ºC.

2.4 Conclusion

The optimized method for isolation and enrichment of LPA subspecies over other related phospholipids developed herein affords the five major LPAs (LPA 14:0, 16:0, 18:0, 18:1 and 20:4) with essentially no other potentially interfering phospholipids. Using this enriched mixture during analysis can eliminate matrix related errors caused by the

presence of other phospholipids which can potentially generate LPAs upon hydrolysis. The HPLC separation of the individual LPA subspecies reported herein is relatively rapid (15 min), and non-destructive optical detection simplifies the selection of detection instrumentation. Optical detection was validated using ESI/MS/MS detection, for which the optimized sample enrichment procedure reduced or completely eliminated ionization suppression effects that have been reported to complicate the measurement.

Chapter 3 Clinical study of LPA levels in ovarian cancer patients

3.1 Introduction

Xu et al. [66] first reported that LPA levels were elevated in ovarian cancer patients and LPA may be a biomarker of ovarian cancer, especially for early stages. Many other groups have reported clinical studies supporting LPA as a diagnostic biomarker of ovarian cancer. [17, 67] For example, Sedlakova et al. [19, 68] found that LPA levels in ovarian cancer patients plasma were elevated by ~140% thus LPA could be useful as diagnostic marker for ovarian cancer.

However, Baker et al. [20] found that neither individual LPA species nor total LPA levels in plasma of ovarian cancer patients was significantly different than a healthy control group. More recently, Lu et al. [69] studied more than 600 patients including healthy women and those with ovarian cancer. The results showed that measurement of total LPA levels in serum was highly accurate and sensitive towards the diagnosis of ovarian cancer. Even among studies that showed plasma LPA levels were elevated in ovarian cancer patients, the total LPA concentrations reported varied widely, from 2.57 to 43.2 μM for ovarian cancer patients. [17, 19, 34, 66] To help understand this controversial issue, we performed a clinical study of LPA levels in ovarian cancer patients using the method developed by our group, which is described in Chapter 2, in collaboration with Women and Infants Hospital of Brown University Medical School in Rhode Island.

3.2 Experimental

A total of 183 patient plasma and serum blind samples, including both healthy and ovarian cancer patients, were collected at the Women and Infants Hospital of Brown University Medical School in Rhode Island. Five subspecies of LPA including LPA 14:0, LPA 16:0, LPA 18:0, LPA 18:1 and LPA 20:4 were extracted, enriched with a liquid-liquid extraction followed by a solid phase extraction method as described in Chapter 2. The concentrations of each LPA subspecies were determined with the HPLC post-column fluorescence detection method we developed. [70]

3.3 Results and discussion

Plasma LPA levels in all patients ranges (n = 183): LPA 14:0 (0.109-2.609 μmol/L), LPA 20:4 (0-1.953 μmol/L), LPA 16:0 (0.229-9.497 μmol/L), LPA 18:1 (0-0.632 μmol/L), LPA 18:0 (0-2.466 μmol/L), total LPA (0.519- 13.925 μmol/L). Serum LPA levels in all patients ranges (n = 183): LPA 14:0 (0-2.649 μmol/L), LPA 20:4 (0-3.156 μmol/L), LPA 16:0 (0-11.853 μmol/L), LPA 18:1 (0- 0.729 μmol/L), LPA 18:0 (0-2.543 μmol/L), total LPA (0-15.109 μmol/L).

We noticed most of the plasma and serum samples are yellow and white. However, some samples showed different colors, such as orange and red. These colors might be from the residual red blood cells from sample processing.

All samples were quantified in 3 runs or 2 runs depending on the sample volume.

Plasma and serum concentrations of LPA species and total LPA of all patients are shown in Figure 3.1-3.6. Statistical analysis of the data for determination of the relevance of LPAs as an ovarian cancer biomarker is currently underway by collaborators.

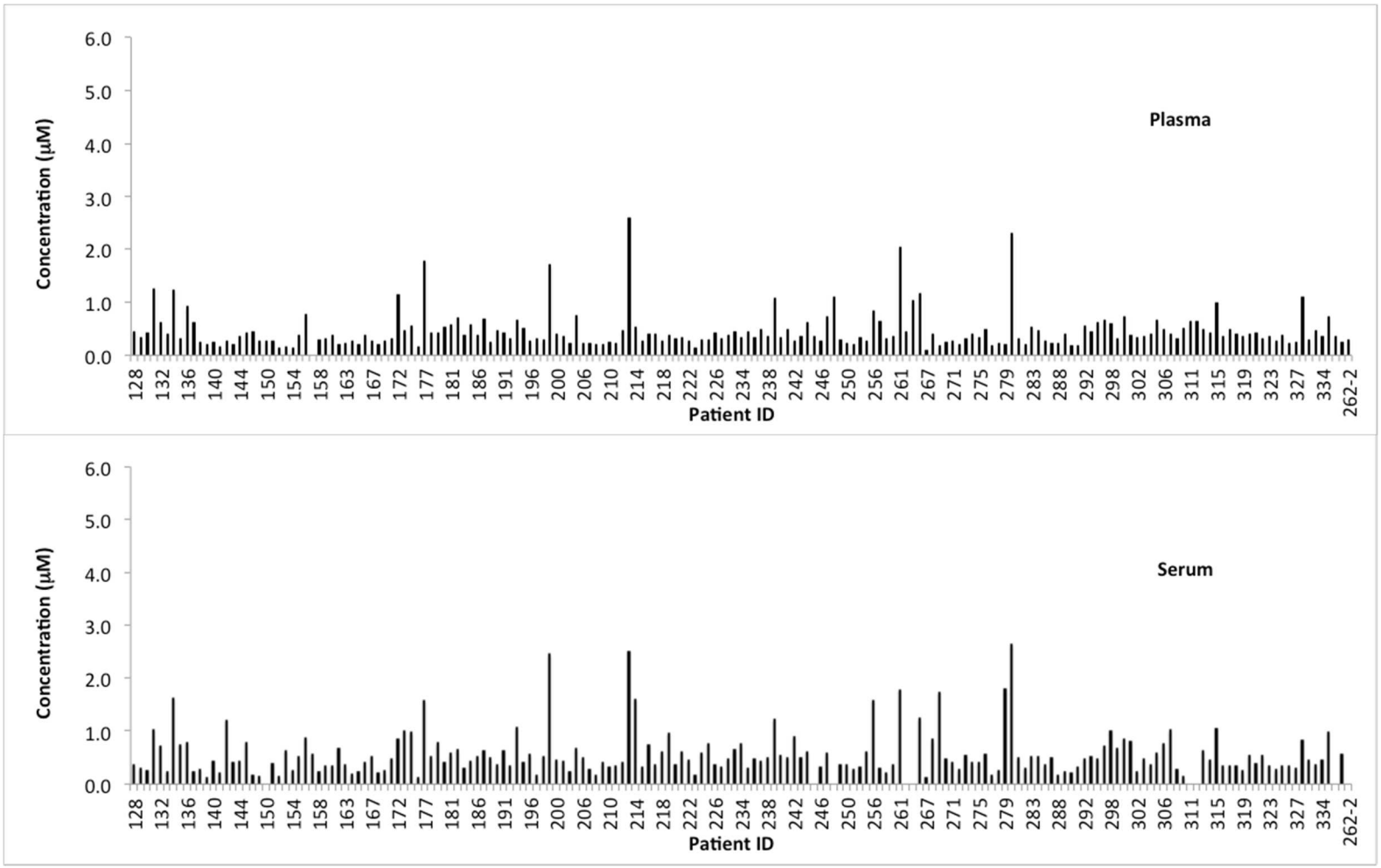

Figure 3.1 LPA 14:0 concentrations in plasma and serum samples of 183 patients.

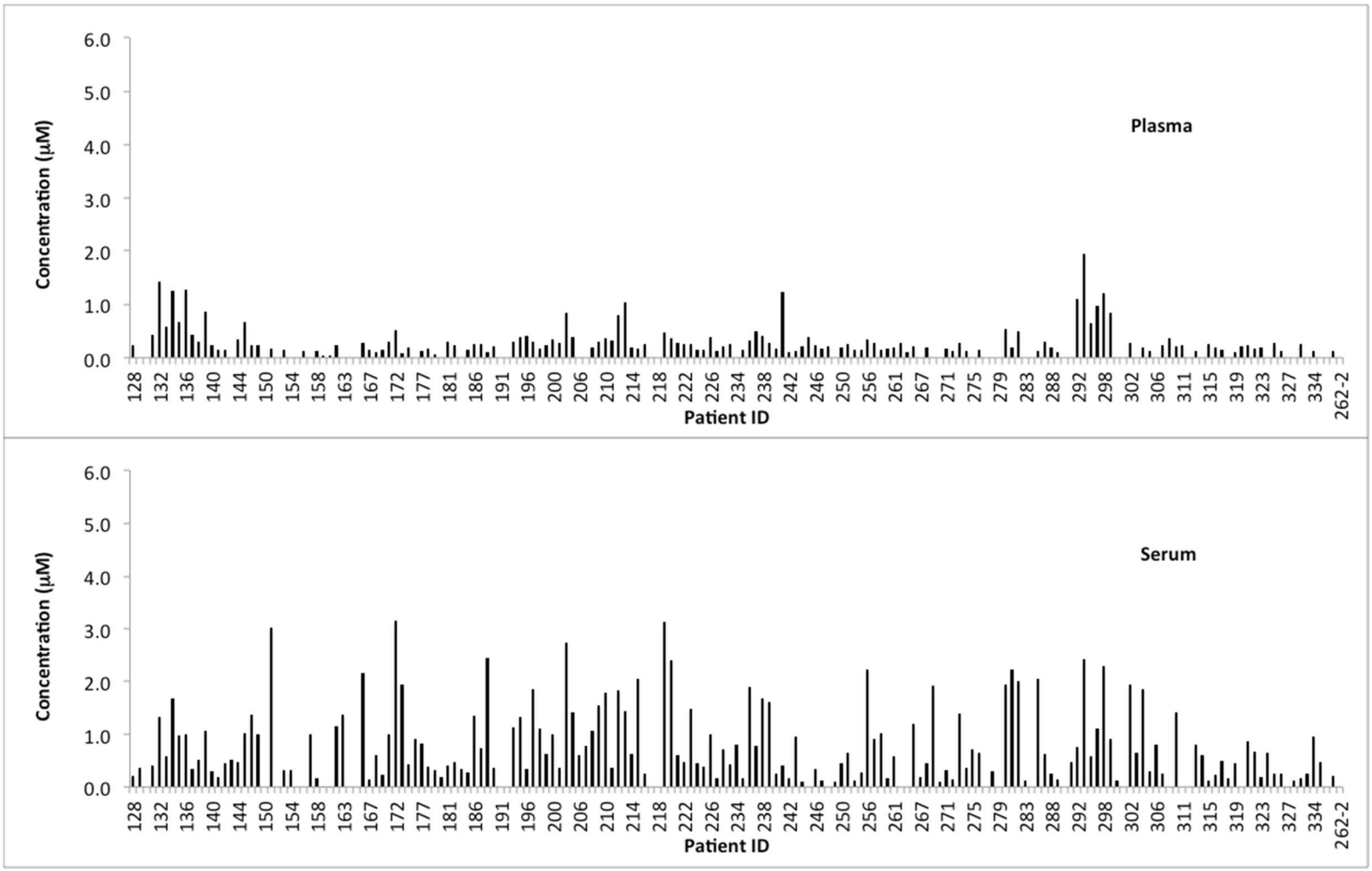

Figure 3.2 LPA 20:4 concentrations in plasma and serum samples of 183 patients.

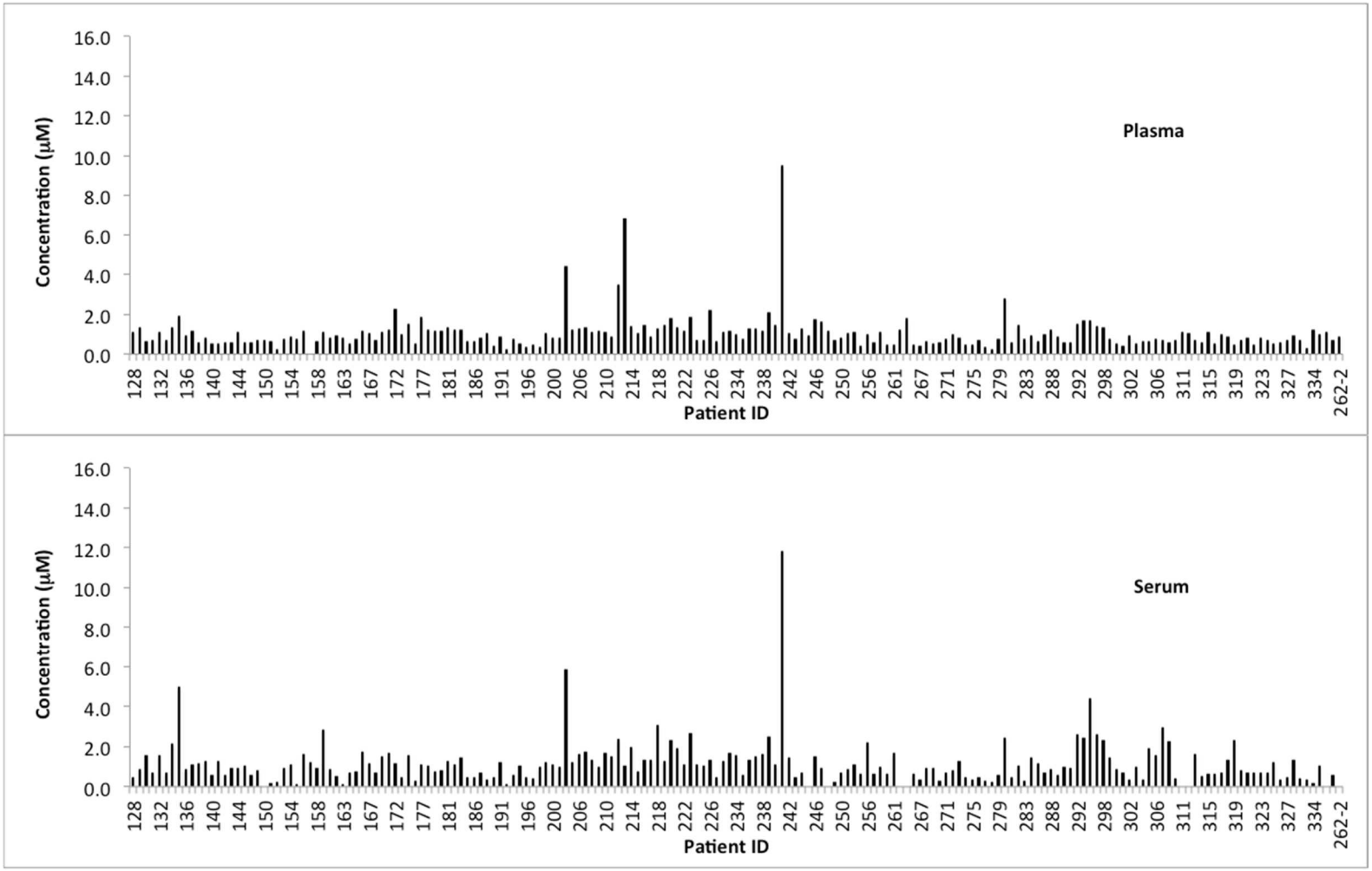

Figure 3.3 LPA 16:0 concentrations in plasma and serum samples of 183 patients.

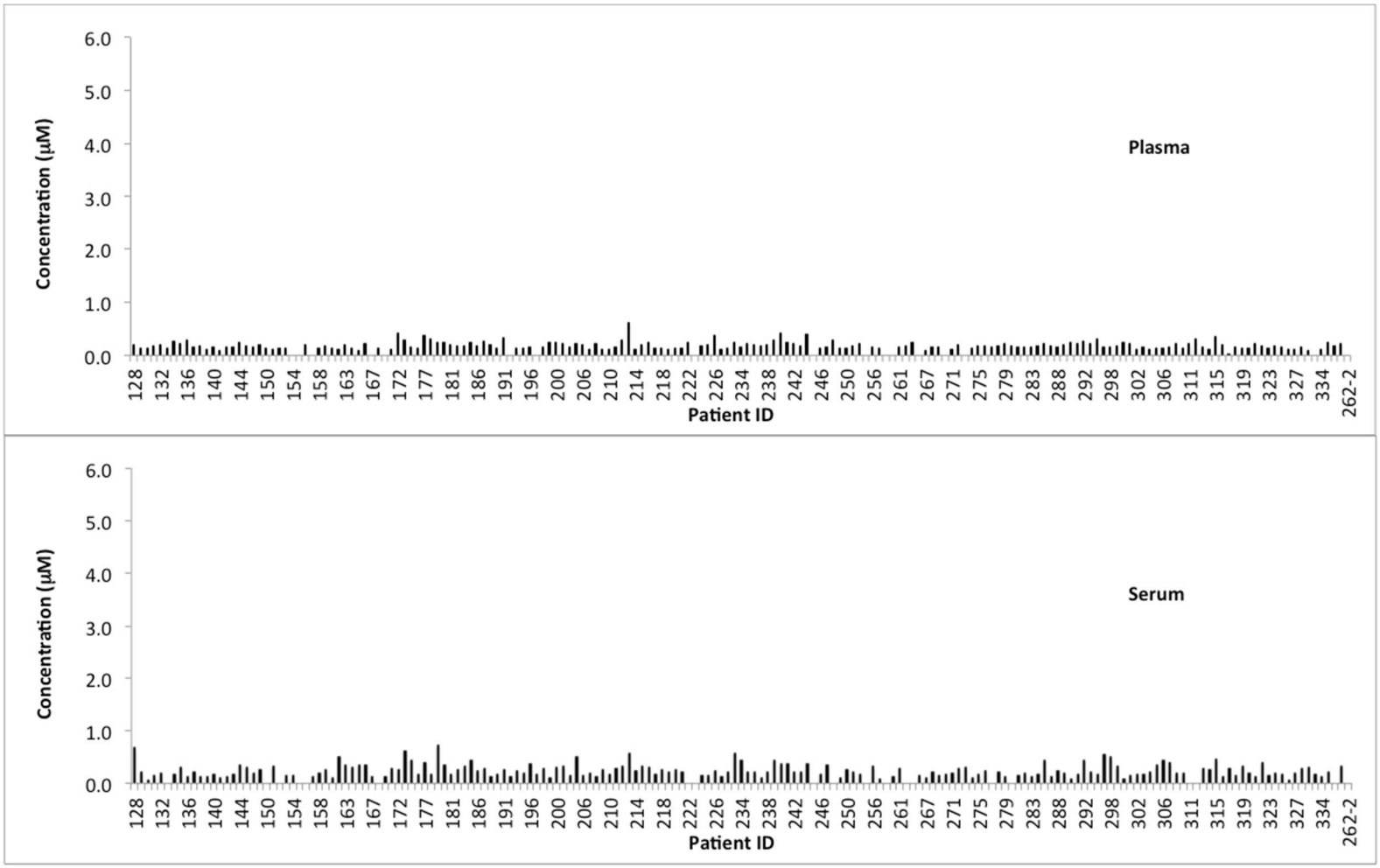

Figure 3.4 LPA 18:1 concentrations in plasma and serum samples of 183 patients.

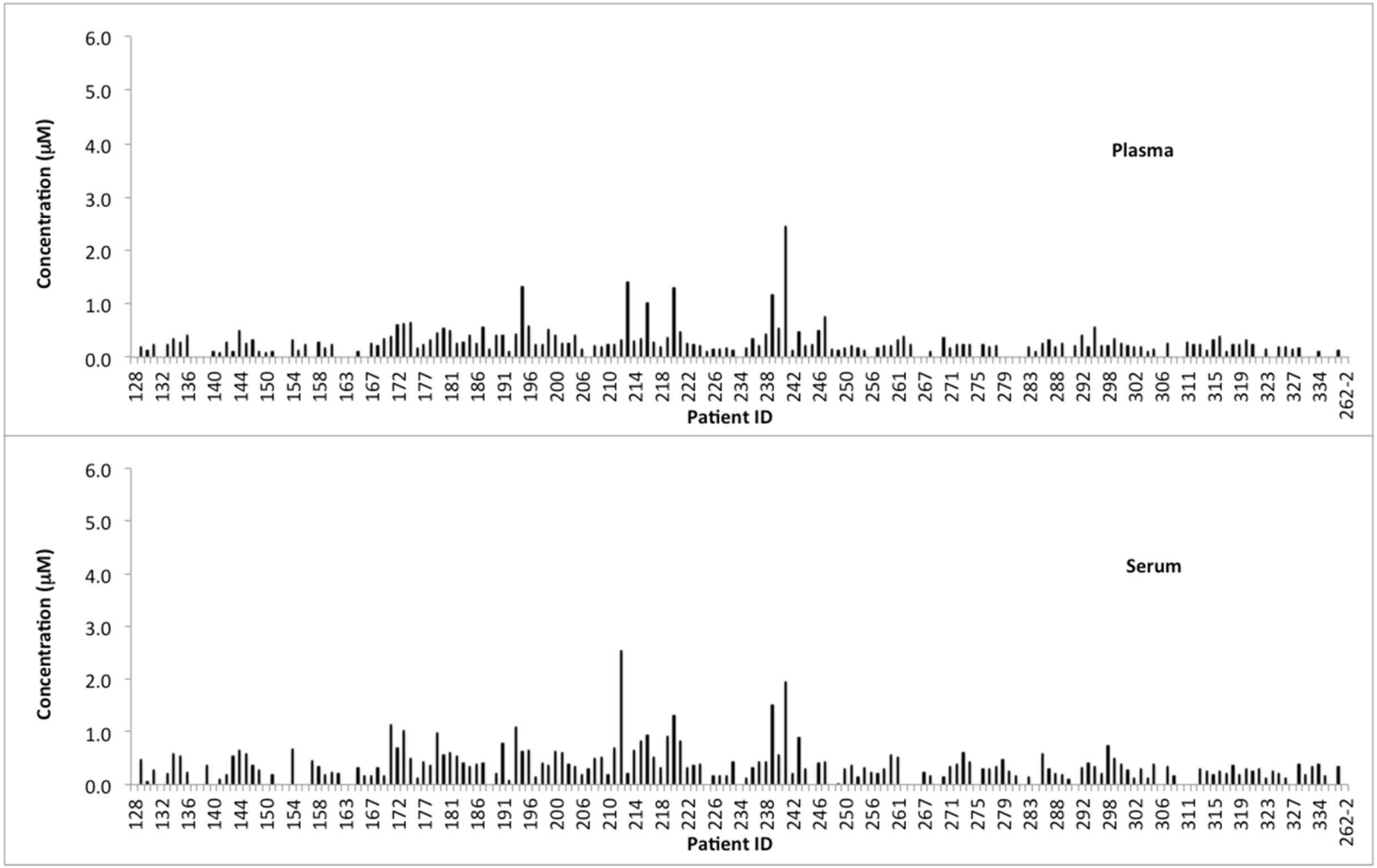

Figure 3.5 LPA 18:0 concentrations in plasma and serum samples of 183 patients.

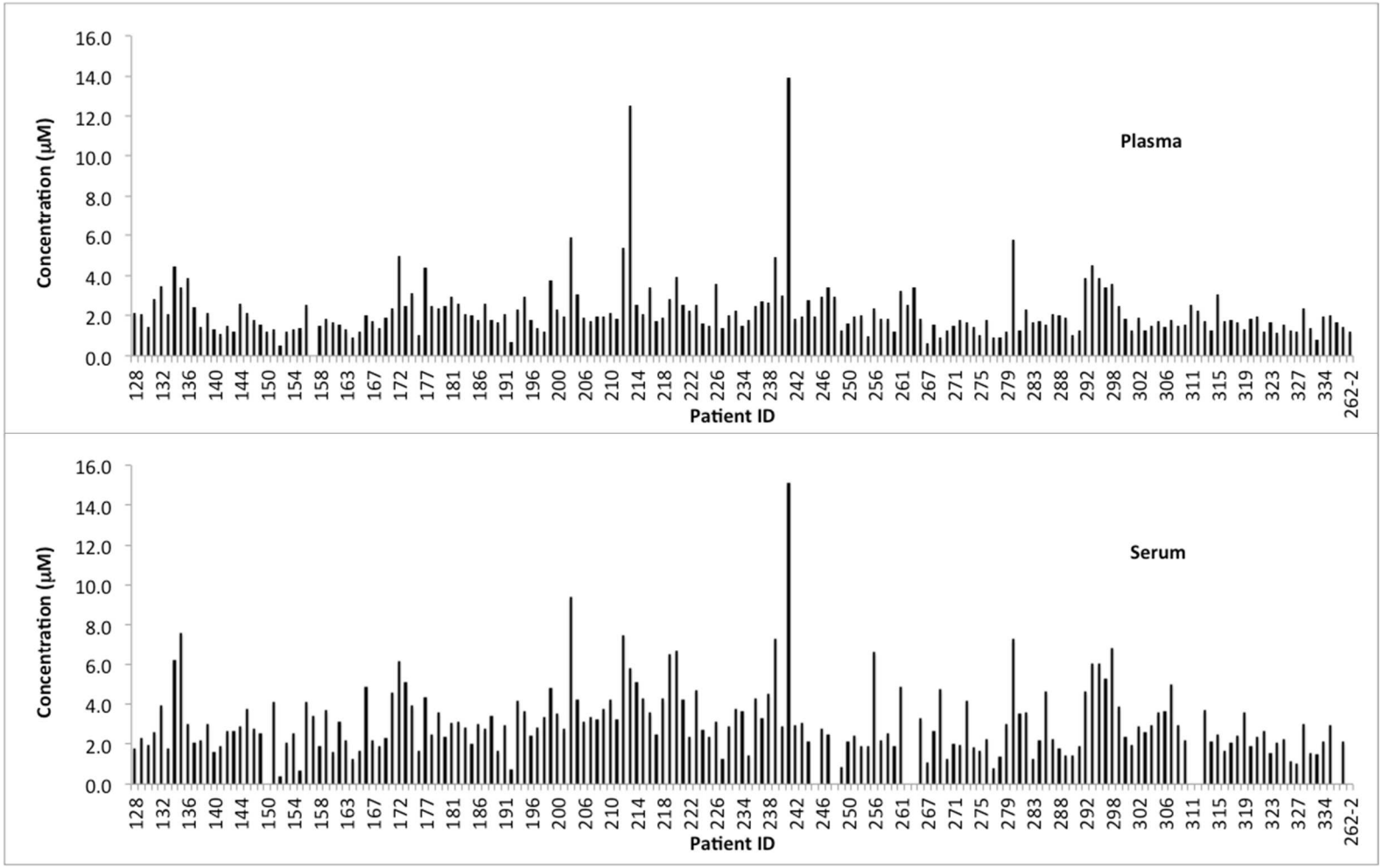

Figure 3.6 Total LPA concentrations in plasma and serum samples of 183 patients.

Chapter 4 Molecular imprinted polymer synthesis and evaluation

4.1 Introduction

A wide variety of methods for LPA sample preparation have been developed. Liquid-liquid extraction (LLE) is the most common methodology for LPA enrichment from biological samples. The LLE method developed by Bligh and Dyer [50] has been modified and used in many studies. These modified methods that require one or two steps are easy and fast. [3, 71, 42, 49] However, they can also be less than ideal because abundant potential interferences, such as lysophosphotidyl choline (LPC), can be co-extracted with LPA and affect LPA quantifications.

For example, Zhao et al. found that lysophosphatidylcholine (LPC) and lysophosphatidylserine (LPS) artificially generate LPA signals in electrospray ionization tandem mass spectrometry (ESI-MS/MS) at the ion source via loss of the head group. [72] This fact may highly effect the quantification, since the biological concentration of total LPC is about 300 μM, which is two orders of magnitude higher than LPA (< 5 μM) in healthy people. [67, 73] Meanwhile, phospholipids such as glycerophosphocholines and lysophosphatidylcholines, can cause matrix effects that suppress or enhance MS ionization and also shift HPLC retention times and elevate baselines. [44, 46, 74] These factors can hamper the accuracy and reproducibility of the quantification of LPA in LC-MS. Other quantification methods besides LC-MS may also be affected by the presence of interfering phospholipids in LPA samples because of the structural similarities between LPA and other phospholipids. For example, phosphatidic acid (PA) has the same head group as LPA; lysophosphatidylethanolamine (LPE), lysophosphatidylserine (LPS)

and LPC all have the same or similar length of alkyl chains as LPA. Thus, if the detection is based on phosphate group binding or deaggregation of a binding group induced by the alkyl chain of LPA, the phospholipids that co-extract with LPA would interfere. Thus, removal of interferences is critical for an accurate quantification of LPA.

Our group has reported a method for LPA extraction and enrichment by using LLE followed by a solid phase extraction (SPE) [70]. With that method, LPA could be extracted with a high recovery and purity level. To improve the efficiency of the sample preparation and reduce the labor intensity and operational difficulties caused by LLE, we eliminated the LLE step by using a synthetic MIP as the stationary phase in SPE. Compared to LLE, SPE has advantages including high recoveries without partition issues, and it is less labor intensive and time consuming, and is potentially automatable.

Molecularly imprinted polymers (MIPs) are highly cross-linked polymers that can be used as artificial receptors for specific molecules. [75-77] MIPs have been mostly used in chromatography [78-80], electrophoresis [81, 82], solid phase extraction [83], chemical sensing [84-88] and catalysis [89 90]. New applications of MIPs also include drug delivery [91 92 93 94], crystallization [95-98], synthetic antibodies [99, 100] and cell culturing [101-103]. To synthesize MIPs, the template and functional monomers are bound covalently or non-covalently before copolymerized with the presence of a high concentration of crosslinking monomers. After the removal of the template, a polymer with cavities and binding sites is formed and can be used to bind target molecules selectively. MIPs have many advantages as a material for the extraction of specific compounds. MIPs can be customized and modified simply by varying the selection and composition of the functional and

crosslinking monomers. Functional monomers may not only be selected from the ones that are commercially available [104], but also designed and synthesized for target compounds, which allows the possibility of MIP being highly selective. The synthesis is also relatively easy and inexpensive.

Compared to using only commercially available functional monomers such as methacrylic acid (MAA), multifunctional monomers that contain more than one functional group can bind with a higher affinity to the template molecule and with reduced nonspecific binding to other molecules. [87 105 106]

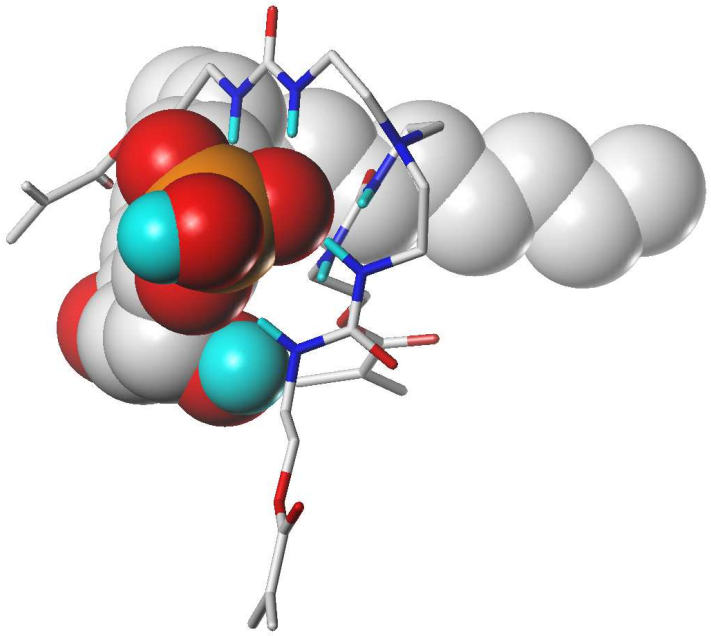

Figure 4.1 Energy-minimized model of the complex of a tris-urea scaffold and LPA 18:1.

MIPs with urea moieties as receptors for the phosphate group have been designed and synthesized. The N-H groups of urea can bind to phosphates via hydrogen bonding

and electrostatic interactions. [107] [108] [109] However, no prior studies have been reported involving specific LPA analysis. Figure 4.1 shows an energy-minimized model of a 1:1 complex of a tris-urea scaffold and LPA using molecular mechanics and Gasteiger-Hückel charges.

In this study, we synthesized an MIP that could be used as the stationary phase in an SPE cartridge. The functional monomer selected and synthesized was multifunctional, containing three urea groups. Because of the selectivity of this MIP, interfering phospholipids could be removed from LPA-containing samples. The elimination of the LLE step not only improved recoveries of LPA, but also simplified and shortened the protocol.

4.2 Experimental

4.2.1 Instruments and materials

NMR spectra were recorded on ARX-400 Advance Bruker spectrometer. FTIR spectra were obtained on a ThermoFisher Nicolet iS10 infrared spectrometer (Thermo Scientific, Madison, WI) in reflection geometry using a single bounce diamond attenuated total reflectance (ATR) accessory. LPA were separated on a Luna^{TM} C-8 (50 × 2 mm, 3 μm) column connected to a guard cartridge with 2.0 to 3.0 mm internal diameters (Phenomenex) in an Accela UPLC system (Thermo Fisher, San Jose, CA). MS data were collected via an LTQ-Orbitrap XL Discovery instrument (San Jose, CA, USA), equipped with an ESI ion max source. SEM image were collected with a CEMN's Zeiss Sigma VP SEM.

All phospholipids were purchased from Avanti Polar Lipids (Alabaster, AL, USA). Hexadecylphosphonic acid, octadecylphosphonic acid, tris(2- aminoethyl) amine, 2-isocyanatoethyl methacrylate, methacrylic acid (MAA), ethylene glycol dimethacrylate (EGDMA), and 2,2'-azobisisobutyronitrile (AIBN) were purchased from Sigma- Aldrich (USA). EGDMA was purified by distillation in vacuo. Human plasma were collected by Lampire Biological Laboratories Inc., from female donors, processed to obtain platelet-free plasma, and frozen at -80 ºC Empty SPE tubes and frits were purchased from Sigma-Aldrich (USA). HPLC grade methanol, chloroform and water were purchased from VWR (USA).

4.2.2 Synthesis of monomer **1**.

2-Propenoic acid, 2-methyl-, 18-methyl-8-[2-[[[[2-[(2-methyl-1-oxo-2-propen-1-yl)oxy]ethyl]amino]carbonyl]amino]ethyl]-4,12,17-trioxo-16-oxa-3,5,8,11,13-pentaazanonadec-18-en-1-yl ester was synthesized as described in literature[110] Tris(2-aminoethyl) amine (2.2 g, 15.04 mmol) was dissolved in 110 mL dichloromethane and cooled to 0 ºC before 2-isocyanatoethyl methacrylate was added in dropwise. The mixture was stirred at room temperature for 4 h. The solvent was evaporated and dried under vaccum. The yield of the product was 9.2 g (100%). ^{1}H-NMR data was in agreement with literature. ^{1}H NMR (400 MHz, CDCl3): δ 6.09 (s, 3H), 6.03 (bs, 3H), 5.80 (bs, 3H), 5.55 (s, 3H), 4.16 (bs, 6H), 3.43 (bs, 6H), 3.12 (bs, 6H), 2.48 (bs, 6H), 1.90 (s, 9H). ^{13}C NMR (400 MHz, $CDCl_3$): δ18.40, 38.72, 39.32, 55.36, 64.29, 126.06, 136.17, 159.45, 167.52. NMR spectra of monomer **1** are shown in Figure 4.2 and 4.3.

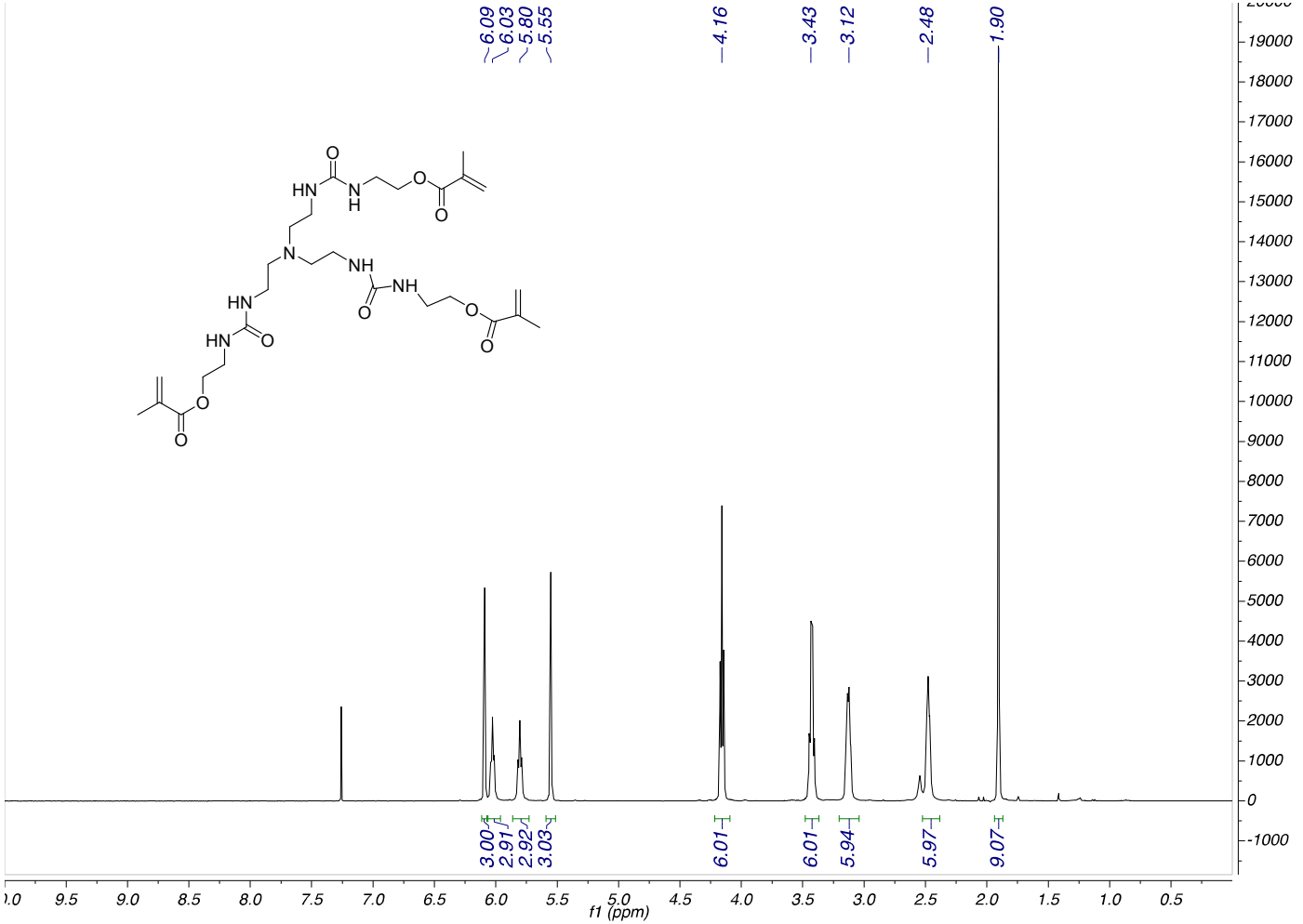

Figure 4.2 ^{1}H-NMR spectrum of monomer **1**.

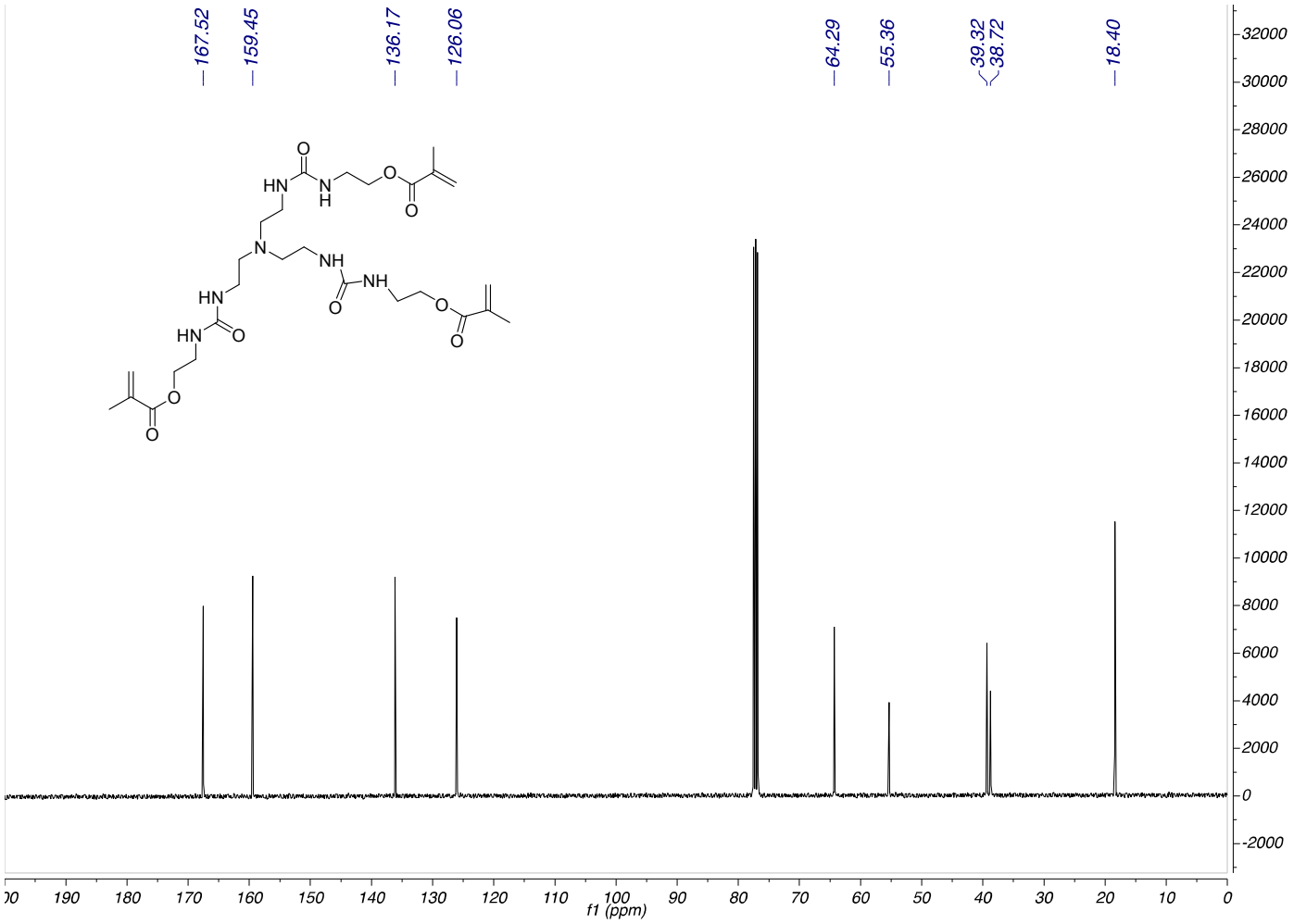

Figure 4.3 ^{13}C-NMR spectrum of monomer **1**.

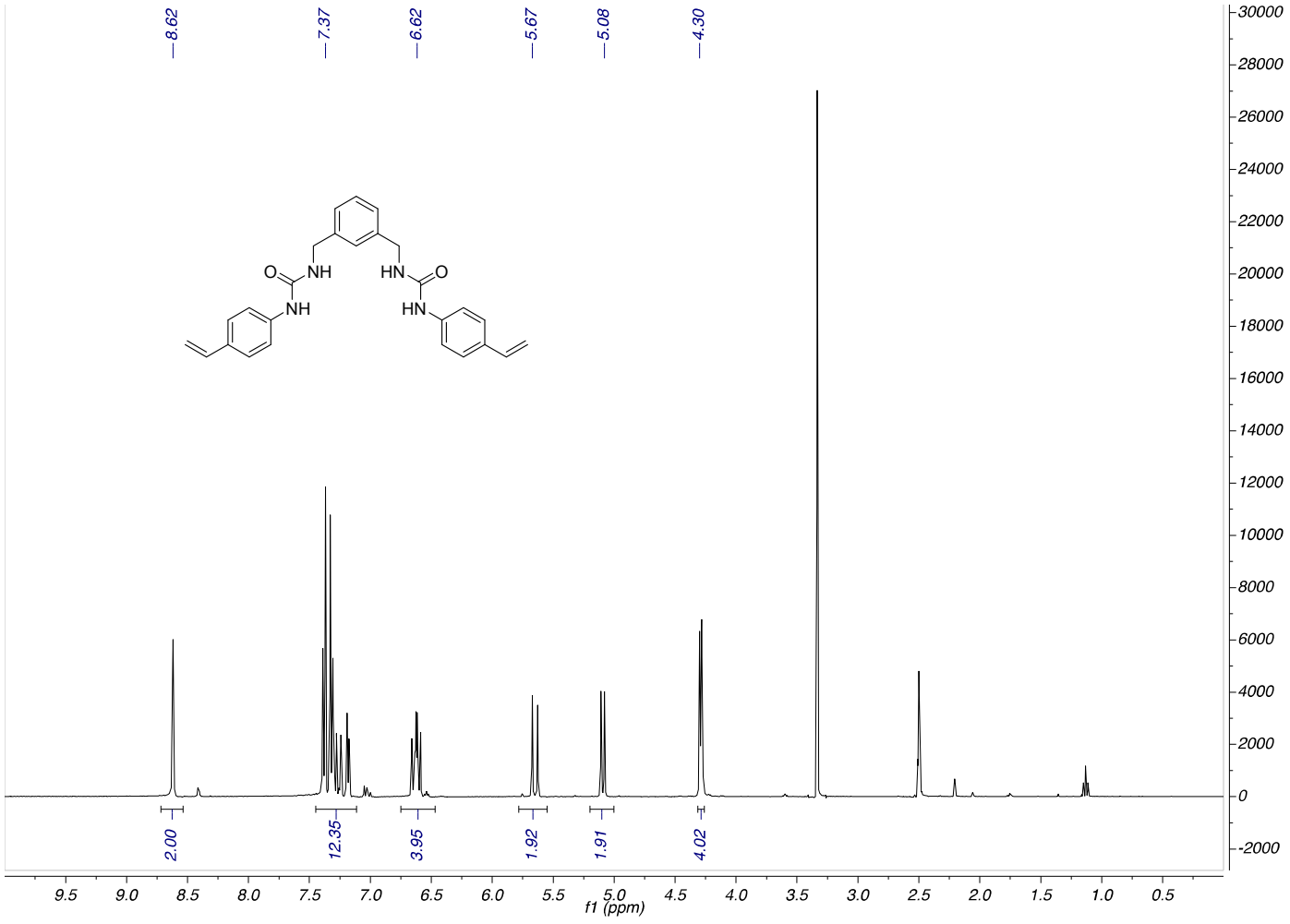

Figure 4.4 ^{1}H-NMR spectrum of monomer **2**.

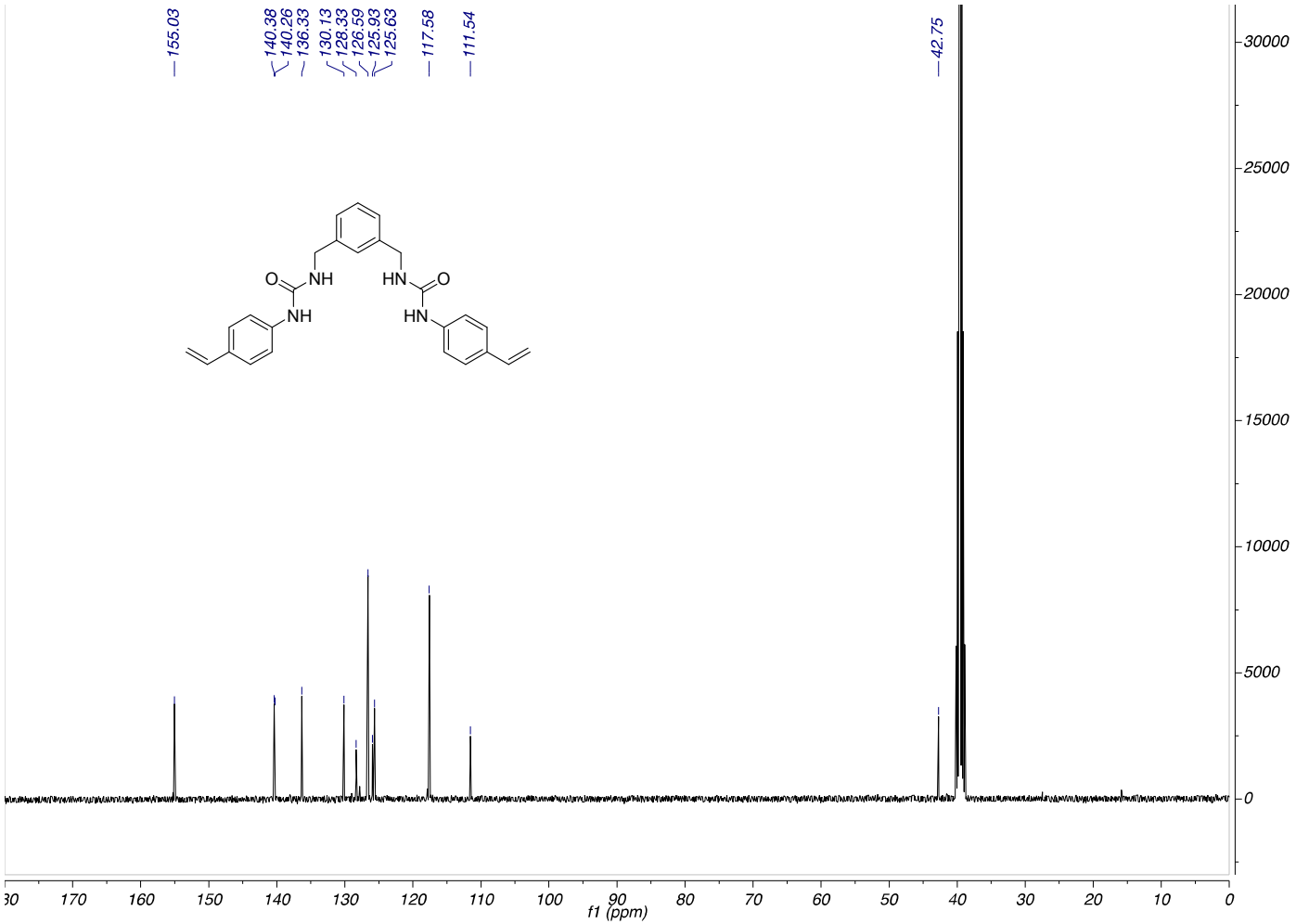

Figure 4.5 ^{13}C-NMR spectrum of monomer

4.2.3 Synthesis of monomer **2**

1,1'-(1,3-phenylenebis(methylene))bis(3-(4-vinylphenyl)urea) was synthesized as described in literature[111]. A solution of 4-aminostyrene (1.19 g, 10 mmol) in anhydrous THF (40 mL) was stirred at room temperature before 1,3-bis(isocyanatemethyl)benzene (0.78 mL, 5 mmol) was added under N_2. The reaction was stirred overnight to form a white precipitate. The precipitate was filtered and dried under vacuum to afford the product (1.62 g, 76.1%). ^{1}H-NMR (400 MHz, [d_6] DMSO): δ4.30 (d, 4 H), 5.08 (d, 2 H), 5.67 (d, 2 H), 6.62 (dd, 4 H), 7.15–7.45 (m, 12 H), 8.62 ppm (s, 2 H). ^{13}C-NMR (400 MHz, [d_6] DMSO): δ 42.75, 111.54, 117.58, 125.63, 125.93, 126.59, 128.33, 130.13, 136.33, 140.26, 140.38, 155.03. NMR spectra of monomer **2** are shown in Figure 4.4 and 4.5.

4.2.4 Synthesis of monomer **3** and **4**.

Vinyl-benzyl-cyclen monomer and Zn (II) vinyl-benzyl-cyclen monomer were synthesized as described in literature[112].

1,4,7-tris(*tert*-butyloxycarbonyl)-1,4,7,10-tetraazacyclododecane. Di-*tert*-butyl-dicarbonate (3.59g, 16.43 mmol) solution in $CHCl_3$ (50 mL) was added dropwise to the solution of cyclen (1.0 g, 5.80 mmol) and triethylamine(1.81 g, 17.88 mmol) in $CHCl_3$ (60 mL) over a 3 hour period. The reaction was stirred for 24 h at rt before the solvent was removed under reduced pressure. The crude product was purified via column chromatography using silica gel to afford 1,4,7-Tris(*tert*-butyloxycarbonyl)-1,4,7,10-tetraazacyclododecane as a colorless solid (1.92 g, 70.1%).

1-(4-vinylbenzyl)-4,7,10-tris(*tert*-butyloxycarbonyl)-1,4,7,10-tetraazacyclododecane. A solution of 1,4,7-Tris(*tert*-butyloxycarbonyl)-1,4,7,10-tetraazacyclo- dodecane (1.7 g, 3.60 mmol), K_2CO_3 (0.75 g, 5.4 mmol), KI (0.60 g, 3.6 mmol) , and 4-vinylbenzene chloride (0.82 g, 5.40 mol) in MeCN (60 mL) was stirred at 70 ºC for 3 h. After the insoluble inorganic salts were removed by filtration, the solvent of the filtrate was evaporated under reduced pressure. The crude product was purified by column chromatography to provide 1-(4-vinylbenzyl)-4,7,10- tris(tert - butyloxycarbonyl) -1,4,7,10-tetraazacyclododecane (1.56 g, 73.6%).

1-(4-vinylbenzyl)-1,4,7,10-tetraazacyclododecane 2TFA salt. Trifluoroacetic acid (12.78 g, 112.1 mmol) is added dropwise to the solution of 1-(4-vinylbenzyl)-4,7,10-tris(tert-butyloxycarbonyl)-1,4,7,10-tetraazacyclododecane (1.20 g, 2.04 mmol) in CH_2Cl_2 (130 mL) at 0 ºC. The reaction is stirred overnight at rt. The solvent was evaporated under reduced pressure before toluene (10 mL) was added to the residue and evaporated under reduced pressure. The residue was recrystallized from Et_2O-EtOH to afford 1-(4-Vinylbenzyl)-1,4,7,10-tetraazacyclododecane 2TFA salt (0.98 g, 93.4 %).

1-(4-vinylbenzyl)-1,4,7,10-tetraazacyclododecane. A solution of 1-(4-vinylbenzyl)-1,4,7,10-tetraazacyclododecane 2TFA salt (0.8g, 1.55 mmol) in water was added to 1M NaOH solution. The aqueous solution was extracted with $CHCl_3$ (50 mL × 5) and the organic layers were combined and dried over anhydrous Na_2SO_4. The solvent was evaporated under reduced pressure to afford 1-(4-vinylbenzyl)-1,4,7,10-tetraazacyclododecane (0.44 g, 98.4 %) ^{1}H NMR (400 MHz, CDCl3): δ 0.40-0.80 (m, 16 H), 1.62 (s, 2H), 3.25 (d, 1H), 3.79 (d, 1H), 4.76 (dd, 1H), 5.30 (d, 2H), 5.44 (d, 2H). ^{13}C

NMR (400 MHz, $CDCl_3$): δ43.69, 44.84, 45.68, 50.28, 57.80, 51.98, 113.46, 125.99, 129.53, 136.23, 136.36, 138.52. NMR spectra of monomer **3** are shown in Figure 4.6 and 4.7.

1-(4-vinylbenzyl)-1,4,7,10-tetraazacyclododecane $Zn(NO_3)_2$ salt, $[ZnL_2(NO_3)_2]$. A solution of $Zn(NO_3)_2 \cdot 6H_2O$ (0.23 g) in EtOH (4 mL) was added to a solution of 1-(4-vinylbenzyl)-1,4,7,10-tetraazacyclododecane (0.20 g, 0.70 mmol) in EtOH (0.3 mL) at 60 ºC and stirred for 1 h. The solvent was evaporated under reduced pressure and the residue was recrystallized from EtOH-H_2O to afford 1-(4-vinylbenzyl)-1,4,7,10-tetraazacyclododecane Zn $(NO_3)_2$ salt, $[ZnL_2(NO_3)_2]$. (0.23 g, 69.7 %) ^{1}H NMR (400 MHz, CDCl3): δ 0.30-1.1 (m, 16 H), 1.80 (s, 2H), 3.19 (d, 1H), 3.73 (d, 1H), 4.62 (dd, 1H), 5.17 (d, 2H), 5.34 (d, 2H). ^{13}C NMR (400 MHz, $CDCl_3$): δ 41.69, 41.81, 43.26, 44.03, 44.15, 48.64, 54.85, 114.47, 125.94, 130.62, 131.22, 135.71, 137.45. NMR spectra of monomer **4** are shown in Figure 4.8 and 4.9.

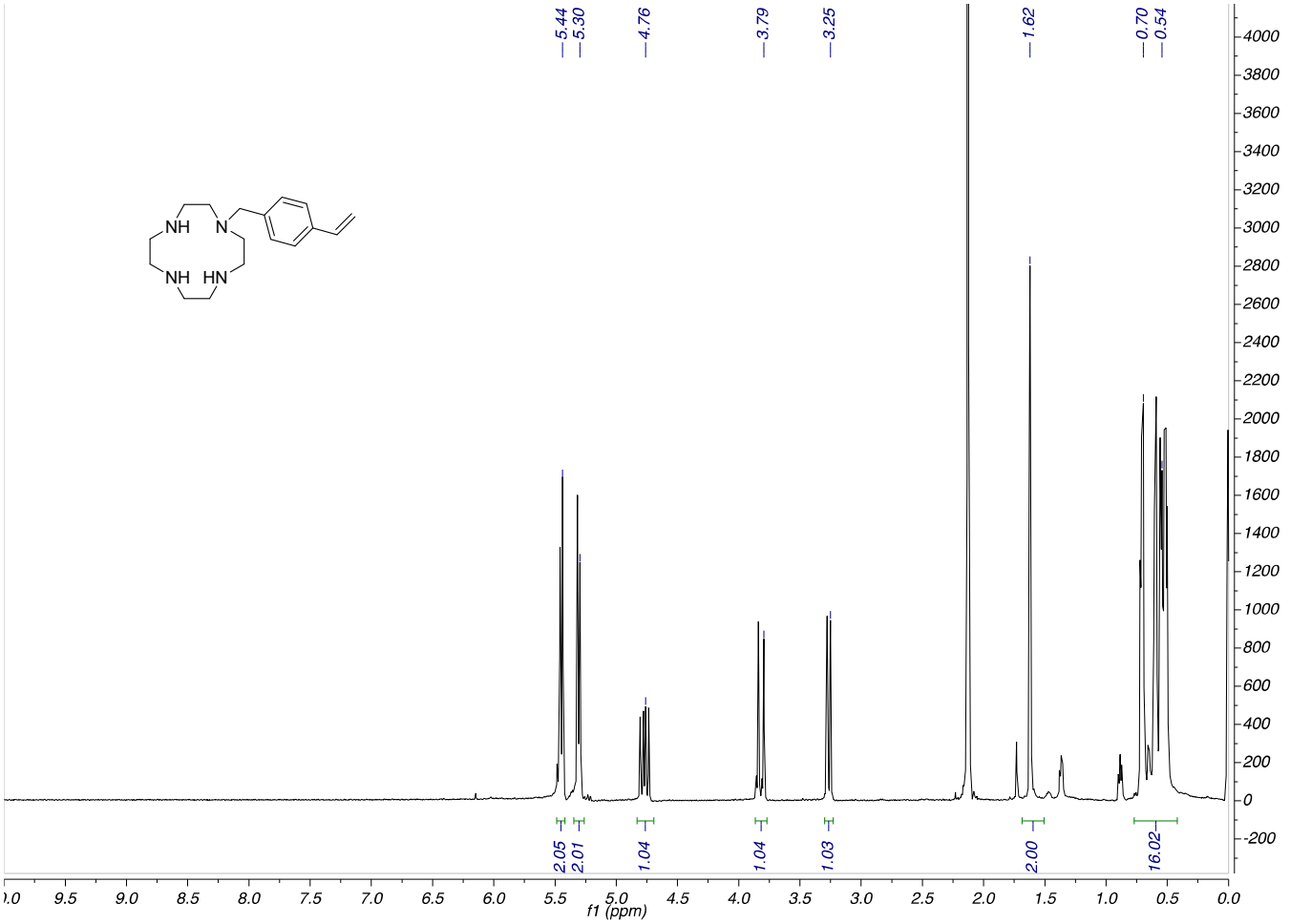

Figure 4.6 ^{1}H-NMR spectrum of monomer **3**.

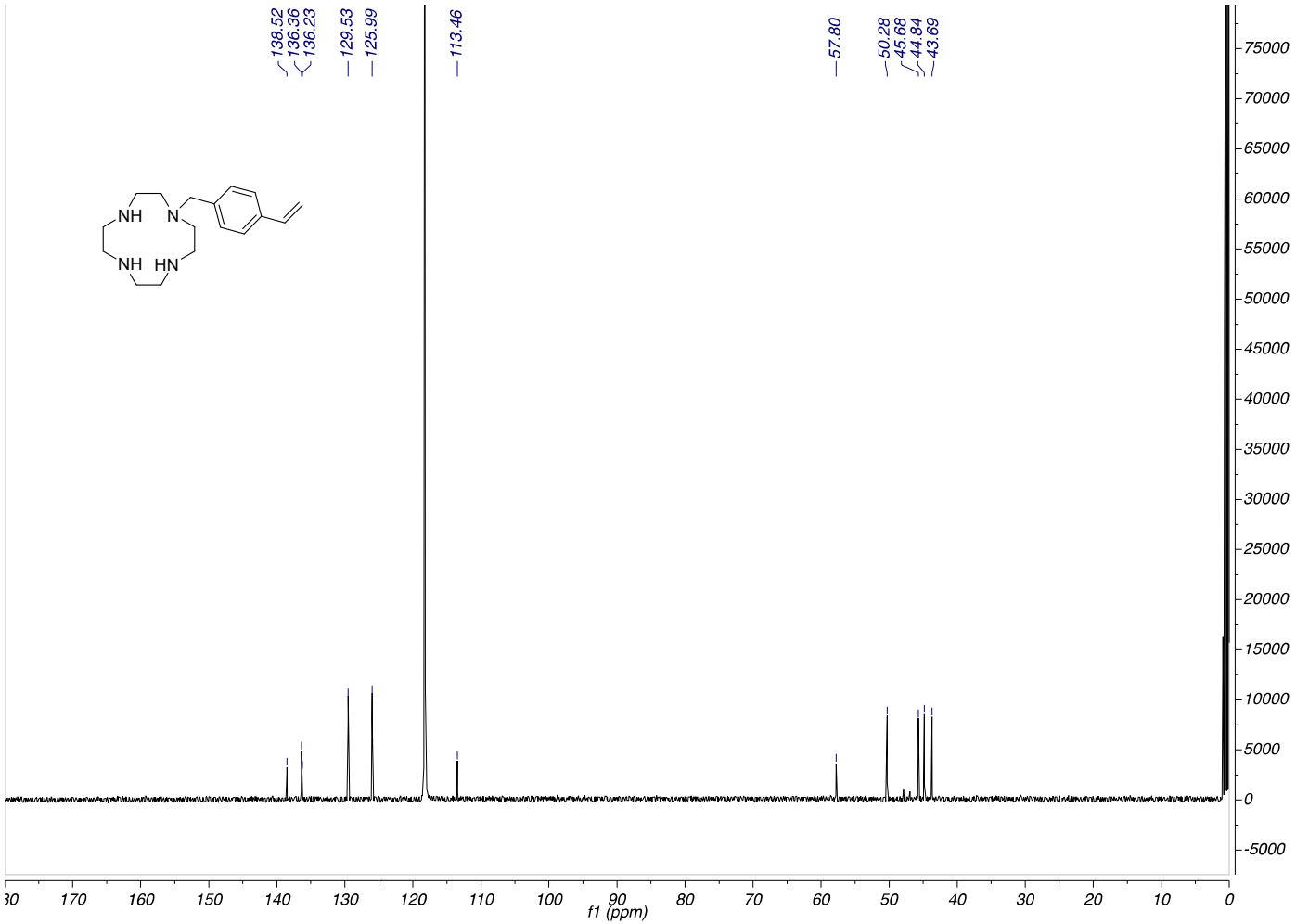

Figure 4.7 ^{13}C-NMR spectrum of monomer **3**.

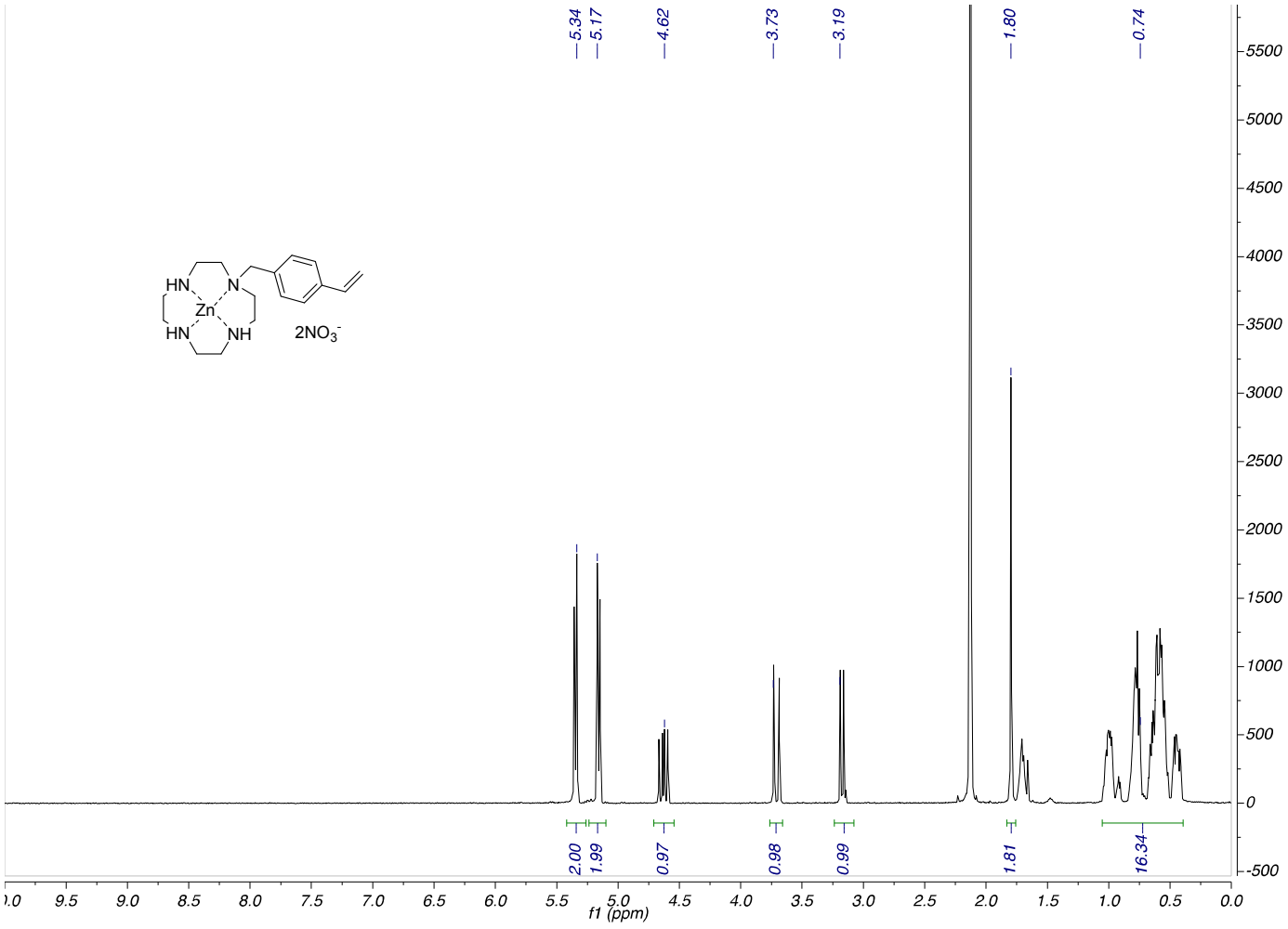

Figure 4.8 ^{1}H-NMR spectrum of monomer **4**.

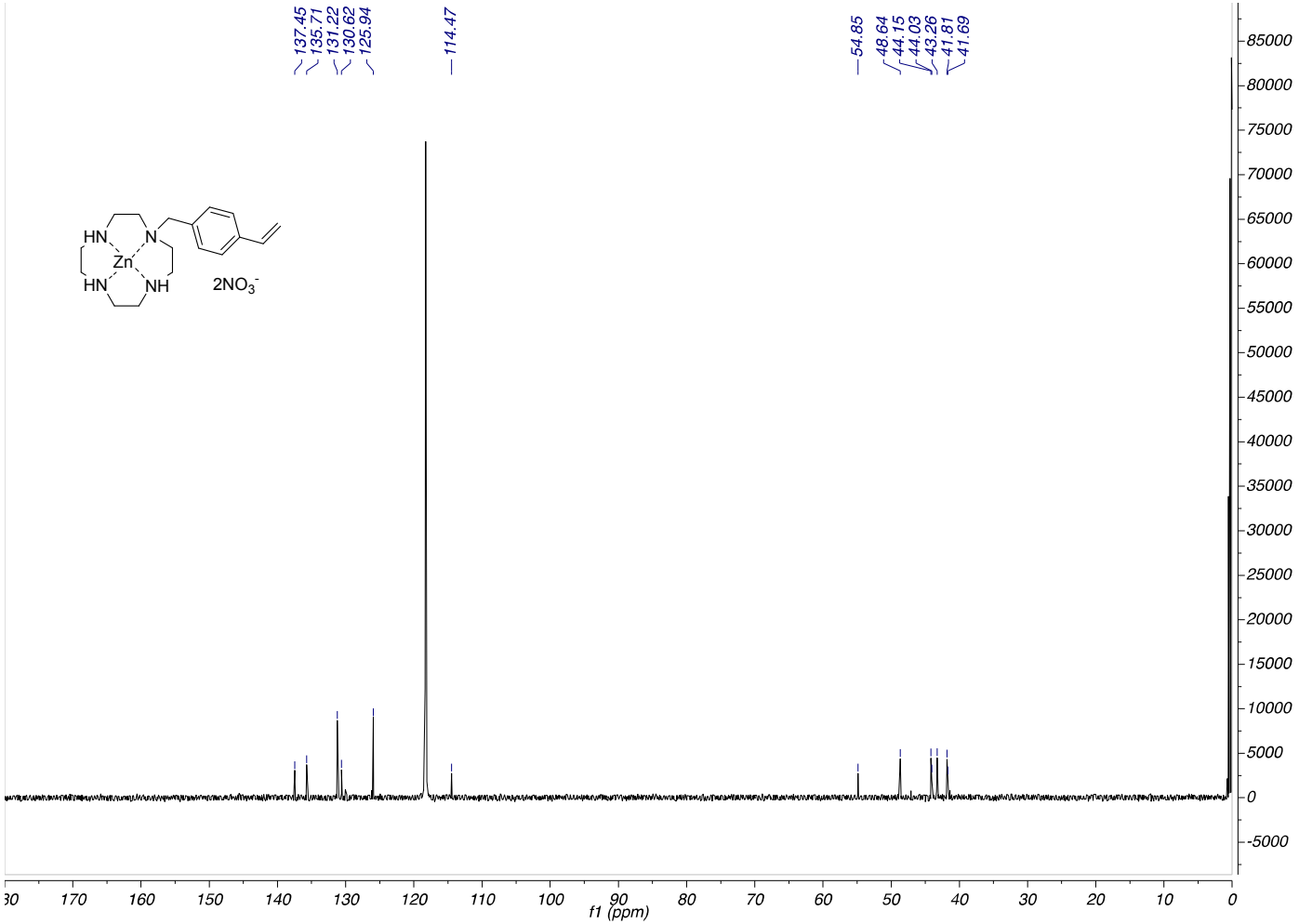

Figure 4.9 ^{13}C-NMR spectrum of monomer **4**.

4.2.5 Preparation of imprinted polymer and non-imprinted polymer

Octadecylphosphonic acid (1.00 g, 2.99 mmol), monomer **1** (1.83 g, 2.99 mmol) and methacrylic acid (0.257 g, 2.99 mmol) were dissolved in 37 mL chloroform and allowed to stand for 60 min for complex formation. EGDMA (11.9 g, 59.8 mmol) was added to the mixture in one portion. The mixture was purged by bubbling nitrogen for 5 min before and after AIBN (0.245g, 1.49 mmol) was added. Polymerization was carried at 55 ºC for 16 h. Polymers were crushed into small pieces before washing with MeOH, and extracted using a Soxhlet apparatus with MeOH for 48 h, before grinding and sieving to 63-90 μm.

A non-imprinted polymer was synthesized using the same protocol, but without the presence of the template octadecylphosphonic acid.

4.2.6 ^{1}H NMR titrations

Stock solutions of monomer **1** (40 mM) and octadecylphosphonic acid (20 mM) were prepared in $CDCl_3$. The initial concentration of template was 5 mM and kept constant. The monomer concentration was 0, 0.5, 1, 1.5, 2, 3, 4, 5, 7.5, 10, 15 mM, respectively. The chemical shifts of proton in urea group and the adjacent methylene group were monitored. Titration of methacrylic acid and template octadecylphosphonic acid were performed using the same protocol.

4.2.7 Job plots for monomers with template

Stock solutions of functional monomers and templates were the same as in the ^{1}H-NMR titration experiment. The concentration of the solution was 10 mM and the mole ratio of template and monomer were varied from 0/10 to 9/1. The chemical shifts of the proton of the urea group and the adjacent methylene group were monitored. A titration of the methacrylic acid and octadecylphosphonic acid was performed using the same protocol.

4.2.8 LPA enrichment procedure with MIP

600 μL human plasma was mixed with 2 mL MeOH-$CHCl_3$ 2:1, vortexed at 2000 rpm for 30 s and incubated at 4 ºC for 20 min. After warming to rt, the mixture was centrifuged at 2000 rpm for 10 min. The supernatant was decanted and loaded onto a cartridge packed with the non-imprinted polymer (NIP). The cartridge was eluted with 2 mL 0.05% NH_4OH in MeOH. The eluent was acidified to pH 3.0 with concentrated formic acid and loaded to a cartridge packed with 30 mg MIP. The cartridge was washed with 2 mL $CHCl_3$, followed by 2 mL MeOH. LPAs were eluted with 3 mL 0.05% NH_4OH in MeOH. The solvent was evaporated under N_2 stream and the residue was reconstituted in 0.2 mL MeOH-H_2O 9:1.

4.2.9 LC-ESI/MS procedure for plasma analysis

Samples (10 μL) after the enrichment with SPE step were injected to a Luna C-8 (50 × 2 mm, 3 μm) column at 40 ºC. The mobile phase, MeOH–HCOOH (pH 2.5) 9:1,

was delivered at a flow rate of 0.6 mL/min. Ions were created in negative ion mode by setting the sprayer voltage at 3.0 kV and the capillary temperature at 300 ºC.

4.2.10 Swelling of polymers

Dry polymer was placed in a 10 mL graduated cylinder and weighed. The weight and volume of the dry polymer were used to calculate the density of the polymer. Excess $CHCl_3$ was added and air bubbles removed by stirring. The polymer was allowed to swell for 24 h. The swelling factor was calculated as the ratio of the volume of the swollen polymers to the dry polymers.

4.3 Results and discussion

4.3.1 Monomer selection and synthesis

Functional monomers and crosslinking monomers were selected from a virtual library of 22 functional monomers containing functionalities for phosphate binding and 7 crosslinking monomers. A Leapfrog algorithm from Tripos Inc. was used to determine the binding of the functional monomer candidates and target analyte LPA 18:0. Functional monomers with the highest binding score and crosslinking monomers with the lowest binding score were selected as the best candidates for polymer preparation. Selected functional monomers **1-5** are shown in Figure 4.10. Monomer **1-4** are synthesized following the protocols in literature. The synthesis schemes are shown in Scheme 4.1-4.3.

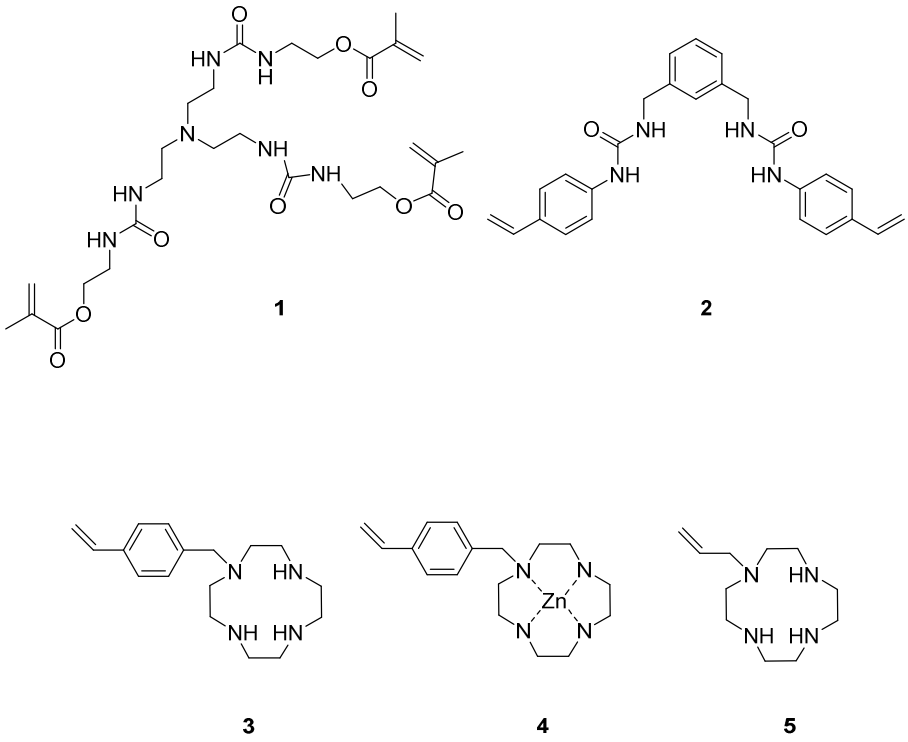

Figure 4.10 Chemical structures of selected functional monomers.

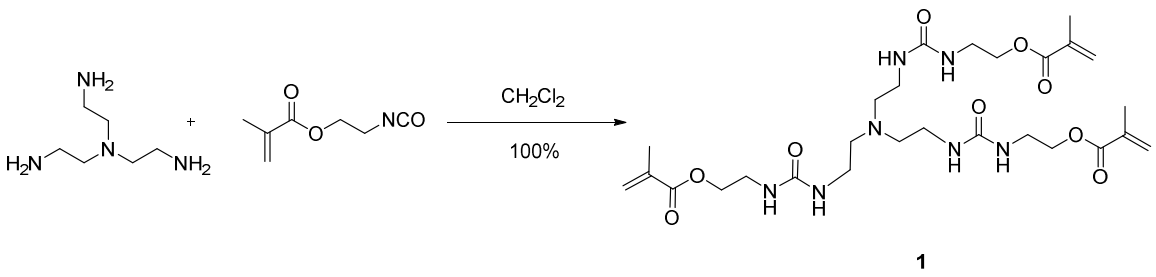

Scheme 4.1 Synthesis of monomer **1**.

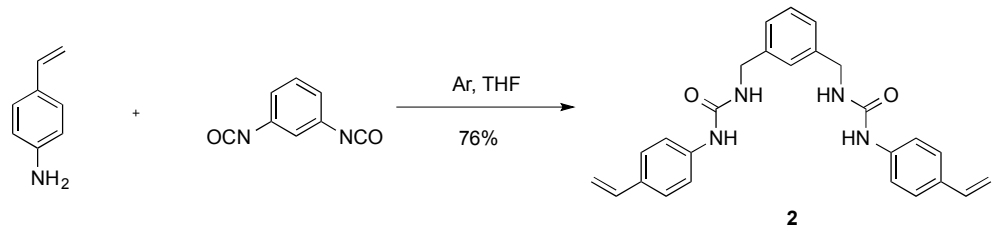

Scheme 4.2 Synthesis of monomer **2**.

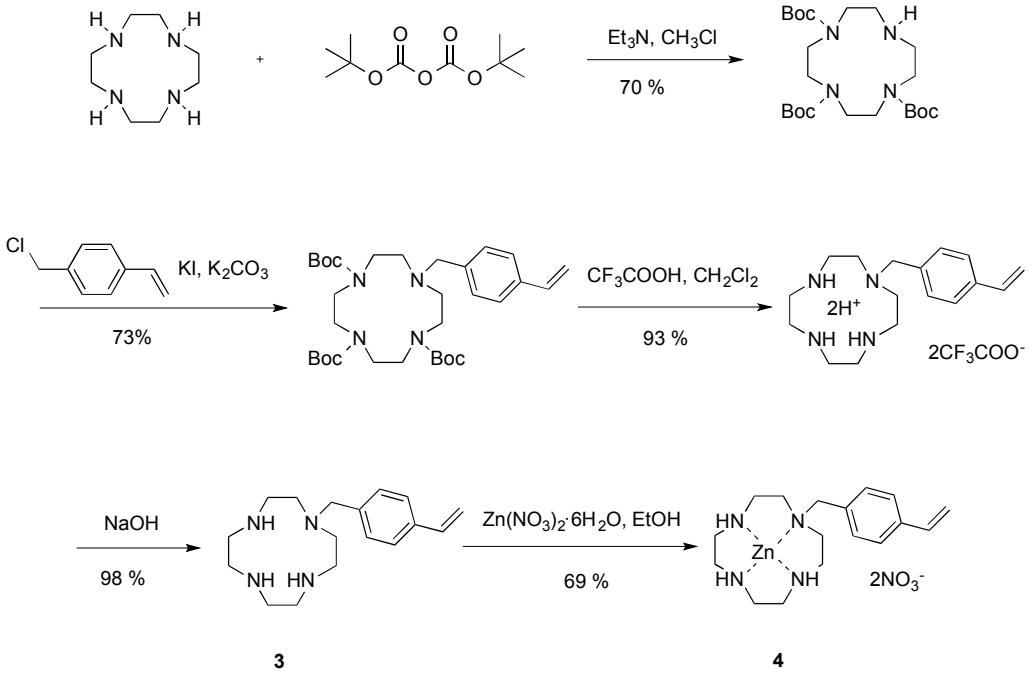

Scheme 4.3 Synthesis of monomer **3** and **4**.

4.3.2 Characterization of monomer binding properties

To study the binding properties of monomer **1**, octadecylphosphonic acid was used as the anionic guest. Octadecylphosphonic acid was also selected as the template for imprinting instead of LPA, to avoid interfering from potential LPA residue after template extraction. Weakly polar aprotic solvent chloroform was used as the solvent to avoid hydrogen bonding between the solvent and the template or the monomers. Data and ^{1}H-

NMR spectra of the Job plot are shown in Table 4.1 and Figure 4.11. The binding affinity of the urea functional group to the phosphate group was monitored using ^{1}H NMR. Downfield chemical shift of the urea N-H group and adjacent methylene protons were observed and monitored. Based on the results from Job plots, the maximum chemical shift was obtained when the mole ratio of monomer and guest was 1:1. Job plot is shown in Figure 4.12.

Table 4.1 Data for the Job plot performed by ^{1}H NMR titration in $CDCl_3$.

Mixture No.	Monomer **1** (mM)	Template (mM)	Mole fraction (monomer **1**)	δ (ppm)	Δδ (ppm)	Δδ × Mole fraction
1	10	0	1	3.1683	0.0000	0.0000
2	9	1	0.9	3.1901	2.1683	0.0196
3	8	2	0.8	3.2291	2.1901	0.0486
4	7	3	0.7	3.2784	2.2291	0.0770
5	6	4	0.6	3.3346	2.2784	0.0998
6	5	5	0.5	3.4273	2.3346	0.1295
7	4	6	0.4	3.4633	2.4273	0.1180
8	3	7	0.3	3.5123	2.4633	0.1032
9	2	8	0.2	3.5538	2.5123	0.0771
10	1	9	0.1	3.5563	2.5538	0.0388
11	0	10	0	-	-	-

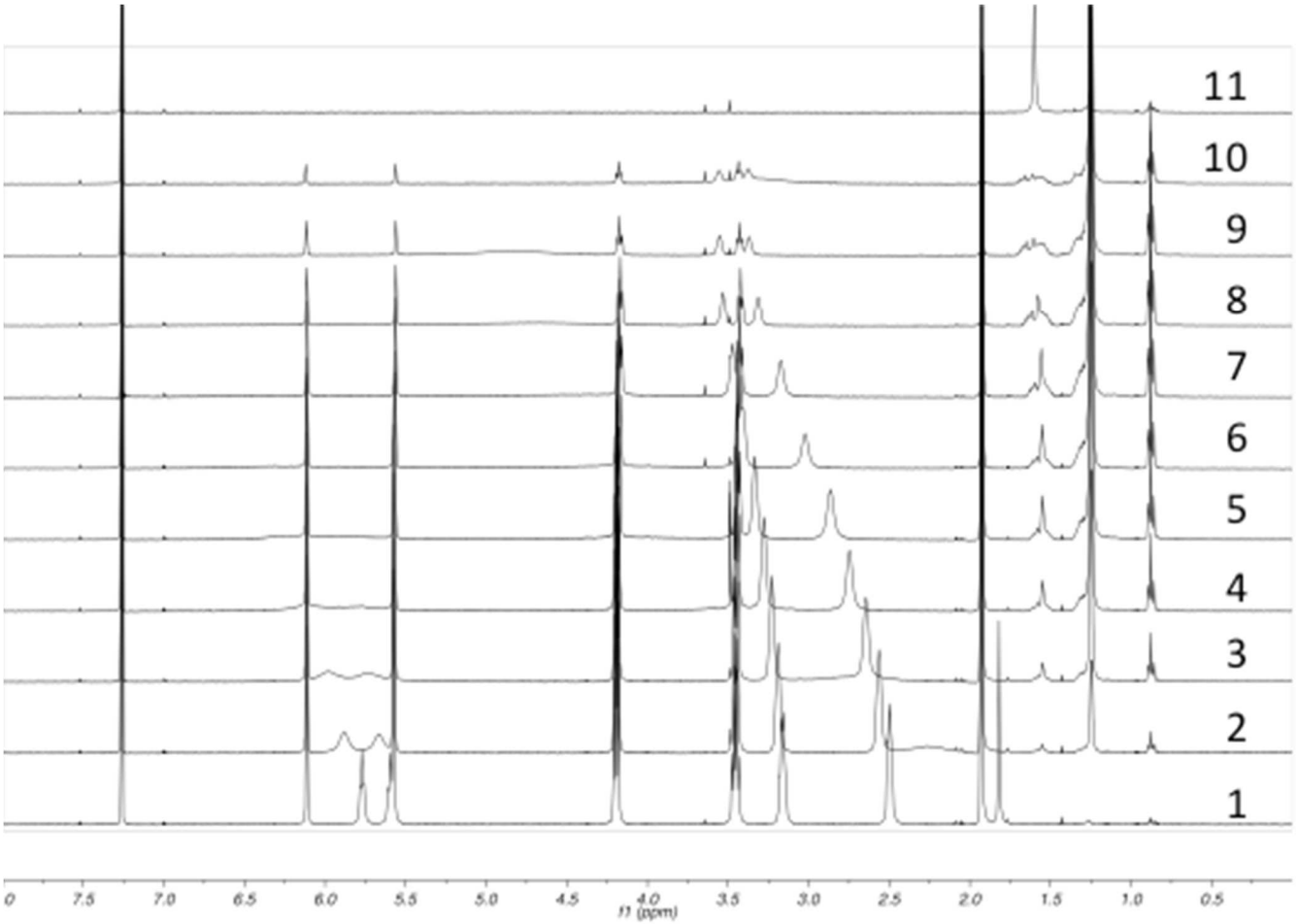

Figure 4.11 ^{1}H NMR spectra of Job plot data for trisurea and octadecylphosphonic acid. Each spectrum is labeled with the mixture numbers in Table 3.1.

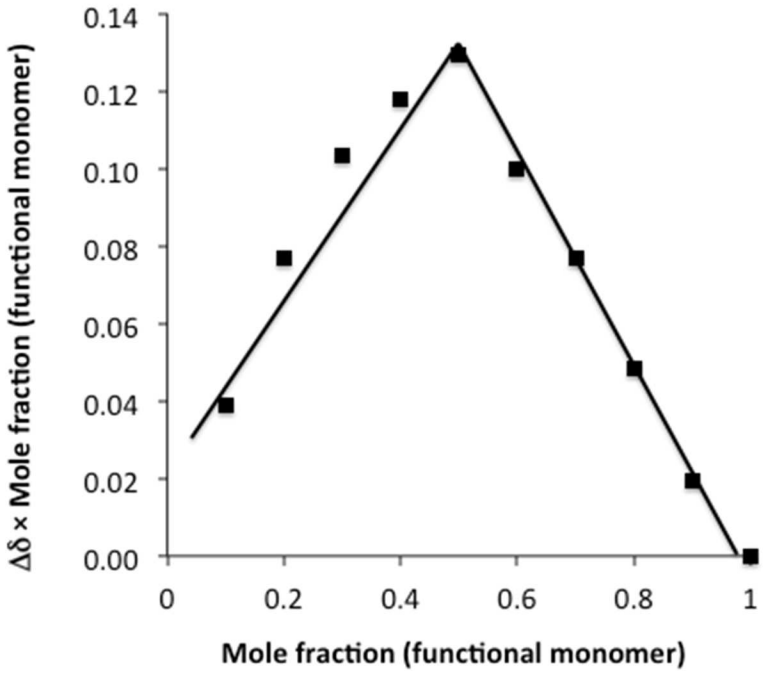

Figure 4.12 Job plot of monomer 1 with octadecylphosphonic acid in $CDCl_3$ showing a maximum at 0.5 mole fraction of trisurea.

The ^1H NMR titration experiment in $CDCl_3$ was carried out to determine the association constant of monomer **1** and octadecylphosphonic acid. Data and results are shown in Table 4.2 and Figure 4.13. ^1H NMR titration of monomer **1** using octadecylphosphonic acid as the guest is shonw in Figure 4.14. The association constant *K* is calculated to be 83.17 M^{-1}.

Job plot and NMR titration experiments were also done using monomer methacrylic acid as the host and octadecylphosphonic acid as the guest. No chemical shift was observed for the proton in N-H group or the adjacent methylene groups.

Table 4.2 Data of ^{1}H NMR titration of monomer **1** with template in $CDCl_3$.

Mixture No.	Monomer **1** (mM)	Template (mM)	Δδ (ppm)	Δδ (ppm)	Δδ (ppm)
1	5	0	0	0	0
2	5	0.5	0.12	0.02	0.06
3	5	1	0.19	0.04	0.1
4	5	1.5	0.26	0.07	0.16
5	5	2	0.33	0.09	0.2
6	5	3	0.46	0.13	0.29
7	5	4	0.6	0.17	0.38
8	5	5	0.64	0.21	0.47
9	5	7.5	0.66	0.29	0.64
10	5	10		0.33	0.74
11	5	15		0.37	0.84

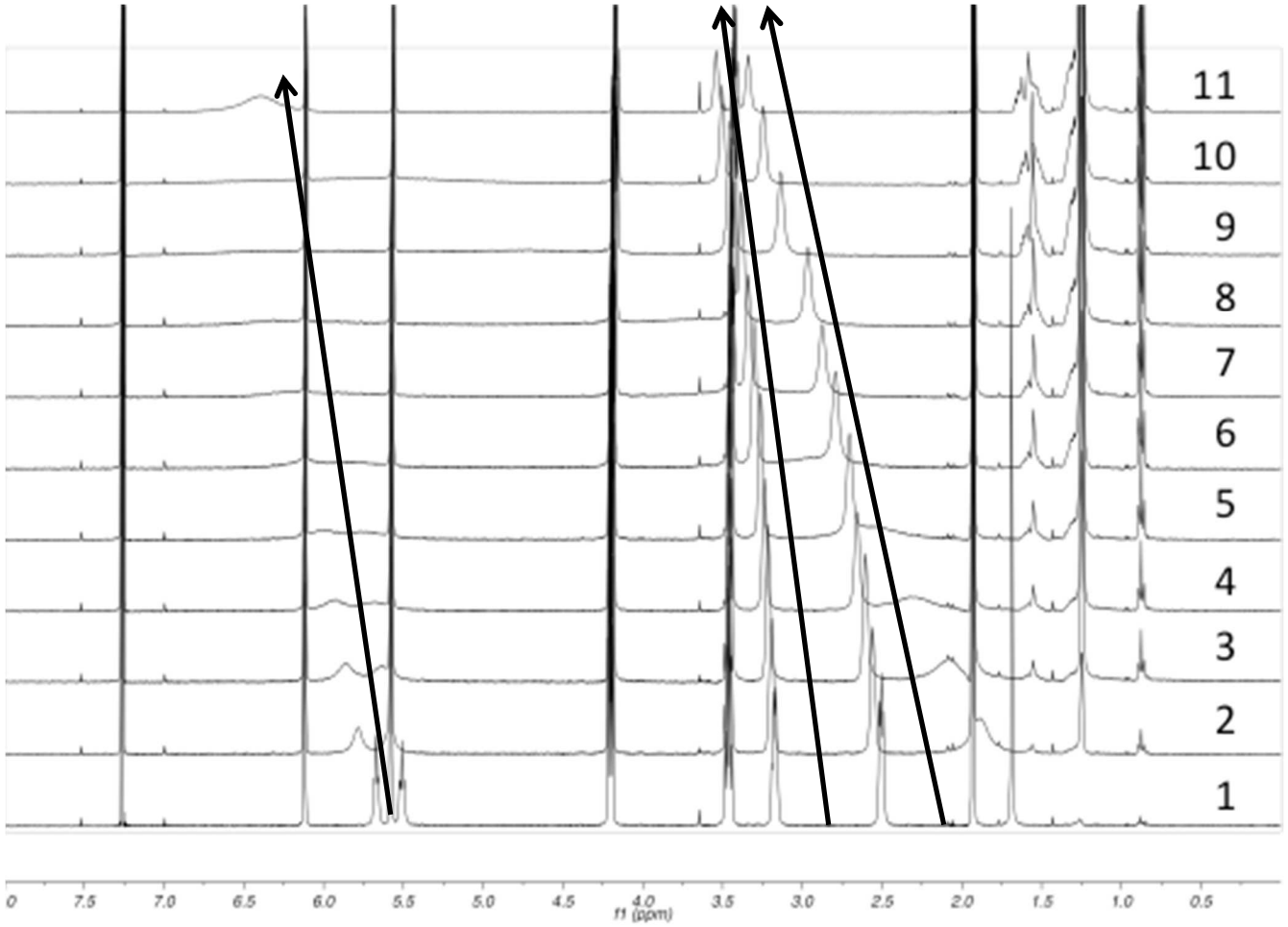

Figure 4.13 ^{1}H NMR titration spectra of trisurea and octadecylphosphonic acid. Each spectrum is labeled with the mixture number in Table 3.2.

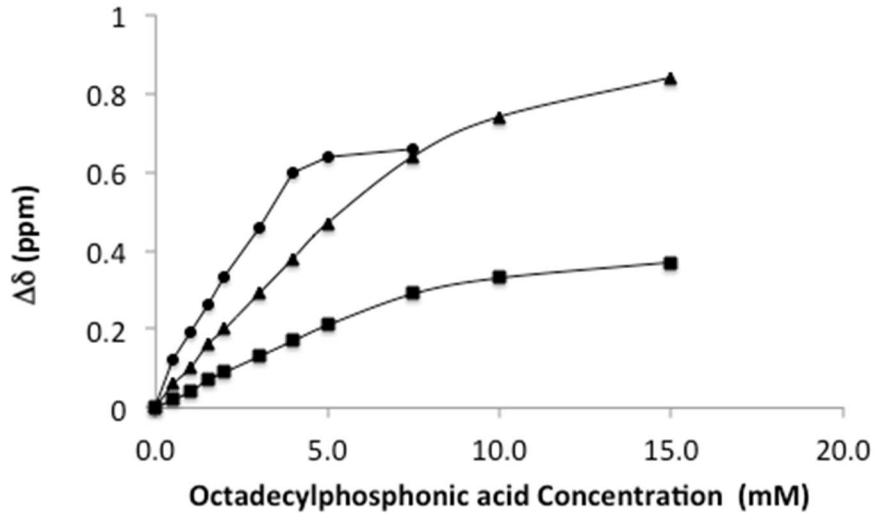

Figure 4.14 ^{1}H NMR titration of monomer **1** using octadecylphosphonic acid as the guest.

4.3.3 Infrared spectroscopy of MIP

Fourier transform infrared spectroscopy (FTIR) spectra of the non-imprinted polymer and imprinted polymer after template removal were collected and shown in Figure 4.15. IR of non-imprinted polymer, 3547, 3377, 2961, 1713, 1547, 1445, 1382, 1236, 1126, 1039, 938, 841, 806, 745 cm^{-1}. IR of imprinted polymer after template removal, 3531, 3375, 2943, 1714, 1632, 1551, 1448, 1384, 1242, 1137, 1043, 943, 845, 784, 748 cm^{-1}. No phosphate group peaks were observed in the spectrum of imprinted polymer, because 95 % of the octadecylphosphonic acid was removed in the template extraction step.

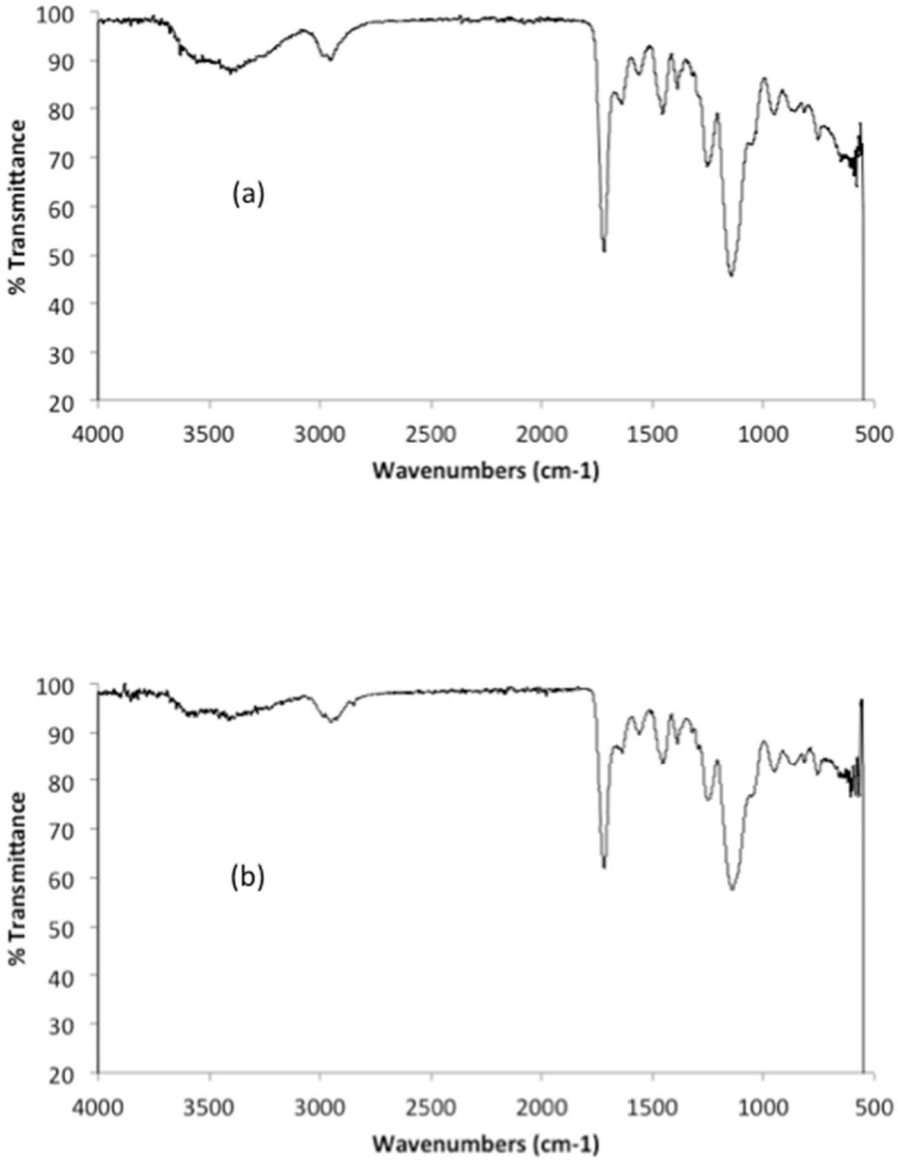

Figure 4.15 IR spectra of (a) non-imprinted polymer and (b) imprinted polymer after template removal.

4.3.4 SEM microphotographs of polymers

A scanning electron microscope (SEM) microphotographs in Figure 4.16 show that both non-imprinted and imprinted polymers obtained from bulk polymerization are irregular shaped particles.

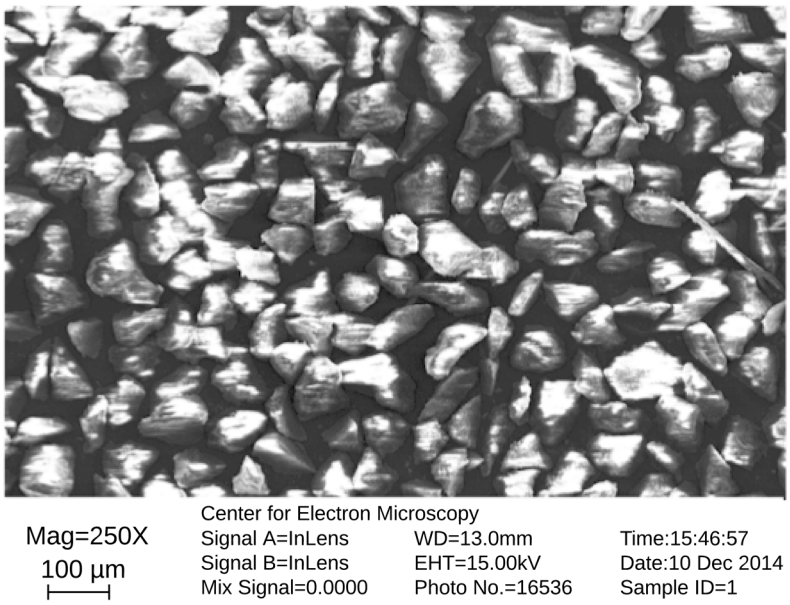

(a)

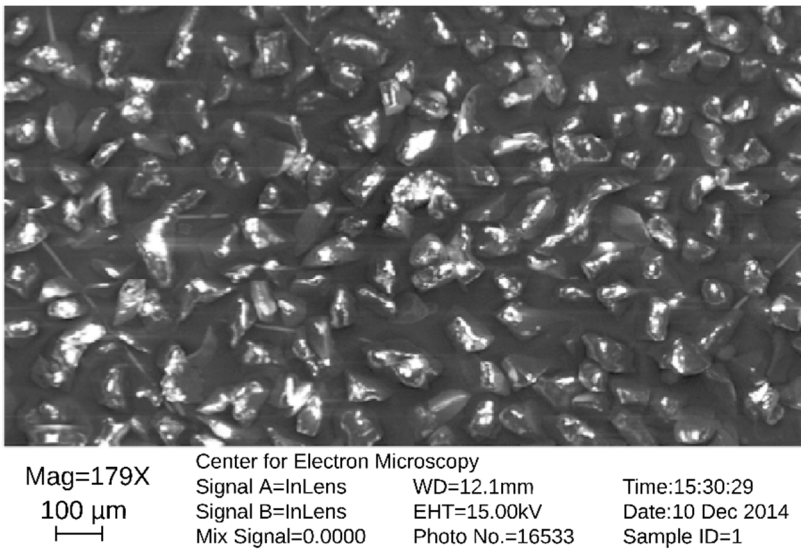

(b)

Figure 4.16 SEM microphotographs of non-imprinted (a) and imprinted (b) polymers.

4.3.5 Swelling of polymers

Swelling factors and density of MIP and NIP are shown in Table 4.3.

Table 4.3 Swelling factor and density of non-imprinted and imprinted polymers.

	Non-imprinted polymer	Imprinted polymer
Density	0.331 g/mL	0.647 g/mL
Swelling factor	2.05	3.47

Monomer **1** was firstly synthesized and used as the functional monomer in the MIP preparation. Optimization of the formulations was carried out after promising screening results were obtained. MIP with monomer **2** was also prepared and screened. The binding of LPA to the polymer was also quite strong, necessitating further study. MIP with monomer **4** as the functional monomer was not prepared because the complex formed by this monomer and the template octadecylphosphonic acid could not be dissolved in any aprotic solvent.

4.3.6 Formulation optimization of MIP

Other functional monomers including 2-vinylpyridine, 4-vinylpyridine (4-VP), and 1-allylthiourea were also evaluated for LPA binding. However, the template OPA did not dissolve completely in $CHCl_3$ at the desired concentration; and the addition of the functional monomer did not help to dissolve the template under the conditions used for template-monomer complex formation. A bulk polymerization procedure was chosen. Soxhlet extraction of the polymer pieces removed 95 % of the template from the

imprinted polymer. An optimal MIP should afford high recovery and high selectivity for LPA.

A series of MIPs formulations were prepared as shown in Table 4.4. The first formulation attempted (Table 4.4, entry 1) included only monomer **1** as the functional monomer. Screening results for this formulation showed that 60-80% of each individual LPA could be recovered, but 70-80% of PA was bound to the polymer and co-eluted with LPA from the MIP. Because of the high cross-reactivity observed between PA and LPA, a second monomer was included in the formulation. For this purpose, methacrylic acid (MAA) and 4-vinylpyridine (4-VP) were used in order to increase non-covalent interactions *via* hydrogen bonding.

In the presence of MAA in the formulation, (Table 4.4, entry 2) the recovery of PA was lowered by 50% due to the absence of the hydroxyl group in the PA structure. The recovery of LPA was also increased to 70-115 %. The formulation containing, 4-VP, (Table 4.4, entry 3) as the second monomer, showed a similar LPA recovery to the second formulation, but with less selectivity. Thus, the second formulation (Table 4.4, entry 2) was found to have the best required properties for the purpose of this study. A comparison of percent recoveries of LPA and possible interferences in preliminary screening experiments with all three formulations of MIP are shown in Figure 4.18.

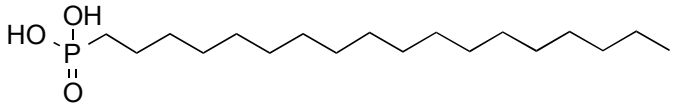

octadecylphosphonic acid (OPA)

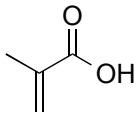

methacrylic acid (MAA)

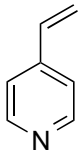

4-vinylpyridine (4-VP)

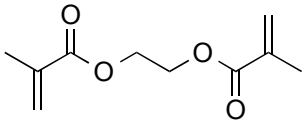

EGDMA

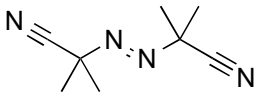

AIBN

Figure 4.17 Structures of OPA, MAA, 4-vinylpyridine, EGDMA and AIBN.

Table 4.4 Formulations of MIP and NIP.

Entry	Polymer	Template	Functional monomer 1	Functional monomer 2	Crosslinking monomer	Initiator	Solvent
1	NIP-1	—	Monomer **1** (0.81 M)	—	EGDMA (16.2 M)	AIBN (0.41 M)	$CHCl_3$
	MIP-1	OPA (0.81 M)	Monomer **1** (0.81 M)	—	EGDMA (16.2 M)	AIBN (0.41 M)	$CHCl_3$
2	NIP-2	—	Monomer **1** (0.81 M)	MAA (0.81 M)	EGDMA (16.2 M)	AIBN (0.41 M)	$CHCl_3$
	MIP-2	OPA (0.81 M)	Monomer **1** (0.81 M)	MAA (0.81 M)	EGDMA (16.2 M)	AIBN (0.41 M)	$CHCl_3$
3	NIP-3	—	Monomer **1** (0.81 M)	4-VP (0.81 M)	EGDMA (16.2 M)	AIBN (0.41 M)	$CHCl_3$
	MIP-3	OPA (0.81 M)	Monomer **1** (0.81 M)	4-VP (0.81 M)	EGDMA (16.2 M)	AIBN (0.41 M)	$CHCl_3$

Structures of OPA, MAA, 4-vinylpyridine, EGDMA and AIBN are shown in Figure 4.17.

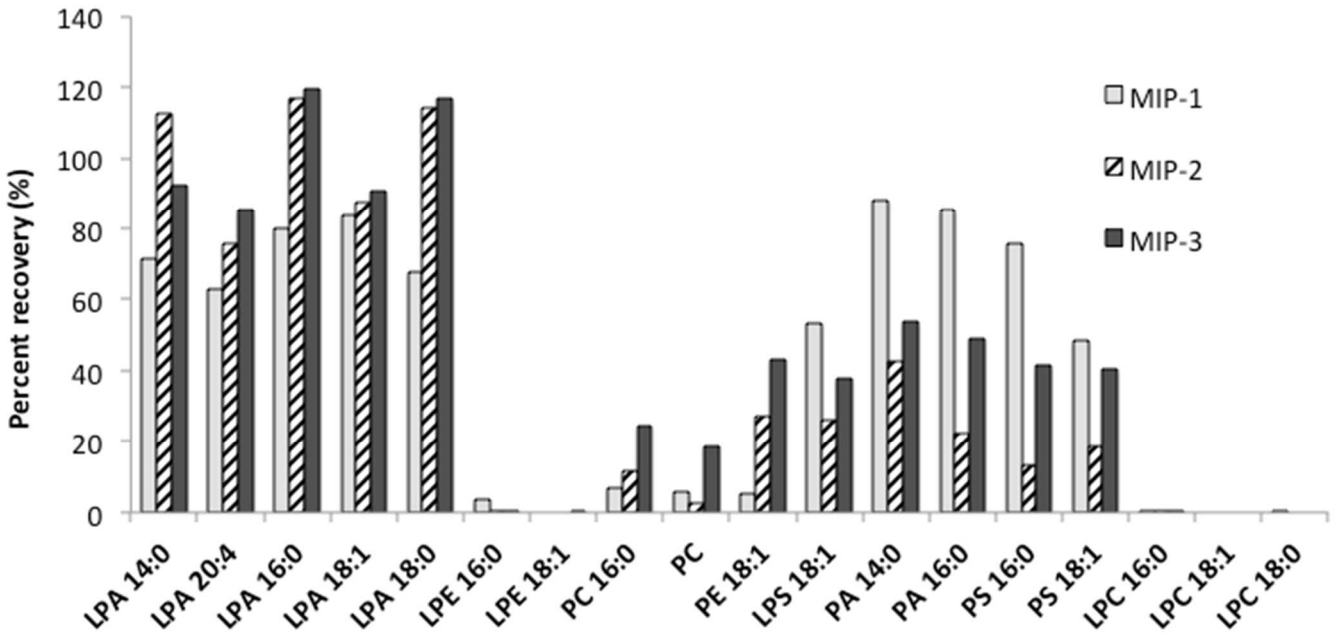

Figure 4.18 Percent recoveries of LPA and possible interferences in preliminary screening experiments of three formulations of MIP.

4.3.7 SPE protocol optimization

The MIP showed a good binding affinity with LPA in organic media. About 75 % of each LPA subspecies were bound to MIP in a $CHCl_3$-MeOH mixture. Formic acid was added to protonate LPA, and increased the binding to 95 %. MeOH or $CHCl_3$ alone could only elute 60-70% of the bound LPA from the MIP. However, more than 90 % of the LPA could be eluted with 0.05% NH_4OH in MeOH. $CHCl_3$ followed by MeOH was used in the washing step for the removal of neutral phospholipids, such as LPC, PC, etc. Using $CHCl_3$ in the washing removed only 50 % LPC; MeOH removed the remainder.

From the evaluation results, we noticed that the non-imprinted polymer showed a stronger binding property to PA than the imprinted polymer under the same loading and elution conditions. About 80% of the PA was retained in the non-imprinted polymer (NIP-2), compared to 50% in the imprinted polymer (MIP-2) when samples were loaded in 0.05% HCOOH in $CHCl_3$ and eluted in 0.05% NH_4OH in MeOH. This can be interpreted as arising from the differences in selectivity between the non-imprinted and imprinted polymers. The non-imprinted polymer has no selectivity in its binding to phosphate head groups, while the imprinted polymer contains cavities that are specific shaped for LPA molecules. This imprinting effect allows us to use the non-imprinted polymer to retain PA before the sample was loaded to the imprinted polymer. On the other hand, LPA was not retained in the non-imprinted polymer because of less non-specific interaction with the polymer compare to PA, which has (double) fatty acid chains.

4.3.8 LPA extraction and quantification in plasma

Mixtures of LPA 14:0, LPA 20:4, LPA 16:0, LPA 18:1 and LPA 18:0 with concentrations ranging from 0.5-10 μM were evaluated with non-natural LPA 17:0 as an internal standard. All LPAs showed linear responses in this range. Statistical values from calibration curves are shown in Table 4.5. Calibration curves of LPA species are shown in Figure 4.19. For all LPA species, acceptable correlation factors (R^2) were obtained. The limit of detection (LOD) was determined as the amount of analyte that corresponds to three times the signal of the background noise.

Table 4.5 Statistical values from calibration curves for LPA species using LC/MS as the quantification method.

LPA species	Retention time (min)	Equation	R^2	LOD (μM)
14:0	3.78	y = 0.0804x + 0.0164	0.9958	0.126
20:4	4.41	y = 0.0939x + 0.0219	0.9941	0.153
16:0	4.87	y = 0.0821x + 0.0156	0.9972	0.166
18:1	5.32	y = 0.0775x + 0.0156	0.9954	0.182
18:0	6.60	y = 0.0734x + 0.0114	0.9967	0.225

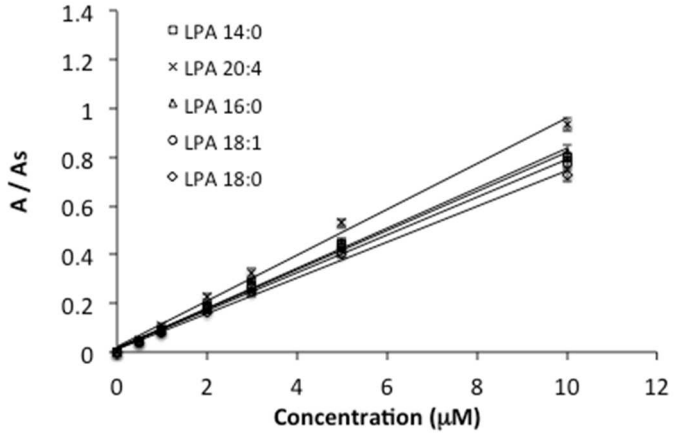

Figure 4.19 Calibration curves of LPA subspecies with LC/MS as the quantification method. The area ratio is the peak area of individual LPA divided by the peak area of the internal standard (LPA 17:0). Data points represent the average of 3 runs.

The recoveries of LPA were determined using LPA control samples and the results are summarized in Table 4.6. Hexadecylphosphonic acid (5 μM) was used as an internal standard instead of octadecylphosphonic acid to eliminate the potential interfere from the residue of template in MIP. Two concentration LPA mixtures including 0.5 μM and 2.5 μM were evaluated for three times.

Table 4.6 Recoveries of individual LPA species after SPE. (n = 3)

LPA species	Recovery (%)	σ
14:0	87.1	1.5
20:4	86.2	1.6
16:0	89.5	1.4
18:1	87.6	1.5
17:0	85.1	1.6
18:0	87.3	1.3

Plasma samples and plasma samples spiked with 0.5 μM, 1 μM and 2 μM of each LPA subspecies were used to evaluate the method and determine potential matrix interferences. All samples were prepared and analyzed in triplicates. Results of non-spiked plasma samples and spiked samples are summarized in Table 4.7. Representative HPLC traces of plasma sample and LPA control sample are shown in Figure 4.20.

Table 4.7 Results for LPA analysis in human plasma using LC-ESI/MS.

LPA species	Non-spiked		Spiked with 0.5 μM			Spiked with 1 μM			Spiked with 2 μM		
	average	σ	average	σ	% recovery	average	σ	% recovery	average	σ	% recovery
14:0	0.25	0.02	0.70	0.03	91.23	1.19	0.03	94.59	2.16	0.04	95.83
20:4	0.23	0.02	0.74	0.01	103.10	1.25	0.06	101.84	2.26	0.02	101.44
16:0	0.37	0.02	0.93	0.04	111.56	1.42	0.05	105.17	2.45	0.03	103.98
18:1	0.26	0.03	0.78	0.03	103.24	1.29	0.04	103.28	2.30	0.04	101.91
18:0	0.34	0.01	0.87	0.02	106.34	1.36	0.05	101.70	2.39	0.22	102.62
Total LPA	1.45	0.05	4.02	0.07	103.09	6.51	0.10	101.32	11.56	0.23	101.16

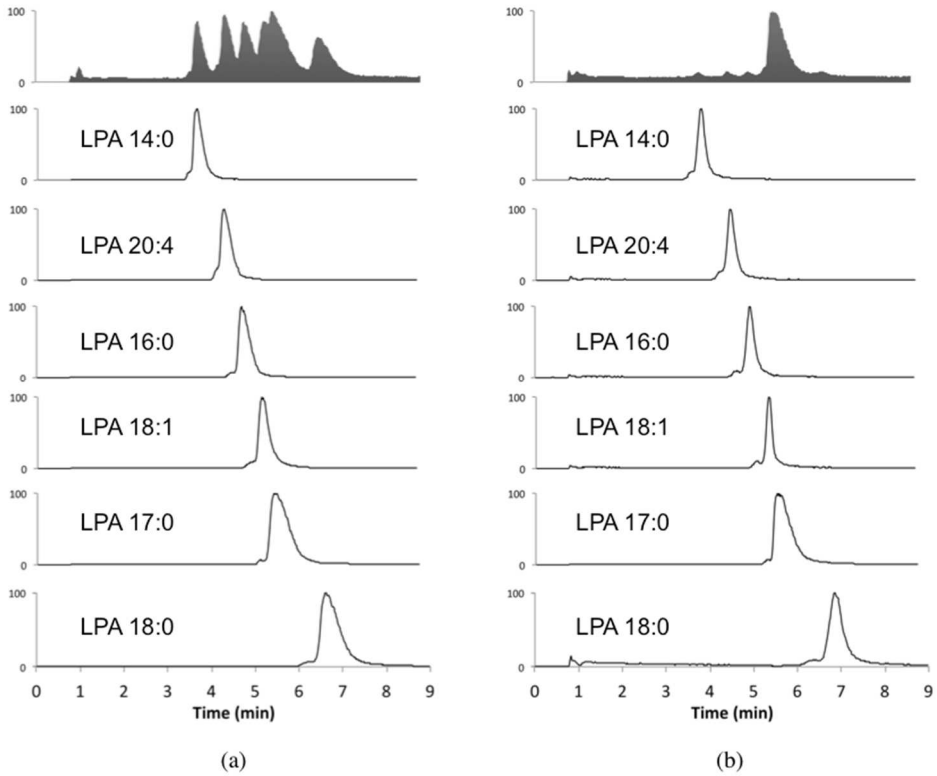

Figure 4.20 LC-ESI/MS traces. (a) A 10 uM standard mixtures of LPAs. (b) Plasma sample. Column: Luna ™ C-8 (50 × 2 mm, 3 µm) at 40 ºC. Injection volume: 10 µL. Mobile phase: 9:1 MeOH–HCOOH (pH 2.5). Flow rate: 0.6 mL/min. Ions were detected in negative ion mode. Sprayer voltage: 3.0 kV and Capillary temperature at 300 ºC

To determine the existence of non-LPA phospholipids in the plasma extraction after SPE with NIP and MIP, an LC/MS full scan in negative and positive modes was used. A mixture of phospholipids was used as the control sample and confirmed to be detectable in either negative or positive mode. The plasma sample after extraction was tested using the same method. Signals were compared to the LIPID MAPS Structure Database (LMSD)[64]. No interfering phospholipids except traces amount of LPC could be detected. Using the presence of LPC 15:0 as the internal standard, the concentration of LPC 16:0, LPC 18:1 and LPC 18:0 were estimated to be 0.05 μM, 0.01 μM and 0.02 μM, respectively. The level represents less than 0.1 % of the total physiological LPC in human plasma.[73] This result is comparable to our previous method [70].

4.4 Conclusion

The MIP prepared using monomer **1** and methacrylic acid as functional monomers showed significant advantages for LPA extraction and enrichment in selectivity. Using this MIP as an SPE cartridge stationary phase allows fast and simple extraction of LPA from human plasma with high recoveries and high purities. Compared to the previous extraction method we developed[70], the current method is faster and less labor intensive, because most of the vortexing and centrifugation steps in liquid-liquid extraction are replaced. The extraction and quantification of plasma LPA can be automated easily because of the elimination of liquid-liquid extraction.

Chapter 5 Future Work

5.1 Optimization of current formulations of MIP

Synthesize MIPs with a more optimized formulation (e.g., stoichiometries of monomers) to remove PA completely without passing the sample through the extra SPE filled with NIP. This may be realized by adding more hydrophobic crosslinking monomer to retain PA that contains double fatty chains. We could also attempt by modify the ratio of functional monomers and crosslinking monomers in the formulation.

5.2 MIP with other functional monomers

Synthesize and evaluate MIPs with other functional monomers, such as monomers **2-5** in Chapter 4. MIPs with other functional monomers could possibly be more advantageous for simplifying LPA extraction. For example, MIPs that could be used in aqueous media could enable bypassing bypassing treatment with MeOH and $CHCl_3$. In other words, the plasma could potentially be passed directly through a MIP cartridge if the MIP effectively binds LPA in water. To date, a MIP with 1-vinylimidazole as the functional monomer showed good binding affinity to LPA (>90 % LPA bound; however, elution was problematic) according to preliminary screening results.

5.3 MIP for specific LPA subspecies

The MIP we are currently using is selective for LPA over other phospholipids, but is not selective for individual LPA species. The synthesis of MIPs

for each individual LPA can eliminate separation with HPLC, which will simplify and shorten the analysis. Individual subspecies quantification could also be accomplished directly with fluorescence.

5.4 Molecularly imprinted membrane (MIM) for LPA analysis

Along with MIPs, we can also synthesize MIMs for selective LPA analysis. Plasma LPA extractions with MIM as a filter could be advantageous because of the potentially shorter retention time of LPA in the material. Functional monomers, described herein could also be used as a starting point for creating LPA-selective MIMs.

5.5 MIPs with fluorescent probes

MIPs that contain fluorescence probes within their interior could allow for the direct determination of LPA in plasma via an optical signal. Fluorescence probes that have been synthesized specifically for LPA detection in our research group can be modified with vinyl groups and be incorporated during polymerization.

References

1. van Dijk, M.C.M. et al. Exogenous phospholipase D generates lysophosphatidic acid and activates Ras, Rho and Ca2+ signaling pathways. *Current Biology* **8**, 386-392 (1998).

2. van Corven, E.J., Groenink A Fau - Jalink, K., Jalink K Fau - Eichholtz, T., Eichholtz T Fau - Moolenaar, W.H. & Moolenaar, W.H. Lysophosphatidate-induced cell proliferation: identification and dissection of signaling pathways mediated by G proteins. *Cell* **59,** 45-54(1989).

3. Baker, D.L., Desiderio, D.M., Miller, D.D., Tolley, B. & Tigyi, G.J. Direct quantitative analysis of lysophosphatidic acid molecular species by stable isotope dilution electrospray ionization liquid chromatography-mass spectrometry. *Analytical Biochemistry* **292**, 287-295 (2001).

4. Stähle, M. et al. Mechanisms in LPA-induced tumor cell migration: critical role of phosphorylated ERK. *Journal of Cell Science* **116**, 3835-3846 (2003).

5. Simon Mf Fau - Chap, H., Chap H Fau - Douste-Blazy, L. & Douste-Blazy, L. Platelet aggregating activity of lysophosphatidic acids is not related to their calcium ionophore properties. *FEBS Lett.* **166**, 115-119 (1984).

6. Schumacher Ka Fau - Classen, H.G., Classen Hg Fau - Spath, M. & Spath, M. Platelet aggregation evoked in vitro and in vivo by phosphatidic acids and lysoderivatives: identity with substances in aged serum (DAS). *Thromb. Haemostasis*, **42**, 631-640(1979).

7. Estivill-Torrús, G. et al. Absence of LPA1 signaling results in defective cortical development. *Cerebral cortex* **18**, 938-950 (2008).

8. Teo, S.T., Yung, Y.C., Herr, D.R. & Chun, J. Lysophosphatidic acid in vascular development and disease. *IUBMB life* **61**, 791-799 (2009).

9. Sims, S.M., Panupinthu, N., Lapierre, D.M., Pereverzev, A. & Dixon, S.J. Lysophosphatidic acid: A potential mediator of osteoblast–osteoclast signaling in bone. *Biochimica et Biophysica Acta (BBA) - Molecular and Cell Biology of Lipids* **1831**, 109-116 (2013).

10. Mills, G.B. & Moolenaar, W.H. The emerging role of lysophosphatidic acid in cancer. *Nature Reviews Cancer* **3**, 582-591 (2003).

11. Pua, T.L., Wang Fq Fau - Fishman, D.A. & Fishman, D.A. Roles of LPA in ovarian cancer development and progression. *Future Oncol* **5**, 1659-1673 (2009).

12. American Cancer Society. Cancer Facts & Figures 2014. *Atlanta: American Cancer Society* (2014).

13. Engel, J. et al. Moderate progress for ovarian cancer in the last 20 years: prolongation of survival, but no improvement in the cure rate. *European Journal of Cancer* **38**, 2435-2445 (2002).

14. Xu, Y., Shen, Z., Wiper, D.W. & et al. LYsophosphatidic acid as a potential biomarker for ovarian and other gynecologic cancers. *JAMA* **280**, 719-723 (1998).

15. Xiao, Y. et al. Electrospray ionization mass spectrometry analysis of lysophospholipids in human ascitic fluids: comparison of the lysophospholipid contents in malignant vs nonmalignant ascitic fluids. *Analytical Biochemistry* **290**, 302-313 (2001).

16. Shen, Z. et al. Fatty acid composition of lysophosphatidic acid and lysophosphatidylinositol in plasma from patients with ovarian cancer and other gynecological diseases. *Gynecologic Oncology* **83**, 25-30 (2001).

17. Sutphen, R. et al. Lysophospholipids are potential biomarkers of ovarian cancer. *Cancer Epidemiology Biomarkers & Prevention* **13**, 1185-1191 (2004).

18. Meleh, M., Pozlep, B., Mlakar, A., Meden-Vrtovec, H. & Zupancic-Kralj, L. Determination of serum lysophosphatidic acid as a potential biomarker for ovarian cancer. *Journal of Chromatography B* **858**, 287-291 (2007).

19. Sedláková, I., Vávrová, J., Tošner, J. & Hanousek, L. Lysophosphatidic Acid in Patients With Ovarian Cancer. *Clinical Ovarian Cancer* **3**, 41-46 (2010).

20. Baker, D.L. et al. Plasma lysophosphatidic acid concentration and ovarian cancer. *Jama-Journal of the American Medical Association* **287**, 3081-3082 (2002).

21. Liu, Y. et al. Lysophosphatidic Acid disrupts junctional integrity and epithelial cohesion in ovarian cancer cells. *Journal of oncology* **2012** (2012).

22. Panupinthu, N., Lee, H.Y. & Mills, G.B. Lysophosphatidic acid production and action: critical new players in breast cancer initiation and progression. *Br J Cancer* **102**, 941-946 (2010).

23. Hao, F. et al. Lysophosphatidic acid induces prostate cancer PC3 cell migration via activation of LPA1, p42 and p38 α . *Biochimica et Biophysica Acta (BBA) - Molecular and Cell Biology of Lipids* **1771**, 883-892 (2007).

24. Shida, D. et al. Aberrant expression of lysophosphatidic acid (LPA) receptors in human colorectal cancer. *Lab Invest* **84**, 1352-1362 (2004).

25. Skill, N.J. et al. Lysophospholipid variants in hepatocellular carcinoma. *J Surg Res* **182**, 241-9 (2013).

26. Sasagawa, T., Okita, M., Murakami, J., Kato, T. & Watanabe, A. Abnormal serum lysophospholipids in multiple myeloma patients. *Lipids* **34**, 17-21 (1999).

27. Cui, M.-Z. Lysophosphatidic acid effects on atherosclerosis and thrombosis. *Clinical Lipidology* **6**, 413-426 (2011).

28. Schober, A. & Siess, W. Lysophosphatidic acid in atherosclerotic diseases. *Br J Pharmacol* **167**, 465-82 (2012).

29. Smyth, S.S., Cheng Hy Fau - Miriyala, S., Miriyala S Fau - Panchatcharam, M., Panchatcharam M Fau - Morris, A.J. & Morris, A.J. Roles of lysophosphatidic acid in cardiovascular physiology and disease.

30. Zhao, Y. & Natarajan, V. Lysophosphatidic acid (LPA) and its receptors: role in airway inflammation and remodeling. *Biochim Biophys Acta* **1831**, 86-92 (2013).

31. Sasagawa, T., Suzuki, K., Shiota, T., Kondo, T. & Okita, M. The Significance of Plasma Lysophospholipids in Patients with Renal Failure on Hemodialysis. *Journal of Nutritional Science and Vitaminology* **44**, 809-818 (1998).

32. Pradere, J.P. et al. LPA1 receptor activation promotes renal interstitial fibrosis. *Molecular and Cell Biology of Lipids*, **1781**, 582-587 (2008).

33. Khaw, K.T., Friesen, M.D., Riboli, E., Luben, R. & Wareham, N. Plasma phospholipid fatty acid concentration and incident coronary heart disease in

men and women: the EPIC-Norfolk prospective study. *PLoS Med* **9**, e1001255 (2012).

34. Bese, T. et al. Comparison of total plasma lysophosphatidic acid and serum CA-125 as a tumor marker in the diagnosis and follow-up of patients with epithelial ovarian cancer. *J Gynecol Oncol* **21**, 248-254 (2010).

35. Takatera, A. et al. Quantification of lysophosphatidylcholines and phosphatidylcholines using liquid chromatography-tandem mass spectrometry in neonatal serum. *Journal of Chromatography, B: Analytical Technologies in the Biomedical and Life Sciences* **838**, 31-36 (2006).

36. Kaewsuya, P., Danielson, N. & Ekhterae, D. Fluorescent determination of cardiolipin using 10-N-nonyl acridine orange. *Analytical and Bioanalytical Chemistry* **387**, 2775-2782 (2007).

37. Kitsos, M., Gandini, C., Massolini, G., De Lorenzi, E. & Caccialanza, G. High-performance liquid chromatography post-column derivatization with fluorescence detection to study the influence of ambroxol on dipalmitoylphosphatidylcholine levels in rabbit eustachian tube washings. *Journal of Chromatography A* **553**, 1-6 (1991).

38. Postle, A.D. Method for the sensitive analysis of individual molecular species of phosphatidylcholine by high-performance liquid chromatography using post-column fluorescence detection. *Journal of Chromatography. B, Biomedical Sciences and Applications* **415**, 241-251 (1987).

39. Chen, Y.L. & Xu, Y. Determination of lysophosphatidic acids by capillary electrophoresis with indirect ultraviolet detection. *Journal of Chromatography. B, Biomedical Sciences and Applications* **753**, 355-363 (2001).

40. Yoon, H.R., Kim, H. & Cho, S.H. Quantitative analysis of acyl-lysophosphatidic acid in plasma using negative ionization tandem mass spectrometry. *Journal of Chromatography B* **788**, 85-92 (2003).

41. Holland, W.L., Stauter, E.C. & Stith, B.J. Quantification of phosphatidic acid and lysophosphatidic acid by HPLC with evaporative light-scattering detection. *Journal of Lipid Research* **44**, 854-858 (2003).

42. Yoon, H.-R., Kim, H. & Cho, S.-H. Quantitative analysis of acyl-lysophosphatidic acid in plasma using negative ionization tandem mass spectrometry. *Journal of Chromatography B* **788**, 85-92 (2003).

43. Shan, L., Jaffe, K., Li, S. & Davis, L. Quantitative determination of lysophosphatidic acid by LC/ESI/MS/MS employing a reversed phase HPLC column. *Journal of Chromatography B* **864**, 22-28 (2008).

44. Chin, C., Zhang, Z.P. & Karnes, H.T. A study of matrix effects on an LC/MS/MS assay for olanzapine and desmethyl olanzapine. *J Pharm Biomed Anal* **35**, 1149-67 (2004).

45. Wang, S., Cyronak, M. & Yang, E. Does a stable isotopically labeled internal standard always correct analyte response? A matrix effect study on a LC/MS/MS method for the determination of carvedilol enantiomers in human plasma. *J Pharm Biomed Anal* **43**, 701-7 (2007).

46. Fu, I., Woolf, E.J. & Matuszewski, B.K. Effect of the sample matrix on the determination of indinavir in human urine by HPLC with turbo ion spray tandem mass spectrometric detection. *Journal of Pharmaceutical and Biomedical Analysis* **18**, 347-357 (1998).

47. Liu, Y. et al. Lysophosphatidic Acid disrupts junctional integrity and epithelial cohesion in ovarian cancer cells. *J Oncol* **2012**, 501492 (2012).

48. Shan, L., Jaffe, K., Li, S. & Davis, L. Quantitative determination of lysophosphatidic acid by LC/ESI/MS/MS employing a reversed phase HPLC column. *Journal of Chromatography B* **864**, 22-28 (2008).

49. Zhao, Z. & Xu, Y. An extremely simple method for extraction of lysophospholipids and phospholipids from blood samples. *Journal of Lipid Research* **51**, 652-659 (2010).

50. Bligh, E.G. & Dyer, W.J. A rapid method of total lipid extraction and purification. *Canadian Journal of Biochemistry and Physiology* **37**, 911-917 (1959).

51. Kooijman, E.E. et al. What makes the bioactive lipids phosphatidic acid and lysophosphatidic acid so special? *Biochemistry* **44**, 17007-15 (2005).

52. Caudron, E., Zhou, J.Y., Chaminade, P., Baillet, A. & Prognon, P. Fluorescence probe assisted post-column detection for lipid analysis in microbore-LC. *Journal of Chromatography A* **1072**, 149-157 (2005).

53. Ibrahim, H., Caudron, E., Kasselouri, A. & Prognon, P. Interest of Fluorescence Derivatization and Fluorescence Probe Assisted Post-column Detection of Phospholipids: A Short Review. *Molecules* **15**, 352-373 (2010).

54. Bernhard, W. et al. High-Performance Liquid Chromatographic Analysis of Phospholipids from Different Sources with Combined Fluorescence and Ultraviolet Detection. *Analytical Biochemistry* **220**, 172-180 (1994).

55. Gebhardt, D.O., Soederhuizen, W. & Feyen, J.H. The fluorimetric determination of the lecithin/sphingomyelin ratio of amniotic fluid after HPLC. *Annals of Clinical Biochemistry* **22**, 321-323 (1985).

56. Zhao, W. et al. A chromo- and fluorogenic sensor for probing the cancer biomarker lysophosphatidic acid. *Analyst* **137**, 1853-1859 (2012).

57. Garcia-Fernandez, M.I., Ceccarelli, D. & Muscatello, U. Use of the fluorescent dye 10-N-nonyl acridine orange in quantitative and location assays of cardiolipin: a study on different experimental models. *Analytical Biochemistry* **328**, 174-180 (2004).

58. Gohil, V.M., Gvozdenovic-Jeremic, J., Schlame, M. & Greenberg, M.L. Binding of 10-N-nonyl acridine orange to cardiolipin-deficient yeast cells: Implications for assay of cardiolipin. *Analytical Biochemistry* **343**, 350-352 (2005).

59. Loew Lm Fau - Simpson, L.L. & Simpson, L.L. Charge-shift probes of membrane potential: a probable electrochromic mechanism for p-aminostyrylpyridinium probes on a hemispherical lipid bilayer. *Biophysical journal*, **34**, 353-365 (1981).

60. Chen, Y.L. & Xu, Y. Isolation and quantitation of plasma lysophosphatidic acids by solid-phase extraction and capillary electrophoresis. *Journal of Liquid Chromatography & Related Technologies* **25**, 843-855 (2002).

61. Chua, S.C. et al. Effect of absorbent in solid-phase extraction on quantification of phospholipids in palm-pressed fiber. *Eur. J. Lipid Sci. Technol.* **110**, 334-340 (2008).

62. Perez-Palacios, T., Ruiz, J. & Antequera, T. Improvement of a solid phase extraction method for separation of animal muscle phospholipid classes. *Food Chemistry* **102**, 875-879 (2007).

63. Xiao, Y., Chen, Y., Kennedy, A.W., Belinson, J. & Xu, Y. Evaluation of plasma lysophospholipids for diagnostic significance using electrospray ionization mass spectrometry (ESI - MS) analyses. *Annals of the New York Academy of Sciences* **905**, 242-259 (2000).

64. Sud, M. et al. LMSD: LIPID MAPS structure database. *Nucleic Acids Res* **35**, D527-32 (2007).

65. Zhu, C. et al. An efficient hydrophilic interaction liquid chromatography separation of 7 phospholipid classes based on a diol column. *Journal of Chromatography A* **1220**, 26-34 (2012).

66. Xu, Y. et al. Lysophosphatidic acid as a potential biomarker for ovarian and other gynecologic cancers. *JAMA, the journal of the American Medical Association* **280**, 719-723 (1998).

67. Bese, T. et al. Comparison of total plasma lysophosphatidic acid and serum CA-125 as a tumor marker in the diagnosis and follow-up of patients with epithelial ovarian cancer. *Journal of Gynecologic Oncology* **21**, 248-254 (2010).

68. Sedlakova, I., Vavrova, J., Tosner, J. & Hanousek, L. Lysophosphatidic acid in ovarian cancer patients. *Ceskoslovenska Gynekologie* **71**, 312-317 (2006).

69. Lu, Z., Chen, Y., Hu, Z. & Hu, C. Diagnostic Value of Total Plasma Lysophosphatidic Acid in Ovarian Cancer. (2014).

70. Wang, J. et al. Simple enrichment and analysis of plasma lysophosphatidic acids. *Analyst* **138**, 6852-9 (2013).

71. Chen, Y.-L. & Xu, Y. Determination of lysophosphatidic acids by capillary electrophoresis with indirect ultraviolet detection. *Journal of Chromatography B: Biomedical Sciences and Applications* **753**, 355-363 (2001).

72. Zhao, Z. & Xu, Y. Measurement of endogenous lysophosphatidic acid by ESI-MS/MS in plasma samples requires pre-separation of

lysophosphatidylcholine. *Journal of Chromatography B* **877**, 3739-3742 (2009).

73. Takatera, A. et al. Quantification of lysophosphatidylcholines and phosphatidylcholines using liquid chromatography–tandem mass spectrometry in neonatal serum. *Journal of Chromatography B* **838**, 31-36 (2006).

74. Matuszewski, B.K., Constanzer, M.L. & Chavez-Eng, C.M. Strategies for the Assessment of Matrix Effect in Quantitative Bioanalytical Methods Based on HPLC–MS/MS. *Analytical Chemistry* **75**, 3019-3030 (2003).

75. Wulff, G. Molecular Imprinting in Cross-Linked Materials with the Aid of Molecular Templates— A Way towards Artificial Antibodies. *Angewandte Chemie International Edition in English* **34**, 1812-1832 (1995).

76. Wulff, G., Gross, T. & Schönfeld, R. Enzyme Models Based on Molecularly Imprinted Polymers with Strong Esterase Activity. *Angewandte Chemie International Edition in English* **36**, 1962-1964 (1997).

77. Zimmerman, S.C. & Lemcoff, N.G. Synthetic hosts via molecular imprinting--are universal synthetic antibodies realistically possible?

78. Qu, P., Lei, J., Ouyang, R. & Ju, H. Enantioseparation and amperometric detection of chiral compounds by in situ molecular imprinting on the microchannel wall. *Analytical chemistry* **81**, 9651-9656 (2009).

79. Fang, L., Chen, S., Zhang, Y. & Zhang, H. Azobenzene-containing molecularly imprinted polymer microspheres with photoresponsive template binding properties. *Journal of Materials Chemistry* **21**, 2320-2329 (2011).

80. Deng, Q.L., Li, Y.L., Zhang, L.H. & Zhang, Y.K. Molecularly imprinted macroporous monolithic materials for protein recognition. *Chinese Chemical Letters* **22**, 1351-1354 (2011).

81. Nilsson, K., Lindell, J., Norrlöw, O. & Sellergren, B. Imprinted polymers as antibody mimetics and new affinity gels for selective separations in capillary electrophoresis. *Journal of Chromatography A* **680**, 57-61 (1994).

82. Vallano, P.T. & Remcho, V.T. Highly selective separations by capillary electrochromatography: molecular imprint polymer sorbents. *Journal of Chromatography A* **887**, 125-135 (2000).

83. Koeber, R. et al. Evaluation of a multidimensional solid-phase extraction platform for highly selective on-line cleanup and high-throughput LC-MS analysis of triazines in river water samples using molecularly imprinted polymers. *Analytical chemistry* **73**, 2437-2444 (2001).

84. Qi, P., Wan, Y. & Zhang, D. Impedimetric biosensor based on cell-mediated bioimprinted films for bacterial detection. *Biosensors and Bioelectronics* **39**, 282-288 (2013).

85. Hayden, O. & Dickert, F.L. Selective microorganism detection with cell surface imprinted polymers. *Advanced Materials* **13**, 1480-1483 (2001).

86. Jenik, M. et al. Sensing picornaviruses using molecular imprinting techniques on a quartz crystal microbalance. *Analytical chemistry* **81**, 5320-5326 (2009).

87. Schirhagl, R., Podlipna, D., Lieberzeit, P.A. & Dickert, F.L. Comparing biomimetic and biological receptors for insulin sensing. *Chemical communications* **46**, 3128-3130 (2010).

88. Schirhagl, R., Latif, U. & Dickert, F.L. Atrazine detection based on antibody replicas. *Journal of Materials Chemistry* **21**, 14594-14598 (2011).

89. Katz, A. & Davis, M.E. Molecular imprinting of bulk, microporous silica. *Nature* **403**, 286-289 (2000).

90. Liu, J.-q. & Wulff, G. Functional Mimicry of the Active Site of Carboxypeptidase A by a Molecular Imprinting Strategy: Cooperativity of an Amidinium and a Copper Ion in a Transition-State Imprinted Cavity Giving Rise to High Catalytic Activity. *Journal of the American Chemical Society* **126**, 7452-7453 (2004).

91. Hilt, J.Z. & Byrne, M.E. Configurational biomimesis in drug delivery: molecular imprinting of biologically significant molecules. *Advanced drug delivery reviews* **56**, 1599-1620 (2004).

92. Alvarez-Lorenzo, C. & Concheiro, A. Molecularly imprinted polymers for drug delivery. *Journal of Chromatography B* **804**, 231-245 (2004).

93. Byrne, M.E., Park, K. & Peppas, N.A. Molecular imprinting within hydrogels. *Advanced drug delivery reviews* **54**, 149-161 (2002).

94. Chien, Y.W. & Lin, S. Optimisation of treatment by applying programmable rate-controlled drug delivery technology. *Clinical pharmacokinetics* **41**, 1267-1299 (2002).

95. Saridakis, E. et al. Protein crystallization facilitated by molecularly imprinted polymers (vol 108, pg 11081, 2011). *Proceedings of the National Academy of Sciences of the United States of America* **108**, 18566-18566 (2011).

96. D'Souza, S.M., Alexander, C., Whitcombe, M.J., Waller, A.M. & Vulfson, E.N. Control of crystal morphology via molecular imprinting. *Polymer international* **50**, 429-432 (2001).

97. D'Souza, S.M. et al. Directed nucleation of calcite at a crystal-imprinted polymer surface. *Nature* **398**, 312-316 (1999).

98. Reddy, S.M. et al. Protein crystallization and biosensor applications of hydrogel-based molecularly imprinted polymers. *Biomacromolecules* **13**, 3959-3965 (2012).

99. Hoshino, Y. et al. Design of synthetic polymer nanoparticles that capture and neutralize a toxic peptide. *Small* **5**, 1562-1568 (2009).

100. Hoshino, Y. et al. Recognition, neutralization, and clearance of target peptides in the bloodstream of living mice by molecularly imprinted polymer nanoparticles: a plastic antibody. *Journal of the American Chemical Society* **132**, 6644-6645 (2010).

101. DePorter, S.M., Lui, I. & McNaughton, B.R. Programmed cell adhesion and growth on cell-imprinted polyacrylamide hydrogels. *Soft Matter* **8**, 10403-10408 (2012).

102. Lim, J.Y. & Donahue, H.J. Cell sensing and response to micro-and nanostructured surfaces produced by chemical and topographic patterning. *Tissue engineering* **13**, 1879-1891 (2007).

103. Curtis, A. & Wilkinson, C. Topographical control of cells. *Biomaterials* **18**, 1573-1583 (1997).

104. Piletsky, S.A. & Turner, A.P.F. Electrochemical sensors based on molecularly imprinted polymers. *Electroanalysis* **14**, 317-323 (2002).

105. Lee, J.-D., Greene, N.T., Rushton, G.T., Shimizu, K.D. & Hong, J.-I. Carbohydrate recognition by porphyrin-based molecularly imprinted polymers. *Organic letters* **7**, 963-966 (2005).

106. Tanabe, K. et al. Recognition of barbiturates in molecularly imprinted copolymers using multiple hydrogen bonding. *J. Chem. Soc., Chem. Commun.*, 2303-2304 (1995).

107. Gale, P.A. Anion and ion-pair receptor chemistry: highlights from 2000 and 2001. *Coordination chemistry reviews* **240**, 191-221 (2003).

108. Brooks, S.J., Edwards, P.R., Gale, P.A. & Light, M.E. Carboxylate complexation by a family of easy-to-make ortho-phenylenediamine based bis-ureas: studies in solution and the solid state. *New journal of chemistry* **30**, 65-70 (2006).

109. Nishizawa, S., Kato, Y. & Teramae, N. Fluorescence sensing of anions via intramolecular excimer formation in a pyrophosphate-induced self-assembly of a pyrene-functionalized guanidinium receptor. *Journal of the American Chemical Society* **121**, 9463-9464 (1999).

110. Wu, X., Goswami, K. & Shimizu, K.D. Comparison of monofunctional and multifunctional monomers in phosphate binding molecularly imprinted polymers. *J Mol Recognit* **21**, 410-8 (2008).

111. Emgenbroich, M. et al. A phosphotyrosine-imprinted polymer receptor for the recognition of tyrosine phosphorylated peptides. *Chemistry* **14**, 9516-29 (2008).

112. Aoki, S., Jikiba, A., Takeda, K. & Kimura, E. A zinc(II) complex-conjugated polymer for selective recognition and separation of phosphates. *Journal of Physical Organic Chemistry* **17**, 489-497 (2004).